New Beamforming and DOA Estimation Techniques in Wireless Communications

by

Nanyan Wang
M.S., Huazhong University of Science and Technology, 1999
B.E., Huazhong University of Science and Technology, 1995

A Dissertation Submitted in Partial Fulfillment of the Requirements
for the Degree of

DOCTOR OF PHILOSOPHY

in the Department of Electrical and Computer Engineering

Supervisors: Dr. P. Agathoklis and Dr. A. Antoniou

ABSTRACT

The development and performance evaluation of new techniques for direction of arrival (DOA) estimation, single-user beamforming (SUB), and multiuser beamforming (MUB) to be used in wireless communications are investigated.

Two of the most commonly used beamformer configurations in direct-sequence code-division multiple access (DS-CDMA) systems, the chip-based (CB) and the symbol-based (SB) configurations for the base station (BS) receiver, are studied and their performance is evaluated. It is shown that using the CB configuration, different interfering components are rejected based on the spatial distribution of their power. In the SB configuration, spatial diversity is exploited after despreading and different interfering components are rejected based on their interfering strength which depends on both their power and code correlation with the signal of interest. For the SB configuration, more effort is applied to rejecting the interfering components with higher interfering strength and thus a more selective and efficient system is achieved. Detailed performance analysis and simulations show that in the presence of multiple-access interference, the SB configuration can lead to a significant improvement in the signal-to-interference-plus-noise ratio relative to that achieved with the CB configuration for both asynchronous and synchronous DS-CDMA systems.

A new technique for DOA estimation is proposed. The new technique, called subarray beamforming-based DOA (SBDOA) estimation, uses two virtual subarrays to form a signal whose phase relative to the reference signal is a function of the DOA. The DOA is then estimated based on the computation of the phase shift between the reference signal and the phase-shifted target signal. Since the phase-shifted target signal is obtained after interference rejection through beamforming, the effect of co-channel interference on the estimation is significantly reduced. The proposed technique is computationally simple and the number of signal sources detectable is

not bounded by the number of antenna elements used. Performance analysis and extensive simulations show that the proposed technique offers significantly improved estimation resolution, capacity, accuracy, and tracking capability relative to existing techniques.

A new SUB algorithm is proposed for the downlink in wireless communication systems. The beam pattern at the BS is determined using a new optimality criterion which takes into consideration the fact that signals from the BS to different mobile stations (MSs) have different power and thus have different resistance to co-channel interference. In this way, the power of co-channel interference in the direction of an MS whose downlink signal has low resistance to co-channel interference can be significantly reduced. Simulation results show that the new algorithm leads to better performance than conventional algorithms in terms of system outage probability.

A new MUB algorithm is proposed for joint beamforming and power control for the downlink in wireless communication systems. The optimization problem of optimal MUB is reformulated by modifying the constraints so that the weight vectors at the BS for different MSs are optimized in a feasible region which is a subset of the one of the original MUB problem. The downlink beamforming weight vectors of different MSs are then jointly optimized in a subspace instead of searching in the entire parameter space. Simulation results show that the modified optimization problem leads to solutions that satisfy the signal-to-noise-plus-interference ratio specification at each MS and, at the same time, the total power transmitted from the BS is very close to the optimal one. The solution of the modified optimization problem requires significantly less computation than that of the optimal MUB problem.

Table of Contents

List of Tables

List of Figures

List of Abbreviations

2G	Second-generation
3G	Third-generation
AWGN	Additive white Gaussian noise
BER	Bit-error rate
BF	Beamformer
BS	Base station
CB	Chip-based
CDMA	Code-division multiple-access
CDMA2000	Code-division multiple-access 2000
CS	Conjugate subarray
DOA	Direction of arrival
DPCCH	dedicated physical control channel
DS-CDMA	Direct-sequence code-division multiple-access
DEML	Decoupled maximum likelihood
ESPRIT	Estimation of signal parameters via rotational invariance technique
FDD	Frequency-division duplexing
GSM	Global system for mobile communications
IS	Interfering strength
IS-95	Interim standard 95
ISI	Inter-symbol interference
LMS	Least-mean-square
LOS	Line of sight
MAI	Multiple-access interference

MF	Matched filter
ML	Maximum likelihood
MMSE	Minimum mean-squared-error
MOS	Maximum overlapping subarray
MS	Mobile station
MSE	Mean-squared-error
MUB	Multiuser beamforming
MV	Minimum variance
MVDR	Minimum-variance distortionless response
MUSIC	Multiple signal classification
S-CPICH	Secondary common pilot channel
QoS	Quality of service
RIS	Relative interfering strength
RLS	Recursive-least-square
RMSE	Root-mean-square error
SB	Symbol-based
SBDOA	Subarray beamforming-based direction-of-arrival
SDP	Semidefinite programming
SINR	Signal-to-interference-plus-noise ratio
SIR	Signal-to-interference ratio
SNR	Signal-to-noise ratio
SOI	Signal of interest
SSBML	Spatial signature based maximum likelihood
SUB	Single-user beamforming
TDD	Time-division duplexing
ULA	Uniform linear antenna array
UMTS	Universal mobile telecommunication system
WCDMA	Wideband code-division multiple-access

Acknowledgement

First, I would like to thank my co-supervisors, Dr. Panajotis Agathoklis and Dr. Andreas Antoniou, for their help, encouragement, and financial support. They have profoundly influenced me during my Ph.D. studies, and it is a pleasure to acknowledge their guidance and support.

I would like to thank the members of my examining committee. I am indebted to Dr. Wu-Sheng Lu for his excellent teaching in Optimization II and careful review of this dissertation. I am grateful to Dr. Colin Bradley and Dr. Majid Ahmadi for being on the examining committee, and for their contribution in improving the quality of this thesis.

My association with DSP lab has been also a source of invaluable experience and friendship for me. I would like to thank my colleagues Brad Riel, David Guindon, Deepali Arora, Haoran Zhang, Dr. M. Watheq El-Kharashi, Paramesh Ramachandran, Dr. Tarek Nasser, Mingjie Cai, Manjinder Mann, Rafik Mikhael, Rajeev Nongpiur, Sabbir Ahmad, Stuart Bergen, Mohamed S. Yasein, Dr. Xianmin Wang, Yajun Kou, and Yihai Zhang for their generous friendship and enlightening discussion.

Outside the DSP Lab, I have also cherished the company of several friends during my stay in Victoria. In particular, I would like to thank Fei Huang, Dr. Jian Wang, Le Yang, Wei Lu, Dr. Wei Li, Xiaoli Lu, Xingming Wang, Yanguo Liu, Yongsheng Shi, and Dr. Zhiwei Mao.

I wish to thank our staff Ms. Catherine Chang, Ms. Lynne Barrett, Ms. Mary-Anne Teo, Ms. Moneca Bracken, and Ms. Vicky Smith, for their help during my Ph.D. studies.

I also thank PMC-Sierra Inc., Micronet and NSERC for sponsoring the projects of this dissertation. The financial support from these sources is greatly appreciated.

Finally, my special thanks go to my family for their love, deep understanding, and strong support on the pursuit of my Ph. D. degree.

Chapter 1

Introduction

The ever-growing number of subscribers and demand for next generation data services have made the issues of capacity increase and performance improvement for wireless communication systems more and more crucial [1][2]. The capacity of wireless communication systems can be increased and the performance improved by adding additional carrier frequencies or increasing cell density in the network which are generally extremely expensive. In recent years, interference cancellation through beamforming [3] has been recognized as one of the most promising and cost-effective techniques to increase the capacity and carrier efficiency of wireless communication systems.

In wireless communication systems, subscribers are usually spatially separated and the use of antenna arrays makes it possible to track the direction-of-arrival (DOA) of each signal and locate the position of a subscriber. Based on the position information, the spatial separation can be exploited through beamforming to multiplex the channel in the spatial dimension as well as in the frequency and time dimensions to receive and transmit signals in a directional manner. In this way, the effect of co-channel interference can be reduced. It has been shown that through the use of beamforming, the capacity, carrier efficiency, and coverage of a wireless communication system can be significantly improved.

The use of beamforming for interference rejection is especially attractive in the third-generation (3G) and future wireless communication systems where capacity, carrier efficiency, and coverage are the most important issues. The 3G standards such as

the wideband code-division multiple-access (WCDMA) and code-division multiple-access 2000 (CDMA2000) standards are well designed to provide the pilot channels which are required for fast and accurate DOA estimation and beamforming. In the universal mobile telecommunications system (UMTS), the dedicated physical control channel (DPCCH) in the uplink is used to transmit pilot symbols at each mobile station (MS) and user-specific beamforming allows the generation of individual beams at the base station (BS) for each MS without any restrictions on the selection of beamforming weight vectors [4]. In the downlink, each beam is associated with a unique secondary common pilot channel (S-CPICH) so that MSs can use it to detect the signal coherently. In CDMA2000 systems, a user-specific pilot signal is available for both uplink and downlink which can be used as a reference signal for DOA estimation and adaptive beamforming [5][6].

In the following section, existing techniques for DOA estimation, single-user beamforming (SUB), and multiuser beamforming (MUB) will be reviewed.

1.1 Previous Work

1.1.1 DOA Estimation

Information about the DOA of signals is required in most smart antenna techniques where signals are transmitted and received in a directional manner. The performance of these techniques relies heavily on the accurate estimation of the DOA of each signal. Various techniques for DOA estimation have been proposed [7]-[18] in the past several decades. The most commonly used among these techniques are multiple signal classification (MUSIC) [9][10], estimation of signal parameters via rotational invariance technique (ESPRIT) [11]-[13], and their variations [14] [15]. These subspace-based techniques lead to an acceptable DOA estimation if the number of signal sources is less than the number of antenna elements. In the case where the total number of

interfering and target signal sources is larger than the number of antenna elements, only some of the DOAs of the signals can be properly estimated. In MUSIC-class techniques, the DOAs are determined by finding the directions for which their antenna response vectors lead to peaks in the MUSIC spectrum formed by the eigenvectors of the noise subspace. The maximum number of DOAs detectable, i.e., the capacity of DOA estimation technique, is equal to the rank of the reciprocal subspace of the selected noise subspace. Thus, the capacity of DOA estimation using MUSIC is no more than $M-1$ where M is the number of antenna elements in the antenna array [19]. For ESPRIT-class techniques, two subarrays are used to obtain two signal subspaces such that the eigenvectors of one signal subspace relative to the eigenvectors of the other are rotated in terms of the DOAs of the signals. The DOAs are then estimated by computing the rotation matrix. As a result, the capacity of DOA estimation using ESPRIT-class techniques is bounded by the number of antenna elements in the subarrays [15] [20]. This limits the application of subspace-based techniques to cases where the number of signal sources is less than the number of antenna elements. In addition, these techniques require subspace estimation and eigendecomposition which entail high computational complexity [13] [21] [22] thereby limiting their use to applications where fast DOA estimation is not required. Another disadvantage of these techniques is that in the presence of multiple signal sources, the DOAs of the target signals and interference are all estimated and as a consequence these techniques cannot identify which signal source corresponds to which estimated DOA.

In some applications such as wireless communication systems, a pilot signal (or decision-directed signal) is usually available [23]. In active radar and sonar systems, the signal received from a target is a reflection of the known transmitted signal. Maximum likelihood (ML) techniques [16]-[18] have been developed to exploit such signals in the DOA estimation. In these techniques, the most likely DOAs are estimated so that the samples of received signals are matched to the known signals. The maximization of the log-likelihood function is a nonlinear optimization problem which

requires multi-dimensional search and thus entails a very large amount computation. The ML algorithm proposed in [16] transforms the multidimensional search problem into an iterative one-dimensional search problem. This technique needs another DOA estimation technique such as MUSIC and ESPRIT to provide initial estimation and further there is no guarantee of global convergence. In [17], another decoupled ML algorithm is described. It is computationally more efficient and it can estimate DOAs in the presence of interference or jamming signals. A spatial signature based ML DOA estimation technique is described in [18]. The DOAs of known signals are computed based on ML estimation of their corresponding spatial signatures. The capacity of DOA estimation of this technique is larger than the number of antenna elements and it can deal with correlated signals. It requires the noise to be spatially and temporally white and, therefore, the performance of this technique is sensitive to directional interference which is present in many applications.

1.1.2 Single-User Beamforming

Spatially selective reception and transmission are accomplished by using adaptive beamformers. A beamformer is a spatial filter with a narrow passband in a target direction that optimally combines signals received at different antenna elements in such a way as to enhance signals arriving from a target source. The goal of SUB in the uplink of mobile communications is to maximize the power received from the target MS and at the same time minimize the received power from MSs other than the target one [24][25]. In early SUB techniques, the beamforming weights for different MSs are optimized individually. Various optimality criteria have been proposed to obtain uplink SUB weights. In [26], beamforming weights are chosen to minimize the mean-squared error (MSE) between the signal at the beamformer output and the reference signal. In [27][28], the signal-to-interference-plus-noise ratio (SINR) of the signal at the beamformer output is maximized. The minimum variance (MV) criterion has been used in [29] to minimize the noise variance at the beamformer output, and the

ML criterion has been used in [30] to obtain the beamforming weights. Based on these optimality criteria, different beamforming algorithms have been developed. Performance analysis of different beamforming schemes can be found in [24][31][32][33]. The computational complexity of beamforming algorithms based on different optimality criteria is discussed in [27]. The effect of receiver nonlinearity and random error on adaptive beamforming is analyzed in [34].

The goal of downlink SUB is to maximize the power transmitted to the target MS and meanwhile minimize it to other MSs sharing the same frequency channel. Conventional generalized eigenvalue-based SUB algorithms [35]-[40] have been widely used to adaptively obtain the weights for transmit beamforming. In [36], the beamforming weights are obtained by maximizing the downlink signal power to the target MS relative to the total power radiated in the direction of other MSs and simultaneously keeping the antenna-array gain constant in the direction of the desired MS. In [37]-[39], the power of the downlink signal to the desired MS is maximized while keeping the total power to other MSs less than or equal to a given constant level. The optimality criterion used in [40] aims at transmitting a given power to the desired MS and simultaneously minimizing the power to other MSs. It can be shown that all these criteria are equivalent in the sense that they lead to the same direction of weight vector and, therefore, the same radiation pattern is obtained.

1.1.3 Multiuser Beamforming

The SUB algorithms are computationally simple but provide suboptimal solutions to the problem of minimizing the BS transmitted power. Recently, a more powerful approach has been proposed, namely, MUB [35]. In the MUB approach, the beamforming weights for all MSs are jointly optimized. For the uplink, MUB is formulated as an optimization problem where the weight vectors at the BS for different MSs are jointly optimized so as to satisfy given SINR specifications at the BS and, at the same time, the total power transmitted from all the MSs is minimized. For the

downlink, MUB is formulated as an optimization problem where the transmit weight vectors at the BS for different MSs are jointly optimized so as to satisfy given SINR specifications at the MSs and, at the same time, the total BS transmitted power is minimized.

Both the uplink MUB and downlink MUB turn out to be optimization problems with nonconvex quadratic constraints. In [44], an iterative algorithm is developed to solve the optimal uplink MUB. Two classes of algorithms have been developed for downlink MUB, namely, duality-based [41][42] and semidefinte programming (SDP) based [45]-[47] MUB algorithms. The duality between the uplink and downlink was originally presented and discussed in [41]. It has been shown that the optimal downlink weight vectors can be obtained through the use of a virtual uplink. Based on this duality, an optimal MUB algorithm is developed to iteratively obtain the optimal downlink weight vectors. An early version of the duality-based algorithm [41] tends to converge more slowly as the SINR requirements become more stringent. The duality between the uplink and downlink is further discussed in [48][49] and a new duality-based MUB algorithm is proposed in [42] where several stopping criteria are proposed to improve the convergence behavior of the iterative algorithm. The SDP based MUB algorithm is described in [45]-[47]. In this algorithm, the optimal MUB optimization problem is relaxed into a SDP optimization problem after Lagrangian relaxation [50]. The weight vectors are then obtained from the optimal solution of the SDP problem. The amount of computation required for the solution of SDP based MUB is high and it increases rapidly as the number of antenna elements is increased.

1.2 Scope and Contributions of the Dissertation

This dissertation consists of seven chapters. In Chapter 2, an introduction to antenna systems and preliminary studies on antenna response, SUB, and MUB for mobile communications is presented. Chapters 3-6 make up the main body of the

dissertation. They describe the analysis of beamformer configurations, a new DOA estimation technique, and several new beamforming and power control algorithms. Chapter 7 provides concluding remarks and suggestions for future research.

In Chapter 3, two beamformer configurations for the BS receiver in direct-sequence code-division multiple access (DS-CDMA) systems, namely, a chip-based (CB) and a symbol-based (SB) configuration, are studied. Though various beamforming schemes have been extensively analyzed and discussed in the past, most beamforming algorithms in the literature have been analyzed independently of the configurations of the CDMA systems they are part of and, most importantly, the effect of code diversity when rejecting interference using beamforming has not been discussed. In Chapter 3, the performance of the CB and SB configurations in rejecting interference is investigated through theoretical analysis and simulations on the basis of closed-form solutions for the beamforming weights. It is shown that in the CB configuration, different interfering components are rejected based on the spatial distribution of their power. In the SB configuration, spatial diversity is exploited after despreading and different interfering components are rejected based on their interfering strength which depends on both their power and code correlation with the signal of interest. For the SB configuration, more effort is applied to rejecting the interfering components with higher interfering strength and thus a more selective and efficient system is achieved. Detailed performance analysis and simulations show that in the presence of multiple-access interference, the SB configuration can lead to a significant improvement in the SINR relative to that achieved with the CB configuration for both asynchronous and synchronous DS-CDMA systems.

The major concern of Chapter 4 is the development of a high-resolution and high-capacity DOA estimation technique. In this chapter, a new subarray beamforming-based DOA (SBDOA) estimation technique that uses a reference signal is proposed. Two virtual subarrays in conjunction with two subarray beamformers are used to obtain an optimum estimation of the phase-shifted reference signal whose phase rela-

tive to the reference signal is a function of the target DOA. The target DOA is then computed from the estimated phase shift between the phase-shifted reference signal and the reference signal. The DOA estimation using the SBDOA technique is no longer bounded by the number of antenna elements as in existing techniques. Further, the DOA is estimated from the phase-shifted reference signal which is obtained after interference rejection through subarray beamforming. The signals from sources which severely interfere with the target signal can be efficiently rejected. Thus their interference on the DOA estimation is reduced. These two facts have the effect that the estimation capacity and resolution of the proposed SBDOA technique are higher than those of existing techniques. Since subspace estimation and eigendecomposition are not required in the SBDOA technique as is the case in other DOA estimation techniques, the SBDOA technique is computationally simpler and can be easily implemented on hardware. In addition, the use of a reference signal which can be either a pilot or a decision-directed signal enables the proposed SBDOA technique to identify which signal source corresponds to which estimated DOA. Performance analysis and extensive simulations show that the proposed technique offers significantly improved estimation resolution, capacity, and accuracy relative to those of existing techniques.

Chapter 5 is devoted to downlink SUB in mobile communication systems. In mobile communication systems, particular the 3G and future wireless communication systems, downlink signals to different MSs have different power levers due to power control, multiple-bit-rate service, and multiple quality-of-services (QoSs). Thus, they have different resistance to the co-channel interference caused by the downlink signals to other MSs. This difference is not taken into consideration in the determination of beamforming weights using the conventional SUB algorithms and, therefore, a system using these algorithms suffers from a near-far problem such that a low-power signal to the target MS is significantly interfered by the high-power signals to other MSs. In the proposed new SUB algorithm, the beam pattern at the BS is determined using a new optimality criterion which takes into consideration the fact that signals from

the BS to different MSs have different power and thus have different resistance to co-channel interference. In this way, the power of co-channel interference in the direction of an MS whose downlink signal has low resistance to co-channel interference can be significantly reduced. Simulation results show that the new algorithm leads to better performance than conventional algorithms in terms of system outage probability.

Chapter 6 is concerned with a low computational-complexity MUB algorithm for the downlink in mobile communication systems. The use of more antenna elements is an effective way to reduce the transmitted power, improve the quality of service, and increase the capacity of a mobile communication system. However, the computational complexity of the optimal MUB using SDP increases rapidly with the number of antenna elements. In the proposed MUB, the optimization problem of optimal MUB is reformulated by modifying the constraints so that weight vectors of different MSs are optimized in a reduced feasible region that is a subset of the one of the optimal MUB problem. The downlink beamforming weight vectors of different MSs are then jointly optimized in a subspace instead of searching in the entire parameter space. The computational complexity of the proposed MUB depends on downlink channels other than the number of antenna elements in the optimal MUB. Simulation results show that the modified optimization problem leads to solutions that satisfy the SINR ratio specification at each MS and that the total power transmitted from the BS is very close to the optimal one. The solution of the modified optimization problem requires significantly less computation than the optimal MUB algorithms.

Chapter 2

Fundamentals of Beamforming for Wireless Communications

2.1 Introduction

In this chapter, the fundamental signal processing aspects of beamforming for wireless communications are presented to provide a basis on which the subsequent chapters are based. The chapter begins with some background knowledge, concepts, and terminology pertaining to radio propagation, and then different antenna systems in wireless communications are introduced. Lastly, the general framework for the study of beamforming configurations, DOA estimation, SUB, and MUB for wireless communications is established.

2.2 Radio Propagation

Wireless communication systems operate in radio environments such as urban areas, mountains, forests, and plains, etc. Depending on the radio environment, a wireless radio channel can comprise a line-of-sight signal path or multipath which is severely obstructed by surrounding buildings, foliage, and mountains. In wireless communication systems, the power of a transmitted signal is attenuated as it propagates through the wireless channel and, therefore, the received signal power is smaller than

the transmit power. This is known as path loss. In this section, the large-scale path loss and small-scale fading due to multipath and Doppler spread will be discussed.

2.2.1 Large-Scale Path Loss

Large-scale path loss describes the variation of the average power of a received signal as a function of the distance between the receiver and the transmitter. The term 'large-scale' refers to small fluctuation of the average power of the received signal during the time that the transmitted signal travels a long distance relative to the carrier wavelength. Measurements have shown that the average power of a received signal decreases in proportion to the logarithm of the distance between the transmitter and the receiver in both indoor and outdoor environments. The average large-scale path loss $\bar{p}(d)$ in dB over a line-of-sight path for an arbitrary transmitter-receiver separation can be expressed as [51]

$$\bar{p}(d) = \bar{p}(d_0) + 10n \log\left(\frac{d}{d_0}\right) \tag{2.1}$$

where d is the distance between the transmitter and receiver, d_0 is the reference distance which is determined from measurements close to the transmitter, and n is the path loss exponent which indicates the rate at which the path loss increases with distance.

If the signal paths are not line-of-sight, the obstructions surrounding the transmitter will reflect the transmitted signal and introduce statistical variability to the average power of a received signal. This is known as shadowing effect. Considering the shadowing effect, the path loss is a random variable having a log-normal distribution [51]. A general expression of the average large-scale path loss is given by

$$\bar{p}_L(d) = \bar{p}(d_0) + 10n \log\left(\frac{d}{d_0}\right) + x_\sigma \tag{2.2}$$

where x_σ is a zero-mean Gaussian distributed random variable in dB with standard deviation σ.

2.2.2 Small-Scale Fading

A transmitted signal may undergo small-scale fading as it propagates through a wireless channel. Depending on the channel, the bandwidth of the transmitted signal, and the velocity of an MS, multipath delay spread and Doppler spread lead to small-scale fading [52]. Relative to large-scale path loss, small-scale fading causes the received signal to change rapidly during the time that the signal travels through a short distance.

2.2.2.1 Multipath Fading

In mobile communication systems, the transmitted signal can be reflected by nearby obstructions and travel through multiple paths to the receiver. Since different paths have different propagation delays and losses, the received signal will be a combination of several time-delayed versions of the transmitted signal. This leads to either flat or frequency-selective fading.

A transmitted signal will undergo flat fading if the mobile radio channel has constant amplitude response and linear phase response over the bandwidth of the transmitted signal. In such a case, the signal bandwidth is narrower than the coherence bandwidth of the mobile radio channel. The root-mean-square path delay is smaller than a signal symbol period and the spectral characteristics of the transmitted signal is unchanged after propagating through the mobile radio channel. This channel is known as flat fading channel. The gain of a flat fading channel varies with time due to the multipath effect and results in amplitude fluctuations in the received signal. The commonly used amplitude distribution for a flat fading channel is the Raleigh distribution. The probability density function of Raleigh distribution is given by [53]

$$p(r) = \begin{cases} \frac{r}{\sigma^2} e^{-r^2/(2\sigma^2)} & 0 \leqslant r \leqslant \infty \\ 0 & \text{otherwise} \end{cases} \tag{2.3}$$

where r is the envelope amplitude of the received signal, and σ^2 is the power of the

multipath signal before envelope detection.

If the signal bandwidth is larger than the coherence bandwidth of the mobile radio channel, the channel is frequency-selective and the transmitted signal will undergo frequency-selective fading. In such a case, the spectral characteristics of the transmitted signal is no longer preserved at the receiver. This causes time-varying distortion. The amplitude and phase of the received signal change rapidly with time. A commonly used multipath fading model is the two-ray Raleigh fading model. The impulse response of the two-ray model is given by [54]

$$h_b(t) = \alpha_1 e^{j\phi_1}\delta(t) + \alpha_2 e^{j\phi_2}\delta(t-\tau) \tag{2.4}$$

where α_1 and α_2 are two independent variables with Rayleigh distribution, ϕ_1 and ϕ_2 are two independent variables with uniform distribution over $[0,\ 2\pi]$, and τ is the time delay between the two rays.

2.2.2.2 Doppler Fading

If an MS is in motion, the transmitted signal will undergo Doppler fading due to the Doppler shift. A Doppler fading channel is characterized by two important parameters, Doppler spread and coherence time. The Doppler spread which is equal to the maximum Doppler shift can be a measure of the spectral change of the Doppler fading channel. The coherence time is the dual of the Doppler spread in time domain. It is a measure of the duration over which the channel is invariant.

If the bandwidth of a transmitted signal is larger than the Doppler spread, a symbol period will be larger than the channel coherence time. In such a case, the channel is static during several symbol periods and thus the transmitted signal will undergo slow fading. On the other hand, if the signal bandwidth is smaller than the Doppler spread, a symbol period will be larger than the channel coherence time. In such a case, the channel is a fast fading channel in that the channel changes in a symbol period. Details of modelling and simulation of the Doppler fading can be

found in [54][55].

2.3 Antenna Systems in Wireless Communications

Four categories of antennas have been used in mobile communications, i.e., omnidirectional, sectored [56], and switched-beam antennas [57], and adaptive antenna arrays. An omnidirectional antenna has a circlular beam pattern with uniform gain in all directions as shown in Fig. 2.1. Using an omnidirectional antenna, signals will be uniformly transmitted and received in all directions. In the uplink of code-division multiple-access (CDMA) communication systems, an omnidirectional antenna at the BS will receive the signal of interest (SOI) from the target MS along with co-channel interference caused by all other MSs in the service area. As a result, high transmitted power is required at the MS to satisfy the SINR requirement at the BS. In the downlink, an omnidirectional antenna will uniformly radiate power in all directions. Since the target MS receives signals at only one place at a time, most of the energy is wasted. In addition, an omnidirectional antenna causes co-channel interference to other MSs and BSs that are using the same frequency channel.

Cell sectorization has been widely used to increase the capacity of mobile communication systems such as the global system for mobile communications (GSM) and the interim standard 95 (IS-95) CDMA communication systems [56][58]. In these systems, each cell is divided into three or more sectors and the same number of directional sector antennas is deployed at the BS. The sectored antenna uses one fixed beam in a sector as shown in Fig. 2.1. Signals are transmitted and received through the beam covering only one sector other than the whole cell when using an omnidirectional antenna. In this way, the uplink and downlink co-channel interference is mostly limited to one sector and the effect of co-channel interference on system performance is reduced. This leads to an increase in cell capacity and a reduction in the transmitted power at the BSs and MSs. If the radiation pattern of a sector is ideal

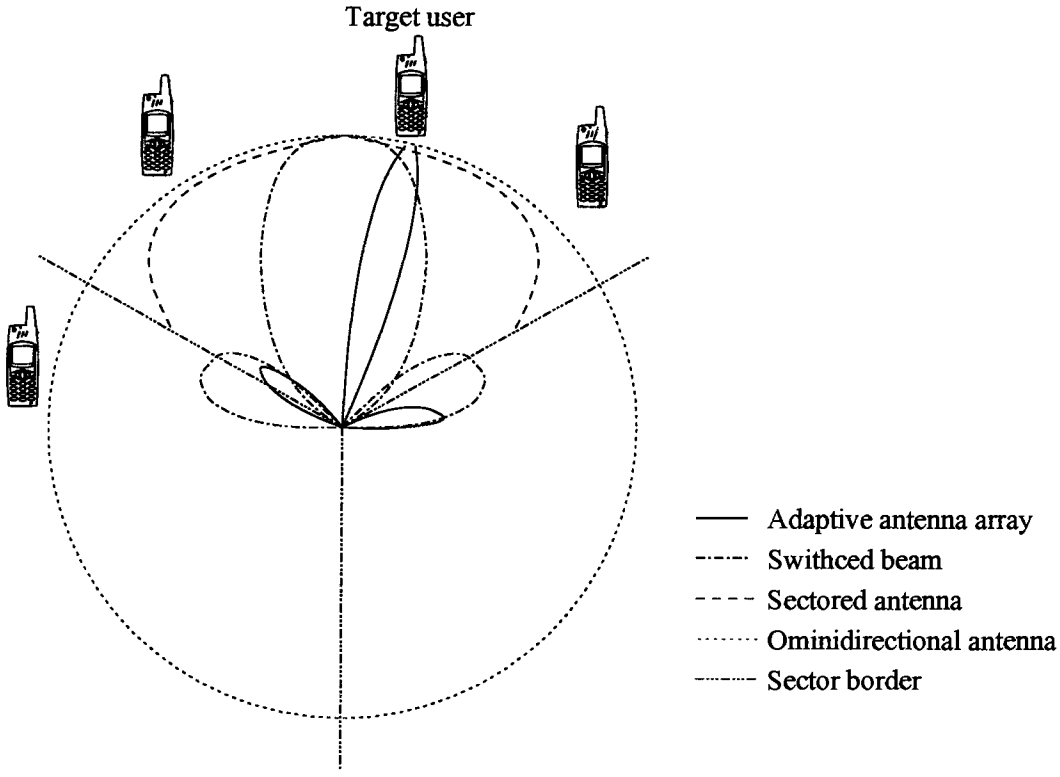

Figure 2.1. *Beam patterns of different antenna systems.*

without overlapping, then a cell with N sectored antennas should have approximately N times more capacity than a cell with an omnidirectional antenna.

A switched-beam antenna forms several fixed narrow beams. Although they cannot be steered to follow an MS, the best beam that leads to the highest SINR is selected to communicate with it. This further reduces the effect of co-channel interference relative to the sectored antenna systems. It has been shown in [59] that in general downlink interference can be reduced by approximately 6 dB by installing an eight-beam antenna system in a 120° sector configuration.

In contrast to an omnidirectional antenna, or a sectored antenna, or a switched beam antenna, an adaptive antenna array combines an antenna array and a digital signal processor to receive and transmit signals in a directional manner. It tracks the movement of an MS and the change of the radio environment, dynamically adjusts a narrow beam towards the MS, and at the same time minimizes the power of co-channel interference. In the uplink, a beam can be steered towards a direction such that the received power of the SOI at BS is maximized and the power of co-channel interference from other MSs is minimized. In the downlink, a beam pattern at the BS is chosen so as to maximize the signal power received at the target MS and at the same time to minimize the power at the other MSs. Using an adaptive antenna array, both the transmitter and receiver are power efficient and, most importantly, the co-channel interference to other MSs and BSs is reduced. As a result, system capacity, frequency efficiency, and coverage will be significantly improved [60].

2.4 Antenna Response Vector

An antenna array consists of a number of antenna elements which are distributed in a certain pattern. In order to simplify the analysis of antenna arrays, a simple antenna array model will be considered in the following chapters. It is assumed that there is no mutual coupling between antenna elements and that the signal amplitude remains

unchanged when received at different antenna elements due to the small element spacing. Bandlimited signals where the signal bandwidth is much smaller than the carrier frequency are also assumed. Based on the above assumptions, the antenna-array response vector of an M-element antenna array with arbitrary configuration is given by

$$\mathbf{a}(\theta,\psi) = \begin{bmatrix} A_1(f_c) \\ A_2(f_c)e^{-j2\pi f_c \tau_2(\theta,\psi)} \\ \vdots \\ A_M(f_c)e^{-j2\pi f_c \tau_M(\theta,\psi)} \end{bmatrix} \tag{2.5}$$

where $A_m(f_c)$ represents the amplitude response at the mth antenna element for the carrier which has frequency f_c, τ_m is the delay of the signal impinging on the mth antenna element relative to that on the first antenna element which is the reference one, and θ and ψ are the azimuth and elevation angles, respectively.

After down-converting to baseband, the signal received from an M-element arbitrary antenna array for a single signal source can be represented by the M-dimension vector as

$$\mathbf{u}(t) = s(t)\mathbf{a}(\theta,\psi) + \mathbf{n}(t) \tag{2.6}$$

where $s(t)$ and $\mathbf{n}(t)$ represent the signal of interest and the background noise, respectively.

Consider an M-element uniform linear antenna array (ULA) along the x axis with isotropic antenna element spacing of D as illustrated in Fig. 2.2. If we assume that a plane wave, i.e., $\psi = 0$, carrying a baseband signal arrives at the ULA in the horizontal plane at an azimuth angle θ, the delay of the signal received at the mth antenna element is given by

$$\tau_m(\theta,0) = \tau_m(\theta) = \frac{(m-1)D\sin\theta}{c} \tag{2.7}$$

where c is the speed of light. Since all the elements are isotropic and have the same amplitude response, without loss of the generality, we can assume that $A_m(f_c) = 1$

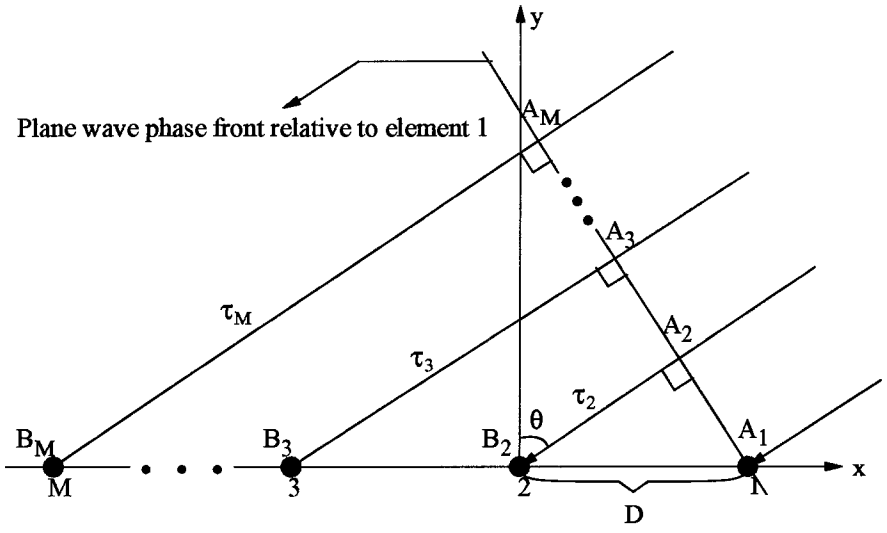

Figure 2.2. *Inter-element signal delay of an uniform linear antenna array.*

for $m = 1, 2, \ldots, M$. The antenna response vector in (2.5) is then simplified as

$$\mathbf{a}(\theta) = [1 \; z(\theta) \; \cdots \; z(\theta)^{M-1}]^T \tag{2.8}$$

where $z(\theta) = e^{-j2\pi D \sin\theta/\lambda_c}$ and λ_c is the carrier wavelength.

2.5 Uplink Beamforming

In the uplink of wireless communication systems, the signal arriving at the antenna array at the BS consists of the signal components from the target MS through multiple paths and co-channel interference from MSs other than the target one. As discussed in Sec. 1.1, the effect of co-channel interference can be reduced through the use of uplink beamforming. In this section, a number of existing uplink SUB and MUB algorithms for wireless communication systems will be discussed.

2.5.1 Uplink Signal Model

Consider an M-element antenna array deployed at a BS and assume that there are L_k paths for the kth MS. After down-converting to baseband, the received signal $\mathbf{x}_{k,l}$ corresponding to the lth path of MS k is given by

$$\mathbf{x}_{k,l}(t) = \sqrt{p_k}\beta_{k,l}s_k(t - \tau_{k,l})\mathbf{a}(\theta_{k,l}) \tag{2.9}$$

where p_k is the transmitted power by the kth MS, $\beta_{k,l}$ is the complex channel response for the lth path, $s_k(t)$ is the normalized transmitted signal, $\tau_{k,l}$ is the path delay, $\theta_{k,l}$ is the DOA of the lth path of MS k, and $\mathbf{a}(\theta_{k,l})$ is the antenna-array response vector. If the number of MSs in a BS service area is K, the received signal at the antenna array can be represented by the M-dimensional vector

$$\mathbf{x}(t) = \sum_{k=1}^{K}\sum_{l=1}^{L_k}\mathbf{x}_{k,l}(t) + \mathbf{n}(t) \tag{2.10}$$

where $\mathbf{n}(t)$ is a M-dimensional complex noise vector with zero mean and covariance

$$E[\mathbf{n}(t_1)\mathbf{n}(t_2)] = \sigma_n^2\delta(t_1 - t_2)\mathbf{I}. \tag{2.11}$$

Given the SOI $\mathbf{x}_{u,v}(t)$ from path v of MS u, the multiple-access interference (MAI) consists of the signal from other paths and other MSs, and the received signal in (2.10) may be rewritten as

$$\mathbf{x}(t) = \mathbf{x}_{u,v}(t) + \mathbf{x}_I(t) \tag{2.12}$$

where

$$\mathbf{x}_I(t) = \sum_{\substack{l=1 \\ l\neq v}}^{L_u}\mathbf{x}_{u,l}(t) + \sum_{\substack{k=1 \\ k\neq u}}^{K}\sum_{l=1}^{L_k}\mathbf{x}_{k,l}(t) + \mathbf{n}(t) \tag{2.13}$$

denotes the interference plus noise.

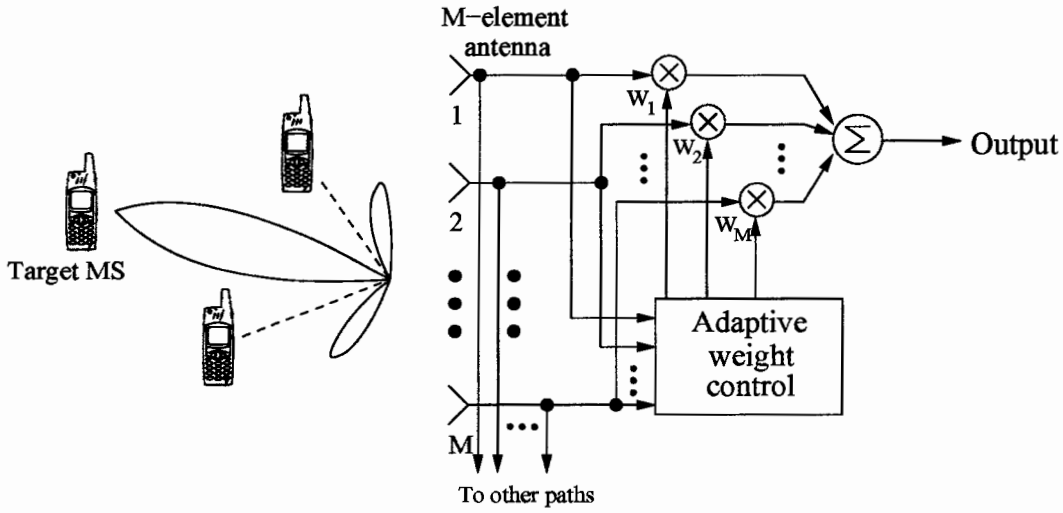

Figure 2.3. *Uplink per-path-per-beamformer SUB.*

2.5.2 Uplink Single-User Beamforming

In the uplink of a mobile communication system, the SOI arriving at the antenna array at the BS rarely has the same DOA as the interfering components and thus the SOI can be spatially resolved from the received signal by passing it and rejecting the interference at the beamformer. This can be achieved by choosing beamforming weights to obtain a high antenna-array gain in the direction of the SOI and a low gain in the directions of the interfering components.

The block diagram of a typical uplink per-path-per-beamformer SUB system is illustrated in Fig. 2.3. The down-converted baseband signals from different antenna elements are optimally combined using the beamforming weights to form a main beam towards the target MS and nulls towards other MSs.

Different criteria have been proposed in the past for the estimation of the beamforming weights.

Maximum Signal-to-Interference-plus-Noise Ratio

One commonly used optimality criterion for uplink beamforming at the BS is to

choose weight vector so as to maximize the SINR at the output of the beamformer [27][28]. If $\mathbf{w}_{u,v}$ denotes the BS weight vector for the SOI arriving from path v of MS u, the maximum SINR optimality criterion is given by

$$\underset{\mathbf{w}_{u,v}}{\text{minimize}} \frac{\mathbf{w}_{u,v}^H \mathbf{R}_{u,v} \mathbf{w}_{u,v}}{\mathbf{w}_{u,v}^H \mathbf{R}_I \mathbf{w}_{u,v}} \tag{2.14}$$

where

$$\mathbf{R}_{u,v} = \mathbf{x}_{u,v} \mathbf{x}_{u,v}^H \tag{2.15}$$

and

$$\mathbf{R}_I = \mathbf{x}_I \mathbf{x}_I^H \tag{2.16}$$

are the correlation matrices of the SOI and the interference plus noise, respectively. The optimum weight vector of a maximum SINR beamformer can be readily derived as

$$\mathbf{w}_{u,v}^{SINR} = \zeta \mathbf{R}_I^{-1} \mathbf{a}_{u,v} \tag{2.17}$$

where ζ can be any nonzero constant.

Minimum Mean-Squared Error

In [26], beamforming weights are chosen to minimize the mean-squared error (MSE) between the signal at the beamformer output and the reference signal, i.e.,

$$\underset{\mathbf{w}_{u,v}}{\text{minimize}} \; E\left[\| \mathbf{x}^H(t) \mathbf{w}_{u,v} - r_u(t) \|^2 \right] \tag{2.18}$$

where $E[\cdot]$ represents the expectation of $[\cdot]$ and r_u is the reference signal which can be a pilot signal, a decision-directed signal, or an estimate of the desired signal. The optimum weight vector of an MMSE beamformer can be obtained in closed-form [34] as

$$\mathbf{w}_{u,v}^{MMSE} = \frac{E(r_u^2)}{1 + E(r_u^2) \mathbf{a}_{u,v}^H \mathbf{R}_I^{-1} \mathbf{a}_{u,v}} \mathbf{R}_I^{-1} \mathbf{a}_{u,v}. \tag{2.19}$$

Minimum-Variance Distortionless response

The minimum-variance distortionless response (MVDR) beamformer [63] can be used in applications where the DOA of the SOI is known at the receiver. The weight vector for an MVDR beamformer is chosen such that the signal power at the beamformer output is minimized and simultaneously the amplitude and phase responses of the beamformer in the direction of the SOI satisfy the condition $\mathbf{w}_{u,v}^H \mathbf{a}_{u,v} = 1$. The optimization problem is formulated as

$$\begin{aligned} \underset{\mathbf{w}_{u,v}}{\text{minimize}} \quad & \mathbf{w}_{u,v}^H \mathbf{R} \mathbf{w}_{u,v} \\ \text{subject to} \quad & \mathbf{w}_{u,v}^H \mathbf{a}_{u,v} = 1 \end{aligned} \tag{2.20}$$

and its optimum solution can be obtained as

$$\mathbf{w}_{u,v}^{MV} = \frac{1}{\mathbf{a}_{u,v}^H \mathbf{R}_I^{-1} \mathbf{a}_{u,v}} \mathbf{R}_I^{-1} \mathbf{a}_{u,v}. \tag{2.21}$$

Many algorithms have been developed to adaptively update the weight vector based on the above optimality criterion. Among them, the least mean square (LMS) algorithm and the recursive least square (RLS) algorithm, and the sample matrix inversion (SMI) algorithm are the commonly used algorithms. A performance analysis of these beamforming algorithms can be found in [8].

2.5.3 Uplink Mutiuser Beamforming

In the uplink of a wireless communication system, MUB is formulated as an optimization problem where the weight vectors at the BS for different MSs are jointly optimized so as to satisfy given SINR specifications at the BS and, at the same time, the total power transmitted from all the MSs in the service area is minimized. If $\mathbf{w}_k$ is the BS weight vector for MS k, the uplink MUB can be formulated as the

optimization problem

$$\begin{aligned} &\underset{\mathbf{p},\mathbf{w}}{\text{minimize}} \sum_{k=1}^{K} p_k \\ \text{subject to } &\frac{p_k \mathbf{w}_k^H \mathbf{R}_k \mathbf{w}_k}{\sum_{\substack{j=1 \\ j\neq k}}^{K} p_j \mathbf{w}_k^H \mathbf{R}_j \mathbf{w}_k + \sigma^2 \mathbf{w}_k^H \mathbf{w}_k} \geq \gamma_k \\ &\text{for } k = 1,\ 2,\ \ldots,\ K \end{aligned} \tag{2.22}$$

where $\mathbf{p} = (p_1\ p_2\ \cdots\ p_K)^T$ is the transmitted power vector, and σ^2 is the noise variance at the BS, γ_k is the required minimum SINR for the uplink signal received from MS k, and correlation matrix $\mathbf{R}_k$ of the signal from MS k is given by

$$\mathbf{R}_k = \sum_{l=1}^{L_k} E[|\beta_{k,l}|^2]\mathbf{a}(\theta_{k,l})\mathbf{a}^H(\theta_{k,l}). \tag{2.23}$$

It can be shown that all the constraints in (2.22) must be active at the optimum solution [61], thus the inequality in (2.22) can be replaced by an equality. The constraints in (2.22) can be written in matrix form as

$$\mathbf{p} = \mathbf{D}_w \mathbf{F}_w \mathbf{p} + \mathbf{u}_w$$

where

$$\mathbf{D}_w = \text{diag}\left[\frac{\gamma_1}{\mathbf{w}_1^H \mathbf{R}_1 \mathbf{w}_1}\ \frac{\gamma_2}{\mathbf{w}_2^H \mathbf{R}_2 \mathbf{w}_2}\ \cdots\ \frac{\gamma_K}{\mathbf{w}_K^H \mathbf{R}_k \mathbf{w}_K}\right] \tag{2.24}$$

$$[\mathbf{F}_w]_{ij} = \begin{cases} = 0 & \text{for } j = i \\ = \mathbf{w}_i^H \mathbf{R}_j \mathbf{w}_i & \text{for } j \neq i \end{cases} \tag{2.25}$$

$$\mathbf{u}_w = \left[\frac{\gamma_1 \|\mathbf{w}_1\|^2}{\mathbf{w}_1^H \mathbf{R}_1 \mathbf{w}_1}\ \frac{\gamma_2 \|\mathbf{w}_2\|^2}{\mathbf{w}_2^H \mathbf{R}_2 \mathbf{w}_2}\ \cdots\ \frac{\gamma_K \|\mathbf{w}_K\|^2}{\mathbf{w}_K^H \mathbf{R}_K \mathbf{w}_K}\right]^T. \tag{2.26}$$

Based on the observation that for a given transmitted power vector, the optimum solution of the BS weight vector for an MS is the one that maximizes the SINR, an iterative algorithm was developed in [44] to solve the optimization problem in (2.22). It has been shown that using this iterative algorithm, the sequence $(\mathbf{p}^n)$ and $(\mathbf{w}_k^n)$ for $n = 1,\ 2,\ \ldots,\ N$ produced will converge to the optimum solution starting from an arbitrary initial power vector $\mathbf{p}^0$. This algorithm is summarized as follows.

Iterative Algorithm for Uplink Multisuer Beamforming

Step 1: Initialize power vector $\mathbf{p}^0$.

Step 2: Compute the weight vector

$$\mathbf{w}_k^n = \arg\max_{\mathbf{w}_k} \frac{p_k \mathbf{w}_k^H \mathbf{R}_k \mathbf{w}_k}{\sum_{\substack{j=1 \\ j\neq k}}^{K} p_j \mathbf{w}_k^H \mathbf{R}_j \mathbf{w}_k + \sigma^2 \mathbf{w}_k^H \mathbf{w}_k}.$$

for $k = 1,\ 2,\ \ldots,\ K$.

Step 3: Update $\mathbf{D}_w(n)$, $\mathbf{F}_w(n)$, and $\mathbf{u}_w(n)$ using (2.24), (2.25), and (2.26), respectively.

Step 4: Update the uplink power vector

$$\mathbf{p}^{n+1} = \mathbf{D}_w(n)\mathbf{F}(n)\mathbf{p}^n + \mathbf{u}_w(n).$$

Step 5: If the sequence of power vectors $\{\mathbf{p}^n\}$ converges, output solutions $\mathbf{p} = \mathbf{p}^n$ and $\mathbf{w}_k = \mathbf{w}_k^n$ for $k = 1,\ 2,\ \ldots,\ K$, and stop. Otherwise, set $n = n + 1$ and repeat from Step 2.

2.6 Downlink Beamforming

In the downlink of wireless communication systems, the signal transmitted to the target MS through BS antenna array will be received by other MSs that share the same frequency channel in the service area, which leads to co-channel interference. The effect of co-channel interference on system performance can be reduced through the use of downlink beamforming. In this section, a number of existing downlink SUB and MUB algorithms for wireless communication systems will be discussed.

2.6.1 Downlink Signal Model

After down-converting to baseband, the downlink signal $x_{k,l}^s(t)$ received from the lth path at MS k is given by

$$x_{k,l}^s(t) = \beta_{k,l}\sqrt{\tilde{p}_k} s_k(t - \tau_{k,l})\mathbf{a}^H(\theta_{k,l})\mathbf{w}_k \tag{2.27}$$

where $\beta_{k,l}$ is the complex channel response for the lth path of MS k, $\tilde{p}_k$ is the BS transmitted power for the downlink signal to MS k, $s_k(t)$ is the normalized transmitted signal to MS k, $\tau_{k,l}$ is the path delay, $\mathbf{w}_k$ is the BS beamforming weight vector of MS k, $\theta_{k,l}$ is the direction of departure of the lth path from the BS antenna array to MS k, and $\mathbf{a}(\theta_{k,l})$ is the M-dimension BS antenna-array response vector.

The co-channel interference $x_{k,l}^{I_i}(t)$ received through the lth path at the target MS k caused by the downlink signal to MS i can be represented by

$$x_{k,l}^{I_i}(t) = \beta_{k,l}\sqrt{\tilde{p}_i}s_i(t-\tau_{k,l})\mathbf{a}^H(\theta_{k,l})\mathbf{w}_i. \tag{2.28}$$

The received signal at MS k consists of the desired downlink signal and the co-channel interference caused by the downlink signals to other MSs. If the number of MSs in a BS service area is K and the number of dominant paths from the BS to MS k is L_k, then the received signal at MS k can be represented by

$$x_k(t) = \sum_{l=1}^{L_k} x_{k,l}^{s}(t) + \sum_{\substack{i=1 \\ i\neq k}}^{K}\sum_{l=1}^{L_k} x_{k,l}^{I_i}(t) + n_k(t) \tag{2.29}$$

where $n_k(t)$ is the noise which is assumed to have zero mean and covariance σ_k^2.

2.6.2 Downlink Single-User Beamforming

In the downlink of a mobile communication system, the goal of SUB is to concentrate the transmitted power in the direction of the target MS and reduce it in the direction of other MSs.

The block diagram of a downlink per-user-per-beamformer SUB system is illustrated in Fig. 2.4. Signal s_u to the target MS u is first split into M signal components corresponding to M antenna elements. The M signal components are then weighted by the beamforming weights which determine the beam pattern of the antenna array at BS. Finally, the weighted signal components are transmitted from their corresponding antenna element.

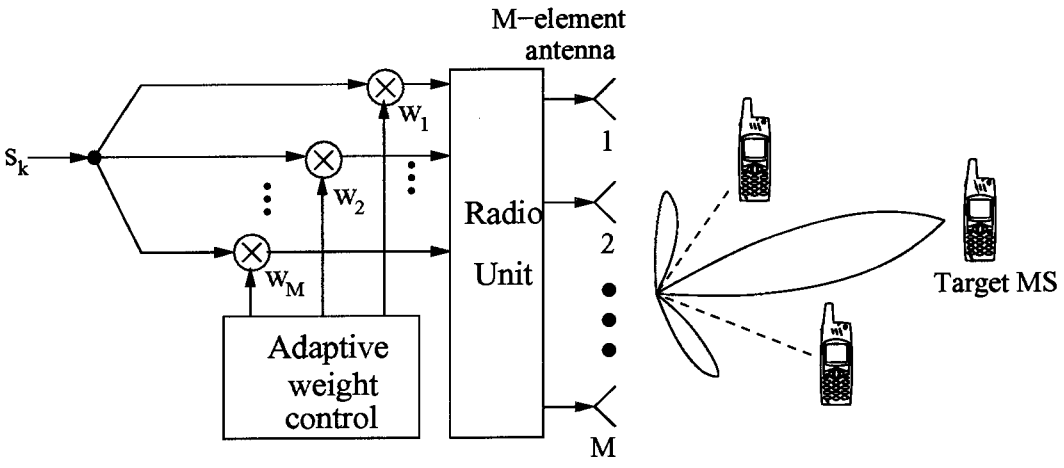

Figure 2.4. *Downlink per-user-per-beamformer SUB.*

As discussed in Sec. 1.1.2, conventional generalized eigenvalue-based beamforming algorithms for the downlink lead to the same beam pattern and, therefore, the same normalized weight vector $\hat{\mathbf{w}}_u$ which has unit norm is obtained. If the number of signal paths to target MS u is L_u and the channel gain $|\beta_{u,l}|$ for lth path is known at the transmitter, $\hat{\mathbf{w}}_u$ can be determined by solving the optimization problem

$$\underset{\hat{\mathbf{w}}_u}{\text{maximize}} \frac{\hat{\mathbf{w}}_u^H \left(\sum_{l=1}^{L_u} \mathbf{R}_{u,l} \right) \hat{\mathbf{w}}_u}{\hat{\mathbf{w}}_u^H \left(\sum_{\substack{k=1 \\ k \neq u}}^{K} \sum_{l=1}^{L_k} \mathbf{R}_{k,l} + \sigma^2 \mathbf{I} \right) \hat{\mathbf{w}}_u} \tag{2.30}$$

where $\sigma^2\mathbf{I}$ is introduced to increase the algorithm robustness to channel uncertainties [35], and

$$\begin{aligned} \mathbf{R}_{u,l} &= E[|\beta_{u,l}|^2] \mathbf{a}_{u,l} \mathbf{a}_{u,l}^H \\ \mathbf{R}_{k,l} &= E[|\beta_{k,l}|^2] \mathbf{a}_{k,l} \mathbf{a}_{k,l}^H \end{aligned} \tag{2.31}$$

are the spatial correlation matrices. The optimum solution of the normalized eigenvector in (2.30) is the eigenvector associated with the largest eigenvalue of the generalized

eigenvalue problem [22] given by

$$\left(\sum_{l=1}^{L_u}\mathbf{R}_{u,l}\right)\hat{\mathbf{w}}_u = \lambda_{max}\left(\sum_{\substack{k=1\\k\neq u}}^{K}\sum_{l=1}^{L_k}\mathbf{R}_{k,l}+\sigma^2\mathbf{I}\right)\hat{\mathbf{w}}_u. \tag{2.32}$$

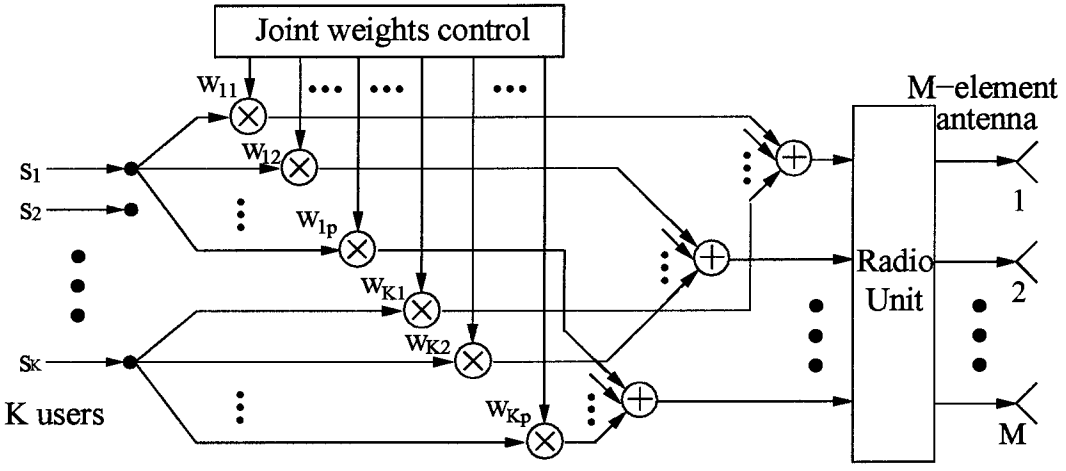

Figure 2.5. *Block diagram of downlink MUB at BS.*

2.6.3 Downlink Mutiuser Beamforming

In the downlink of a wireless communication system, the optimum downlink weight vectors can be determined by minimizing the total power transmitted from the BS such that a given SINR specification at each MS is achieved. Consider the MUB system illustrated in Fig. 2.5 where a M-element antenna array is deployed at the BS and an omnidirectional antenna with unit gain is deployed at each MS. Signal s_k to MS k is first split into M signals corresponding to p antenna elements which are then weighted by the beamforming weights. The beamforming weights corresponding to different MSs, which determine the BS radiation pattern and downlink signal power, are jointly computed based on the channel information obtained. Then the weighted

signal components to different MSs are combined branch by branch and transmitted from each antenna element.

The downlink MUB problem can be formulated as the optimization problem

$$\begin{aligned} &\underset{\tilde{\mathbf{p}},\mathbf{w}}{\text{minimize}} \sum_{k=1}^{K} [\tilde{p}_k \mathbf{w}_k^H \mathbf{w}_k] \\ &\text{subject to } \frac{\tilde{p}_k \mathbf{w}_k^H \mathbf{R}_k \mathbf{w}_k}{\sum_{\substack{j=1 \\ j\neq k}}^{K} \tilde{p}_j \mathbf{w}_j^H \mathbf{R}_k \mathbf{w}_j + \sigma_k^2} \geq \gamma_k \\ &\text{for } k = 1,\ 2,\ \ldots,\ K \end{aligned} \tag{2.33}$$

where

$$\mathbf{R}_k = \sum_{l=1}^{L_k} E[|\beta_{k,l}|^2] \mathbf{a}(\theta_{k,l}) \mathbf{a}^H(\theta_{k,l}). \tag{2.34}$$

is the correlation matrix of the downlink signal to MS k, $\tilde{\mathbf{p}} = [\tilde{p}_1\ \tilde{p}_2\ \cdots\ \tilde{p}_K]^T$ is the downlink transmitted power vector, σ_k^2 and γ_k are the noise variance and the required minimum SINR at MS k, respectively.

In the downlink, signal correlation matrix $\mathbf{R}_k$, for $k = 1,\ 2,\ \ldots,\ K$, needs to be estimated in order to solve the MUB problem. In the case of TDD systems where the uplink and downlink channel are reciprocal, $\mathbf{R}_k$ can be obtained through uplink channel estimation [41]. In the case of FDD systems where the frequency channels used in the downlink and uplink are different, $\mathbf{R}_k$ can be estimated via feedback signaling [42][43]. Based on the estimated $\mathbf{R}_k$, two classes of algorithms have been developed to solve the optimization problem in (2.33), namely, duality-based [41][42] and semidefinte programming (SDP) based [45]-[47] MUB algorithms.

2.6.3.1 Duality-Based Downlink Mutiuser Beamforming

The duality between the uplink MUB and downlink MUB was originally presented and discussed in [41]. It has been shown that the optimal downlink weight vectors can be obtained through the use of a virtual uplink. Based on this duality, an optimal MUB algorithm [41] has been developed to iteratively obtain the optimal downlink weight

vectors. As in the uplink MUB optimization problem, all the constraints in (2.33) must be active at the optimum solution. The minimum downlink BS transmitted power is achieved when the SINR is equal to the minimum SINR. Thus, the constraints in (2.33) can be written in matrix form as

$$\tilde{\mathbf{p}} = \mathbf{D}_w(\mathbf{F}_w)^T\tilde{\mathbf{p}} + \tilde{\mathbf{u}}_w \tag{2.35}$$

where $\tilde{\mathbf{u}}_w$ is defined as

$$\tilde{\mathbf{u}}_w = \left[\frac{\gamma_1 N_1}{\mathbf{w}_1{}^H\mathbf{R}_1\mathbf{w}_1} \quad \frac{\gamma_2 N_2}{\mathbf{w}_2{}^H\mathbf{R}_2\mathbf{w}_2} \quad \cdots \quad \frac{\gamma_K \sigma_k^2}{\mathbf{w}_K{}^H\mathbf{R}_K\mathbf{w}_K}\right]^T. \tag{2.36}$$

Considering one BS in a service area, the iterative algorithm for the downlink MUB is summarized as follows.

Iterative Algorithm for Downlink Multisuer Beamforming

Step 1: Initialize virtual uplink power vector $\mathbf{p}^0$ and downlink power vector $\tilde{\mathbf{p}}^0$.

Step 2: Compute the virtual uplink weight vector

$$\mathbf{w}_k^n = \arg\max_{\mathbf{w}_k} \frac{p_k\mathbf{w}_k^H\mathbf{R}_k\mathbf{w}_k}{\sum_{\substack{j=1\\ j\neq k}}^{K} p_j\mathbf{w}_k^H\mathbf{R}_j\mathbf{w}_k + \sigma^2\mathbf{w}_k^H\mathbf{w}_k}$$

for $k = 1, 2, \ldots, K$.

Step 3: Update $\mathbf{D}_w(n)$, $\mathbf{F}_w(n)$, $\mathbf{u}_w(n)$, and $\tilde{\mathbf{u}}_w(n)$ using (2.24), (2.25), (2.26), and (2.36), respectively.

Step 4: Update virtual uplink power vector

$$\mathbf{p}^{n+1} = \mathbf{D}_w(n)\mathbf{F}(n)\mathbf{p}^n + \mathbf{u}_w(n). \tag{2.37}$$

Step 5: Update downlink power vector

$$\tilde{\mathbf{p}}^{n+1} = \mathbf{D}_w(n)\mathbf{F}^T(n)\tilde{\mathbf{p}}^n + \tilde{\mathbf{u}}_w(n). \tag{2.38}$$

Step 6: If the sequence of downlink power vector $\{\tilde{\mathbf{p}}^n\}$ converges, output solutions $\tilde{\mathbf{p}} = \tilde{\mathbf{p}}^n$ and $\mathbf{w}_k = \mathbf{w}_k^n$ for $k = 1, 2, \ldots, K$, and stop. Otherwise, set $n = n + 1$ and repeat from Step 2.

2.6.3.2 SDP-Based Downlink Mutiuser Beamforming

The SDP-based MUB algorithm can be found in [45]-[47] where the optimal MUB optimization problem is relaxed into an SDP optimization problem after Lagrangian relaxation [50]. The weight vectors are then obtained from the optimal solution of the SDP problem.

For simplicity, but without loss of generality, the BS transmitted power p_k can be merged with the BS weight vector $\mathbf{w}_k$ for $k = 1,\ 2,\ \ldots,\ K$. The optimization problem in (2.33) can be rewritten as

$$\begin{aligned} &\underset{\mathbf{w}}{\text{minimize}} \sum_{k=1}^{K} \left[\mathbf{w}_k^H \mathbf{w}_k\right] \\ &\text{subject to } \frac{\mathbf{w}_k^H \mathbf{R}_k \mathbf{w}_k}{\sum_{\substack{j=1 \\ j\neq k}}^{K} \mathbf{w}_j^H \mathbf{R}_k \mathbf{w}_j + \sigma_k^2} \geq \gamma_k \\ &\text{for } k = 1,\ 2,\ \ldots,\ K. \end{aligned} \tag{2.39}$$

If we define $\mathbf{W} = \mathbf{w}_k \mathbf{w}_k^H$ and let tr[·] denote the trace of a matrix. After relaxing the constraint $\text{rank}(\mathbf{W}_k) = 1$ for $k = 1,\ 2,\ \ldots,\ K$, the optimization problem in (2.39) can be reformulated as the SDP optimization problem

$$\begin{aligned} &\min_{\mathbf{W}} \sum_{k=1}^{K} \text{tr}\left[\mathbf{W}_k\right] \\ &\text{subject to } \text{tr}\left[\mathbf{R}_k \mathbf{W}_k\right] - \gamma_k \sum_{\substack{j=1 \\ j\neq k}}^{K} \text{tr}\left[\mathbf{R}_k \mathbf{W}_j\right] - \sigma_k^2 \gamma_k \geq 0 \\ &\mathbf{W}_k = \mathbf{W}_k^H \\ &\mathbf{W}_k \succeq 0 \\ &\text{for } k = 1,\ 2,\ \ldots,\ K. \end{aligned} \tag{2.40}$$

Based on the solution $\mathbf{W}_k$ for $k = 1,\ 2,\ \ldots,\ K$ of the optimization problem in (2.40), $\mathbf{w}_k$ can be calculated as

$$\mathbf{w}_k = \sqrt{\mu_k}\mathbf{q}_k \quad \text{for } k = 1,\ 2,\ \ldots,\ K \tag{2.41}$$

where $\mathbf{q}_k$ is the eigenvector associated with the nonzero eigenvalue μ_k of matrix $\mathbf{W}_k$.

The solution of the SDP problem after the Lagrangian relaxation in (2.40) cannot guarantee the constraint $\text{rank}(\mathbf{W}_k) = 1$ for $k = 1, 2, \ldots, K$ being satisfied and, therefore, it may not lead to an optimum solution to the original MUB problem in (2.39). However, in practice, these degenerate cases almost never occur and if the algorithm gives a high rank solution, a small perturbation can be added to the correlation matrixes which will make the problem have a rank one solution [62].

2.7 Conclusion

The background knowledge, concepts, and terminology that are necessary for the development of new beamforming and DOA estimation techniques in the following chapters have been reviewed. Specifically, the basic models of antenna arrays have been introduced and several important beamforming techniques using antenna arrays, i.e., the SUB and the MUB for the uplink and downlink in wireless communication systems, have been described.

Chapter 3

Analysis of Uplink Beamformer Configurations for DS-CDMA Systems

3.1 Introduction

In the uplink of DS-CDMA communication systems, the receiver consists of a beamformer, a DSP unit that adjusts the beamforming weights, and matched filters. Two different types of beamformer configurations have been studied, the CB and SB configurations as shown in Figs. 3.2(a) and (b), respectively. In the CB configuration [64]-[68], the beamforming weights are adjusted based on the signal before despreading whereas in the SB configuration [26][31][69][70] they are adjusted after despreading. This difference leads to different beam patterns even though the same optimality criterion is applied to the output signal. The performance of various beamforming schemes has been extensively analyzed and discussed in the past [24][31][32][33]. However, most of the work has been done for the beamformer alone independently of the CDMA system the beamformer is part of. As a result, the difference due to the beamformer configuration has not been clearly understood nor has the effect of code diversity on the performance of the beamformer been discussed before.

In this chapter, the performance of the CB and SB configurations is investigated

based on theoretical analysis and the results are confirmed with simulations. It is shown that the SB configuration offers a better performance with respect to MMSE and SINR than the CB configuration but the improvement comes with an increased hardware complexity relative to that of the CB configuration.

The organization of the chapter is as follows: in Sec. 3.2, the signal model considered is described. The performance achieved using the CB and SB configurations is analyzed and compared with respect to SINR and MMSE in Sec. 3.3. A discussion and conceptual explanation of the difference in the performance of CB and SB configurations are presented in Sec. 3.4. In Sec. 3.5, numerical results obtained through simulations for both asynchronous and synchronous DS-CDMA systems are presented. Conclusions are drawn in Sec. 3.6.

3.2 System Model

Previous work has shown that an improvement of system performance in a multipath environment can be achieved by combining a set of beamformers and a RAKE combiner as in Fig. 3.1 [71]-[73]. Each beamformer and matched filter (BF-MF) unit in Fig. 3.1 uses either the CB configuration or the SB configuration. It resolves the dominant path of the desired signal. It consists of a beamformer and one or multiple symbol-rate matched filters. The beamformer is adapted to the antenna-array response and the symbol-rate MF (which can also be a code correlator) is matched to the path delay. The typical CB and SB configurations are shown in Fig. 3.2(a) and (b), respectively. In the CB configuration, the received signal components from different antenna elements are fed into a beamformer and are then passed through an MF. The beamforming weights are obtained by applying an optimization algorithm to the signal before despreading. In the SB configuration, a beamformer is cascaded with the MFs and the beamforming weights are determined using the despread signal components at the output of the MFs.

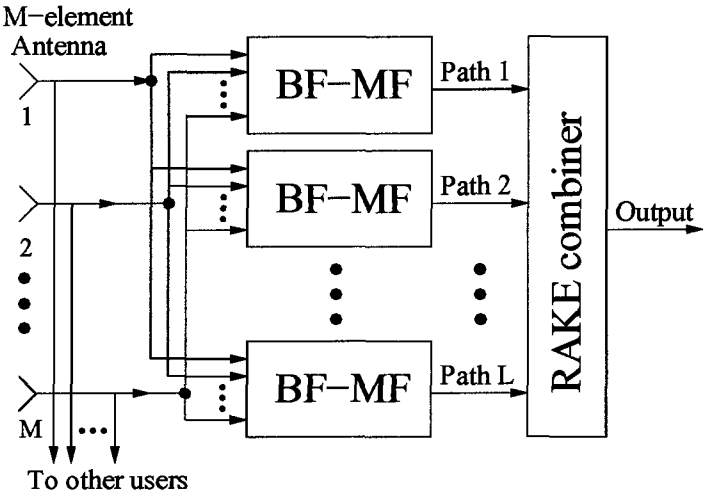

Figure 3.1. *Space-time RAKE receiver.*

Consider a DS-CDMA system deployed with an M-element antenna array at the BS. After down-converting to baseband, the received signal $\mathbf{x}_{k,l}$ in (2.9) corresponding to the lth path of MS k can be written as

$$\mathbf{x}_{k,l}(t) = \sqrt{p_k}\beta_{k,l}b_k(n)d_k(t - nT - \tau_{k,l})\mathbf{a}_{k,l} \tag{3.1}$$

where b_k is the transmitted information bit sequence, T is the symbol duration, $\tau_{k,l}$ is the delay of a resolvable path, which is assumed to be an integer multiple of the chip duration T_c, and $d_k(t)$ is the signature waveform of MS k given by

$$d_k(t) = \sum_{n=0}^{N-1} \mathbf{c}_k(n)g(t - nT_c). \tag{3.2}$$

In the above equation, $N = T/T_c$ is the processing gain, $\mathbf{c}_k(n)$ is the normalized spreading code sequence for MS k, and $g(t)$ is the chip pulse-shaping waveform. Without loss of generality, assume that all the signature waveforms assigned to different MSs are normalized so as to have unit energy, i.e.,

$$\int_0^T d_k^2(t)dt = 1. \tag{3.3}$$

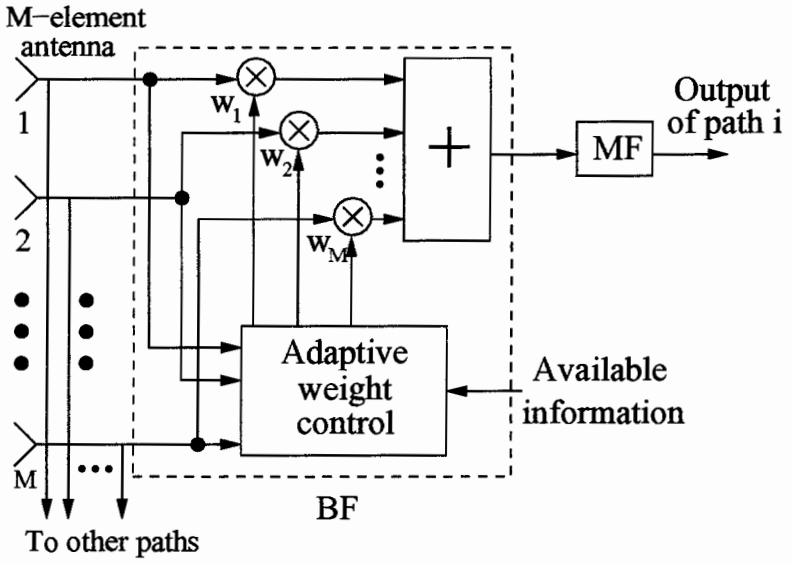

(a)

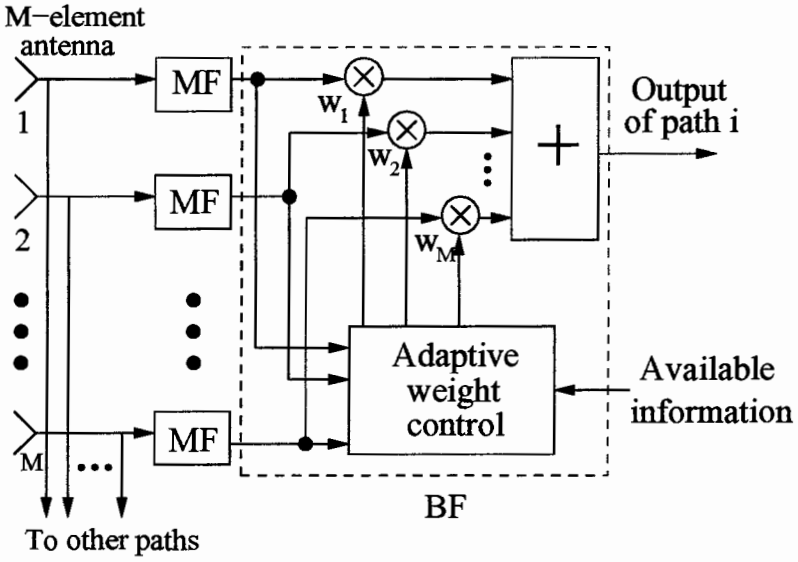

(b)

Figure 3.2. *(a) Chip-based configuration, (b) Symbol-based configuration.*

Assume that the SOI arrives through the vth path of MS u. Consider a signal component from the lth path of MS k. If this signal is asynchronous with the SOI, then during the symbol duration of the SOI, this signal will consist of parts of two symbols. In order to facilitate the analysis of the asynchronous CDMA systems, the asynchronous signal component from the lth path of MS k can be viewed as a signal from two fictitious MSs [74], namely, the left and right MSs k_1 and k_2, respectively. The spreading codes of the left and right MSs, denoted as $\mathbf{c}_{(k_1,l)}$ and $\mathbf{c}_{(k_2,l)}$, respectively, are given by

$$\mathbf{c}_{(k_1,l)} \begin{cases} = [\mathbf{c}_k(m+1)\ \mathbf{c}_k(m+2)\ \cdots\ \mathbf{c}_k(N-1-m)\ 0\ 0\ \cdots\ 0]^H & \text{for } \tau_{k,l} < \tau_{u,v} \\ = [\mathbf{c}_k(N-m)\ \mathbf{c}_k(N-m+1)\ \cdots\ \mathbf{c}_k(N-1)\ 0\ 0\ \cdots\ 0]^H & \text{for } \tau_{k,l} > \tau_{u,v} \end{cases}$$

and

$$\mathbf{c}_{(k_2,l)} \begin{cases} = [0\ 0\ \cdots\ 0\ \mathbf{c}_k(0)\ \mathbf{c}_k(1)\ \cdots\ \mathbf{c}_k(m-1)]^H & \text{for } \tau_{k,l} < \tau_{u,v} \\ = [0\ 0\ \cdots\ 0\ \mathbf{c}_k(0)\ \mathbf{c}_k(1)\ \cdots\ \mathbf{c}_k(N-m-1)]^H & \text{for } \tau_{k,l} > \tau_{u,v} \end{cases}$$

where

$$m = \frac{|\tau_{u,v} - \tau_{k,l}|}{T_c}$$

is the number of chips of the relative delay between the SOI and the signal from the lth path of MS k. Signal $\mathbf{x}_{k,l}$ can be expressed as

$$\mathbf{x}_{k,l}(t) \begin{cases} = \sqrt{p_k}\beta_{k,l}[b_k(n)d_{k_1}(t-nT) + b_k(n+1)d_{k_2}(t-nT)]\mathbf{a}_{k,l} & \text{for } \tau_{k,l} < \tau_{u,v} \\ = \sqrt{p_k}\beta_{k,l}[b_k(n-1)d_{k_1}(t-nT) + b_k(n)d_{k_2}(t-nT)]\mathbf{a}_{k,l} & \text{for } \tau_{k,l} > \tau_{u,v} \\ = \sqrt{p_k}\beta_{k,l}b_k(n)d_k(t-nT)\mathbf{a}_{k,l} & \text{for } \tau_{k,l} = \tau_{u,v} \end{cases}.$$

3.3 Analysis of Beamforming Configuration

3.3.1 Closed-Form Solution of Beamforming Weights

Several techniques have been proposed in the past to adaptively obtain the beamforming weights. The commonly used optimality criteria are MMSE, maximization of

SINR, ML, and MV. It has been shown in [30] and [34] that the closed-form solutions for the weight vectors $\mathbf{w}$ have the same form for the above criteria and are given by

$$\mathbf{w} = \delta \mathbf{w}^o \tag{3.4}$$

where scalar δ assumes different values for different criteria, and $\mathbf{w}^o$ is the optimum Wiener solution [63] which is also the MMSE solution. It can be seen from (3.4) that the same beam pattern can be obtained despite different values assigned to the scalar δ. Moreover, different values of δ lead to the same SINR at the beamformer output. The optimal weight vectors in terms of MMSE for the CB and SB configurations can be derived in closed form and will be used to evaluate the system performance.

A beamformer for DS-CDMA systems is said to be a CB MMSE beamformer if it operates on the received chip-rate signal and the weight vector is obtained by minimizing the mean-squared error (MSE) between the signal at the beamformer output and the reference signal. In [75], the weight vector $\mathbf{w}_{u,v}$ corresponding to the vth path of MS u is determined by solving the optimization problem

$$\underset{\mathbf{w}_{u,v}}{\text{minimize}}\ E\left[\| \mathbf{X}^H(nT)\mathbf{w}_{u,v} - \sqrt{p_u}\beta_{u,v}b_u(n)\mathbf{c}_u \|^2\right] \tag{3.5}$$

where b_u is the information bit transmitted, and $\mathbf{X}(nT)$ is a $p \times N$ matrix given by

$$\mathbf{X}(nT) = \begin{bmatrix} \mathbf{x}^H(nT + \tau_{u,v}) \\ \mathbf{x}^H(nT + T_c + \tau_{u,v}) \\ \vdots \\ \mathbf{x}^H(nT + (N-1)T_c + \tau_{u,v}) \end{bmatrix}^H .$$

In the above equation, N is the processing gain, and T_c is the chip duration. The optimization problem may also be formulated as [64][66]

$$\underset{\mathbf{w}_{u,v}}{\text{minimize}}\ E\left[| \mathbf{x}^H(nT + kT_c + \tau_{u,v})\mathbf{w}_{u,v} - r(kT_c) |^2\right] \tag{3.6}$$

where $k = 0,\ 1,\ \ldots,\ N-1$ and $r(kT_c) = \sqrt{p_u}\beta_{u,v}b_u(n)\mathbf{c}_u(k)$. The optimal weight vector $\mathbf{w}^c_{u,v}$ of (3.5) and (3.6) can be readily obtained in closed form [34] as

$$\mathbf{w}^c_{u,v} = \sigma^2_{u,v}\mathbf{R}_c^{-1}\mathbf{a}_{u,v} \tag{3.7}$$

where $\sigma_{u,v}^2 = E|\sqrt{p_u}\beta_{u,v}b_u(n)\mathbf{c}_u(k)|^2$ is the power of the SOI and

$$\mathbf{R}_c = E[\mathbf{x}\mathbf{x}^H] = \sigma_{u,v}^2\mathbf{a}_{u,v}\mathbf{a}_{u,v}^H + \mathbf{R}_{cI} \tag{3.8}$$

is the autocorrelation matrix of the received signal. $\mathbf{R}_{cI}$ is the correlation matrix of the unwanted signal given by

$$\mathbf{R}_{cI} = \sum_{\substack{l=1 \\ l\neq v}}^{L_u} \sigma_{u,l}^2\mathbf{a}_{u,l}\mathbf{a}_{u,l}^H + \sum_{\substack{k=1 \\ k\neq u}}^{K}\sum_{l=1}^{L_k} \sigma_{k,l}^2\mathbf{a}_{k,l}\mathbf{a}_{k,l}^H + \sigma_n^2\mathbf{I}. \tag{3.9}$$

Using the matrix-inversion lemma [63], (3.7) can be rewritten as

$$\mathbf{w}_{u,v}^c = \frac{\sigma_{u,v}^2}{1+\sigma_{u,v}^2\mathbf{a}_{u,v}^H{\mathbf{R}_{cI}}^{-1}\mathbf{a}_{u,v}}{\mathbf{R}_{cI}}^{-1}\mathbf{a}_{u,v}. \tag{3.10}$$

It can be seen from (3.9) that the higher power $\sigma_{k,l}^2$ of the interfering component from path l of MS k is, the more is its contribution to the correlation matrix $\mathbf{R}_{cI}$. As a consequence, more effort will be applied to reject it. In this light, the rejecting factor $f_{k,l}^c$ of the interference component from path l of MS k is defined as

$$f_{k,l}^c = \sigma_{k,l}^2. \tag{3.11}$$

Thus, different interfering components are rejected in terms of their received power using the CB configuration.

The SB MMSE beamformer developed in [26] and [69] aims at minimizing the MSE between the combined despread signal and the reference symbol signal. It involves solving the optimization problem

$$\underset{\mathbf{w}_{u,v}}{\text{minimize}}\ E\left[\left|\ {\mathbf{c}_u}^H\mathbf{X}^H(nT)\mathbf{w}_{u,v} - \sqrt{p_u}\beta_{u,v}b_u(n)\ \right|^2\right]. \tag{3.12}$$

Similarly, the Wiener solution $\mathbf{w}_{u,v}^s$ of (3.12) can be readily derived as

$$\mathbf{w}_{u,v}^s = N\sigma_{u,v}^2\mathbf{R}_s^{-1}\mathbf{a}_{u,v} \tag{3.13}$$

where

$$\begin{aligned}\mathbf{R}_s &= E[\mathbf{X}(nT)\mathbf{c}_u\mathbf{c}_u^H\mathbf{X}^H(nT)] \\ &= \sigma_{u,v}^2\rho_{(u,v)}^2\mathbf{a}_{u,v}\mathbf{a}_{u,v}^H + \mathbf{R}_{sI}\end{aligned} \tag{3.14}$$

and $\mathbf{R}_{sI}$ is the correlation matrix of the unwanted signal after passing through the MF. It is given by

$$\begin{aligned}\mathbf{R}_{sI} &= \sum_{\substack{l=1\\l\neq v}}^{L_u} \rho_{(u,l)}^2 \sigma_{u,l}^2 \mathbf{a}_{u,l}\mathbf{a}_{u,l}^H \\ &\quad + \sum_{\substack{k=1\\k\neq u}}^{K} \sum_{l=1}^{L_k} \rho_{(k,l)}^2 \sigma_{k,l}^2 \mathbf{a}_{k,l}\mathbf{a}_{k,l}^H + \sigma_n^2 \mathbf{I}\end{aligned} \tag{3.15}$$

where $\rho_{(k,l)}$ is the code correlation between the SOI and the signal component from the lth path of MS k, namely, the synchronous code correlation for $\tau_{u,v} = \tau_{k,l}$ or the asynchronous correlation for $\tau_{u,v} \neq \tau_{k,l}$. It is defined as

$$\rho_{(k,l)} \begin{cases} = \sqrt{|\mathbf{c}_u^H \mathbf{c}_{k_1,l}|^2 + |\mathbf{c}_u^H \mathbf{c}_{k_2,l}|^2} & \text{for } \tau_{u,v} \neq \tau_{k,l} \\ = |\mathbf{c}_u^H \mathbf{c}_k| & \text{for } \tau_{u,v} = \tau_{k,l} \end{cases} \tag{3.16}$$

and

$$\rho_{(k,l)}^2 \begin{cases} = 1 \quad \text{for } (k,l) = (u,v) \\ \ll 1 \quad \text{for } (k,l) \neq (u,v) \end{cases}.$$

By virtue of the matrix-inversion lemma, (3.13) can be rewritten as

$$\mathbf{w}_{u,v}^s = \frac{N\sigma_{u,v}^2}{1 + \sigma_{u,v}^2 \mathbf{a}_{u,v}^H \mathbf{R}_{sI}^{-1} \mathbf{a}_{u,v}} \mathbf{R}_{sI}^{-1} \mathbf{a}_{u,v}. \tag{3.17}$$

Keeping the definition of $f_{k,l}^c$ (3.11) in mind, it can be seen from (3.15) that for the SB beamformer, the rejecting factor is not only dependent on the power of an interfering component but also on its code correlation with the SOI. The rejecting factor $f_{k,l}^s$ of the interference component from the lth path of MS k can be defined as

$$f_{k,l}^s = \rho_{(k,l)}^2 \sigma_{k,l}^2. \tag{3.18}$$

Thus, more effort will be applied to reject the interfering components whose product of power and code correlation with the SOI is high.

3.3.2 Comparison with Respect to SINR

The CB beamformer operates on the received spread signal and the SB beamformer operates on the despread signal. In order to compare the above two configurations on the same basis, the difference in their performance can be evaluated with respect to the SINR of the signal at the BF-MF unit output which is the signal at the matched filter output when using the CB configuration, and the signal at the beamformer output when using the SB configuration. Let

$$\mathbf{X}_{u,v}(nT) = \begin{bmatrix} \mathbf{x}_{u,v}^H(nT + \tau_{u,v}) \\ \mathbf{x}_{u,v}^H(nT + T_c + \tau_{u,v}) \\ \cdots \\ \mathbf{x}_{u,v}^H(nT + (N-1)T_c + \tau_{u,v}) \end{bmatrix}^H$$

and

$$\mathbf{X}_I(nT) = \begin{bmatrix} \mathbf{x}_I^H(nT + \tau_{u,v}) \\ \mathbf{x}_I^H(nT + T_c + \tau_{u,v}) \\ \cdots \\ \mathbf{x}_I^H(nT + (N-1)T_c + \tau_{u,v}) \end{bmatrix}^H$$

be the matrices spanned by the N received signal vectors corresponding to the contribution of SOI and the interference plus noise, respectively. For both the CB and the SB configurations, the SINR of the signal at the BF-MF unit output is given by

$$\gamma_{SINR} = \frac{E|\mathbf{c}_u^H \mathbf{X}_{u,v}^H(nT)\mathbf{w}_{u,v}|^2}{E|\mathbf{c}_u^H \mathbf{X}_I^H(nT)\mathbf{w}_{u,v}|^2} \tag{3.19}$$

which can be rewritten as

$$\gamma_{SINR} = \frac{N\sigma_{u,v}^2 \mathbf{w}_{u,v}{}^H \mathbf{a}_{u,v}\mathbf{a}_{u,v}^H \mathbf{w}_{u,v}}{\mathbf{w}_{u,v}{}^H \mathbf{R}_{sI}\mathbf{w}_{u,v}}. \tag{3.20}$$

Since matrix $\mathbf{R}_{sI}$ is positive definite, it can be decomposed as

$$\mathbf{R}_{sI} = \mathbf{Q}\mathbf{Q}^H \tag{3.21}$$

and

$$\gamma_{SINR} = N\sigma_{u,v}^2 \frac{|(\mathbf{Q}^{-1}\mathbf{a}_{u,v})^H \mathbf{Q}^H \mathbf{w}_{u,v}|^2}{\| \mathbf{Q}^H \mathbf{w}_{u,v} \|^2}. \tag{3.22}$$

As mentioned earlier, the closed-form expressions for the weight vectors corresponding to the MMSE, SINR, ML, and MV criteria have the same form and all maximize the SINR at the beamformer output provided that the same beamformer configuration is used. In this light, quantities γ_{SINR}^c and γ_{SINR}^s, which correspond to the SINR for the CB and the SB configurations, respectively, can be obtained by substituting (3.10) and (3.17) into (3.22). They are given by

$$\gamma_{SINR}^c = N\sigma_{u,v}^2 \frac{|(\mathbf{Q}^{-1}\mathbf{a}_{u,v})^H \mathbf{Q}^H \mathbf{R}_{cI}^{-1} \mathbf{a}_{u,v}|^2}{\| \mathbf{Q}^H \mathbf{R}_{cI}^{-1} \mathbf{a}_{u,v} \|^2} \tag{3.23}$$

and

$$\gamma_{SINR}^s = N\sigma_{u,v}^2 \| \mathbf{Q}^{-1}\mathbf{a}_{u,v} \|^2 . \tag{3.24}$$

Applying the Cauchy-Schwartz inequality to (3.23) and (3.24), it can be shown that

$$\gamma_{SINR}^c \leq \gamma_{SINR}^s \tag{3.25}$$

where equality applies if and only if

$$\mathbf{R}_{cI}^{-1}\mathbf{a}_{u,v} = \zeta \mathbf{R}_{sI}^{-1}\mathbf{a}_{u,v} \tag{3.26}$$

where ζ can be any nonzero constant. Eq. (3.25) implies that the SB beamformer outperforms the CB beamformer in general except in the case where (3.26) is satisfied and in that case, the two beamformers have the same performance. For (3.26) to be satisfied, it is required that the CB and SB beamformers have the same beam pattern. Generally, this condition is not satisfied since the two correlation matrixes $\mathbf{R}_{cI}$ and $\mathbf{R}_{sI}$ are different. Therefore, the SB configuration outperforms the CB configuration in the sense that it leads to a higher SINR for the signal at the BF-MF unit output.

3.3.3 Comparison with Respect to MMSE

The difference in the performance between the CB MMSE beamformer and the SB MMSE beamformer can also be compared with respect to the MSE between the signal at the BF-MF unit output and the reference symbol signal using the closed-form solutions. It is given by

$$J_{min} = E[|\alpha \mathbf{c}_k{}^H \mathbf{X}^H(nT)\mathbf{w}_{u,v} - \sqrt{p_u}\beta_{u,v}b_u(n)|^2] \tag{3.27}$$

where b_u is the information bit transmitted and α is a scaling factor to scale the power of the SOI evaluated. Scaling factor α can be readily obtained by minimizing J_{min} in (3.27). It is given by

$$\alpha = \frac{N\sigma_{u,v}^2 \mathbf{a}_{u,v}^H \mathbf{w}_{u,v}}{\mathbf{w}_{u,v}{}^H \mathbf{R}_s \mathbf{w}_{u,v}}. \tag{3.28}$$

Let α_c and α_s denote the scaling factors corresponding to the CB and the SB MMSE beamformers, respectively. Substituting (3.7) and (3.13) into (3.28), the corresponding scaling factors α_c and α_s can be readily obtained as

$$\alpha_c = \frac{N\mathbf{a}_{u,v}^H \mathbf{R}_c{}^{-1}\mathbf{a}_{u,v}}{\mathbf{a}_{u,v}^H \mathbf{R}_c{}^{-1}\mathbf{R}_s\mathbf{R}_c{}^{-1}\mathbf{a}_{u,v}} \tag{3.29}$$

$$\alpha_s = 1. \tag{3.30}$$

Quantities J_c and J_s, for the CB and SB MMSE beamformers, can then be obtained by substituting (3.7), (3.13), (3.29), and (3.30) into (3.27) as

$$\begin{aligned} J_c &= \alpha_c^2\sigma_{u,v}^4 \mathbf{a}_{u,v}^H \mathbf{R}_c{}^{-1}\mathbf{R}_s\mathbf{R}_c{}^{-1}\mathbf{a}_{u,v} \\ &\quad -2N\alpha_c\sigma_{u,v}^4 \mathbf{a}_{u,v}^H \mathbf{R}_c{}^{-1}\mathbf{a}_{u,v} + \sigma_{u,v}^2 \end{aligned}$$

and

$$J_s = \sigma_{u,v}^2 - N^2\sigma_{u,v}^4 \mathbf{a}_{u,v}^H \mathbf{R}_s^{-1}\mathbf{a}_{u,v}.$$

The performance of these two criteria can be compared by evaluating the difference between J_c and J_s, i.e.,

$$J_c - J_s = N^2\sigma_{u,v}^4 \mathbf{a}_{u,v}^H \mathbf{M}\mathbf{a}_{u,v} \tag{3.31}$$

where

$$\mathbf{M} = \frac{\alpha_c}{N}\mathbf{R}_c{}^{-1}\mathbf{R}_s\frac{\alpha_c}{N}\mathbf{R}_c{}^{-1} - 2\frac{\alpha_c}{N}\mathbf{R}_c{}^{-1} + \mathbf{R}_s^{-1}. \tag{3.32}$$

Since matrix $\mathbf{R}_s^{-1}$ is positive definite, it can be decomposed as

$$\mathbf{R}_s^{-1} = \mathbf{D}\mathbf{D}^H \tag{3.33}$$

where $\mathbf{D}$ is a square matrix. Substituting (3.33) into (3.32), matrix $\mathbf{M}$ can be rewritten as

$$\mathbf{M} = \mathbf{G}\mathbf{G}^H \tag{3.34}$$

where $\mathbf{G} = \mathbf{R}_c^{-1}(\mathbf{R}_c - \frac{\alpha_c}{N}\mathbf{R}_s)\mathbf{D}$. Matrix $\mathbf{M}$ is positive semidefinite and thus

$$J_c \geq J_s. \tag{3.35}$$

Therefore, the MSE of the signal at the BF-MF unit output using the SB configuration is less than that of using the CB configuration.

3.4 Discussion and Conceptual Explanation

In the previous section, it has been shown through theoretical analysis that the SB configuration offers a better performance with respect to SINR and MMSE than the CB configuration. In this section, this result will be discussed and two simple examples, one corresponding to a synchronous and the other corresponding to an asynchronous DS-CDMA systems will be presented to explain the difference in the performance of the SB and CB configurations.

3.4.1 Interfering Strength and Rejecting Factor

The impact of an interfering component on the system performance depends not only on the power of the interfering component but also on its code correlation with

the SOI. This fact is the motivation for defining here the concept of IS. Given an interfering component from path l of MS k and the SOI from path v of MS u, its IS on the SOI is defined as

$$\eta_{k,l} = \sigma_{k,l}^2 \rho_{(k,l)}^2 \tag{3.36}$$

where $\sigma_{k,l}^2$ is the power of the interfering component from path l of MS k and $\rho_{(k,l)}$ is the code correlation as defined in (3.16). Interference with high IS will have a significant impact on the system performance and has to be rejected with a higher priority than interference with lower IS. Since the IS depends on both the power of an interfering component as well as its code correlation with the SOI, an interfering component with high power may have relatively less impact than an interfering component with lower power but higher code correlation with the SOI. Comparing $\eta_{k,l}$ with $f_{k,l}^c$ in (3.11) and $f_{k,l}^s$ in (3.18), the rejecting factors of the CB and SB configurations, respectively, it can be seen that in the case of the SB configuration, the rejecting factor $f_{k,l}^s$ is equal to the IS $\eta_{k,l}$. In contrast, when the CB configuration is used, the rejecting factor $f_{k,l}^c$ is equal to the power of an interfering component. Thus in the SB configuration, the beamforming weights are computed based on the IS, i.e., by taking both the power of the interference and its code correlation with the SOI into consideration whereas for the CB configuration, only the power of the interference is taken into consideration. This difference between the CB and SB configurations leads to different performance. Below, we investigate further two aspects of the difference in the performance of the two configurations. First, we consider the mismatch loss in synchronous DS-CDMA systems where all interfering components have the same code correlation with the SOI. Second, we consider the spatial selectivity in asynchronous DS-CDMA systems where the interfering components have different code correlation with the SOI.

3.4.2 Mismatch Loss in Synchronous DS-CDMA Systems

In adaptive beamforming, the beamforming weights are obtained such that the antenna-array gain is maximized in the direction of the SOI and simultaneously is minimized in the direction of the interference. In most cases, the main beam obtained deviates from the DOA of the SOI and, thus, the received power of the SOI is attenuated (assuming a normalized beamforming weight vector). This attenuation is known as mismatch loss. Since the noise component $\mathbf{n}(t)$ is uniformly distributed in all directions, the SNR of the signal received in the direction of the main beam is less than the SNR of the signal received when the main beam is steered towards the DOA of the SOI. In other words, the price paid for the rejection of the interference by using the spatial diversity between the SOI and the interference is a reduction in the SNR for the received SOI. In the case of the CB configuration, the rejecting factor $f^c_{k,l}$ is far larger than the IS $\eta_{k,l}$ due to the fact that $\rho_{(k,l)} \ll 1$ and, therefore, the impact of the interference is overvalued. This leads to a higher mismatch loss than when using the SB configuration where the rejecting factor $f^s_{k,l}$ is equal to the IS $\eta_{k,l}$. In Example 1, it will be shown that this can lead to more mismatch loss and SNR degradation than the corresponding values for the SB configuration.

Example 1: Synchronous DS-CDMA system

Example 1 concerns a synchronous DS-CDMA system with an antenna array deployed at the BS. Three MSs A, B, and C and one path for each MS were assumed. The power from MSs A and C was assumed to be half of that from MS B when received at the antenna array. The difference of the antenna patterns using the CB and the SB configurations is illustrated in Fig. 3.3. In the CB configuration, the input of the beamformer is the received signal at the antenna array. It can be modeled as a sum of the SOI $\mathbf{x}_A$ from MS A, the interfering component $\mathbf{x}_B$ from MS B, the interfering component $\mathbf{x}_C$ from MS C, and spatially uniformly distributed additive white Gaussian noise (AWGN) $\mathbf{n}(t)$. In the SB configuration, the input of the

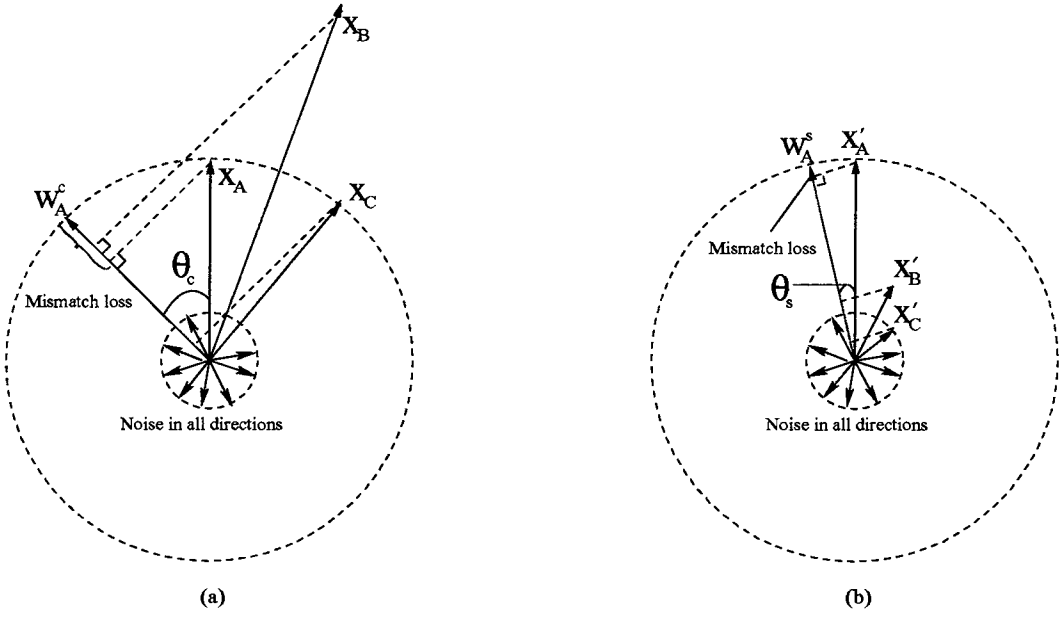

Figure 3.3. *Conceptual explanation for antenna patterns in Example 1: (a) CB configuration, (b) SB configuration.*

beamformer is the sum of $\mathbf{n}(t)$ and the corresponding despread signals of $\mathbf{x}_A$, $\mathbf{x}_B$, and $\mathbf{x}_C$, denoted by $\mathbf{x}'_A$, $\mathbf{x}'_B$, and $\mathbf{x}'_C$, respectively. The weight vectors corresponding to the CB and SB configurations are normalized and denoted by $\mathbf{w}_A^c$ and $\mathbf{w}_A^s$, respectively.

Since in a synchronous DS-CDMA system, the signal components from different MSs arrive at the BS are synchronous, the different interfering components received at the antenna array have equal code correlation with the SOI. Thus, their IS on the SOI is proportional to their power received at antenna array. Using the SB configuration, the power of different interfering components is proportionally reduced by the same amount after despreading. As shown in Fig. 3.3(b), the powers of $\mathbf{x}'_B$ and $\mathbf{x}'_C$ are far less than that of $\mathbf{x}'_A$. Thus, the SB beamformer has a lower input SIR as compared to the CB beamformer and this difference will lead to different beam patterns. It can be seen that the weight vector $\mathbf{w}_A^s$ deviates less from the DOA of the SOI in Fig. 3.3(b) for the SB configuration than that in Fig. 3.3(a) for the CB configuration. Using the CB configuration, the rejecting factor in (3.11) equals the power received at the antenna array, which is far larger than the corresponding IS. Thus, the impact of interference on the system performance is overvalued and, as a result, $\theta_c > \theta_s$, i.e., the weight vector $\mathbf{w}_A^c$ for the CB configuration is steered to deviate more from the DOA of the SOI than in the SB configuration in order to reject the overvalued interference. This indicates that the CB configuration leads to more mismatch loss and more degradation of SNR. Because of this reduction of the SNR in the CB configuration, the performance with respect to the combined SINR for the CB configuration is inferior relative to that of the SB configuration. This will be verified through simulations in the next section.

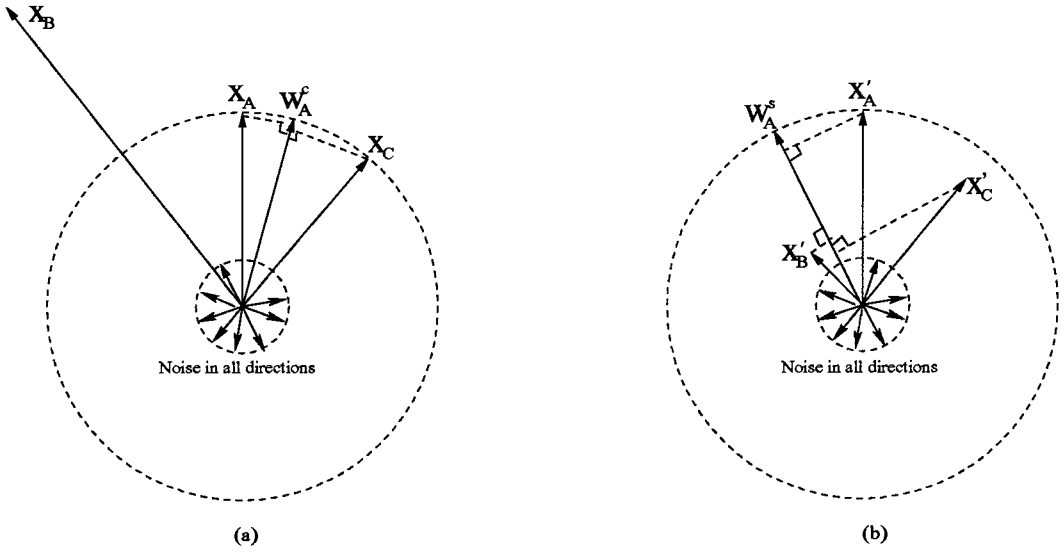

Figure 3.4. *Conceptual explanation for antenna patterns in Example 2: (a) CB configuration, (b) SB configuration.*

3.4.3 Spatial Selectivity in Asynchronous DS-CDMA Systems

In asynchronous DS-CDMA systems or systems over multipath environments, an interfering component with high power may interfere less with the SOI than an interfering component with less power but larger code correlation with the SOI. In such a case, the rejecting factor $f_{k,l}^c$ of the CB configuration does not reflect the relative impact of different interfering components. The interfering component with the highest power is given the highest priority for cancellation even though it may not have the highest IS. In the case of the SB configuration, the rejecting factor $f_{k,l}^s$ is equal to the IS and the highest priority is given to the interfering component with the highest IS. Thus the SB configuration has better spatial selectivity than the CB configuration in that an interfering component that interferes more with the SOI is rejected more efficiently. This will be further explained in Example 2.

Example 2: Asynchronous DS-CDMA system

Example 2 concerns an asynchronous DS-CDMA system with an antenna array deployed at the BS. Three MSs A, B, and C and one path for each MS were assumed. The power of the signals received at the antenna array from MSs A and C was assumed to be half of the power from MS B. The antenna patterns using the CB and SB configurations are illustrated in Fig. 3.4(a) and Fig. 3.4(b), respectively.

Since in an asynchronous DS-CDMA system signal components from different MSs and paths arrive at the BS with different delays, their code correlation with the SOI can be significantly different and, therefore, their power is not proportionally reduced after despreading. In this example, the code correlation between $\mathbf{x}_A$ and $\mathbf{x}_C$ is assumed to be much larger than that between $\mathbf{x}_A$ and $\mathbf{x}_B$ such that the IS of $\mathbf{x}_C$ on the SOI is larger than that of $\mathbf{x}_B$ even though $\mathbf{x}_B$ has higher power. Correspondingly, the power of the despread signal $\mathbf{x}'_B$ shown in Fig. 3.4(b) is far less than $\mathbf{x}'_C$; that is, the interfering component from MS C is a stronger interference and interferes more with the SOI than the interfering component from MS B. Using the CB configuration, the interfering component from MS B is regarded as a stronger interference than the interfering component from MS C and the weight vector $\mathbf{w}_A^c$ in Fig. 3.4(a) is steered so that the interfering component from MS B is more efficiently rejected than the interfering component from MS C. Conversely, using the SB configuration, the interfering component from MS C, which has larger IS on the SOI, is considered as a stronger interference and the direction of the weight vector $\mathbf{w}_A^s$ in Fig. 3.4(b) is chosen so that $\mathbf{x}'_C$ is more efficiently rejected than $\mathbf{x}'_B$. Thus, an interfering component with higher IS is more efficiently rejected using the SB configuration and the performance of the SINR for the SB configuration is superior relative to that of the CB configuration. This will be verified by using simulations in the next section.

3.5 Simulations

In this section, the difference in the performance of the CB and SB configurations will be illustrated through simulations by considering four examples. The discussion and conceptual explanation in Sec. 3.4 will be verified by means of simulations in Example 1 and 2, respectively. The spatial selectivity of the CB and SB configurations is further illustrated in Example 3. In Example 4, the system performance of the CB and SB configurations is compared in terms of bit-error rate (BER).

3.5.1 Example 1

Example 1 deals with a synchronous DS-CDMA system as described in Sec. 3.4. The spacing of a 2-element antenna array was set to $d = \lambda/2$ and Gold codes of length 31 were used as the spreading codes. The information bit-to-background power spectral density ratio (E_b/N_0) of the received signal was set to 25 dB. A single path with a static channel was assumed. It was further assumed that the power from MSs A and C was half of that from MS B when received at the antenna array. Simulations were carried out with the DOA of the SOI from MS A varying from -90^o to 90^o and the DOAs of the interfering components from MSs B and C were kept constant at 30^o and 60^o, respectively. Plots of the relative antenna-array gain for the SOI from MS A for the CB and SB configurations are shown in Fig. 3.5. As can be seen, interference rejection is achieved at the expense of mismatch loss for the SOI and this loss is higher when using the CB configuration. This implies that the SNR obtained using the CB configuration will be lower than that of using the SB configuration, and this is confirmed in Fig. 3.6. Further, the signal-to-interference ratio (SIR) and SINR versus the DOA of the SOI are plotted in Figs. 3.7 and 3.8, respectively. It can be seen that the resulting SIR using the CB configuration is higher than that achieved in the SB configuration. However, this higher SIR for the CB configuration is accompanied with lower SNR relatively to that in the SB configuration and, as shown in Fig. 3.8,

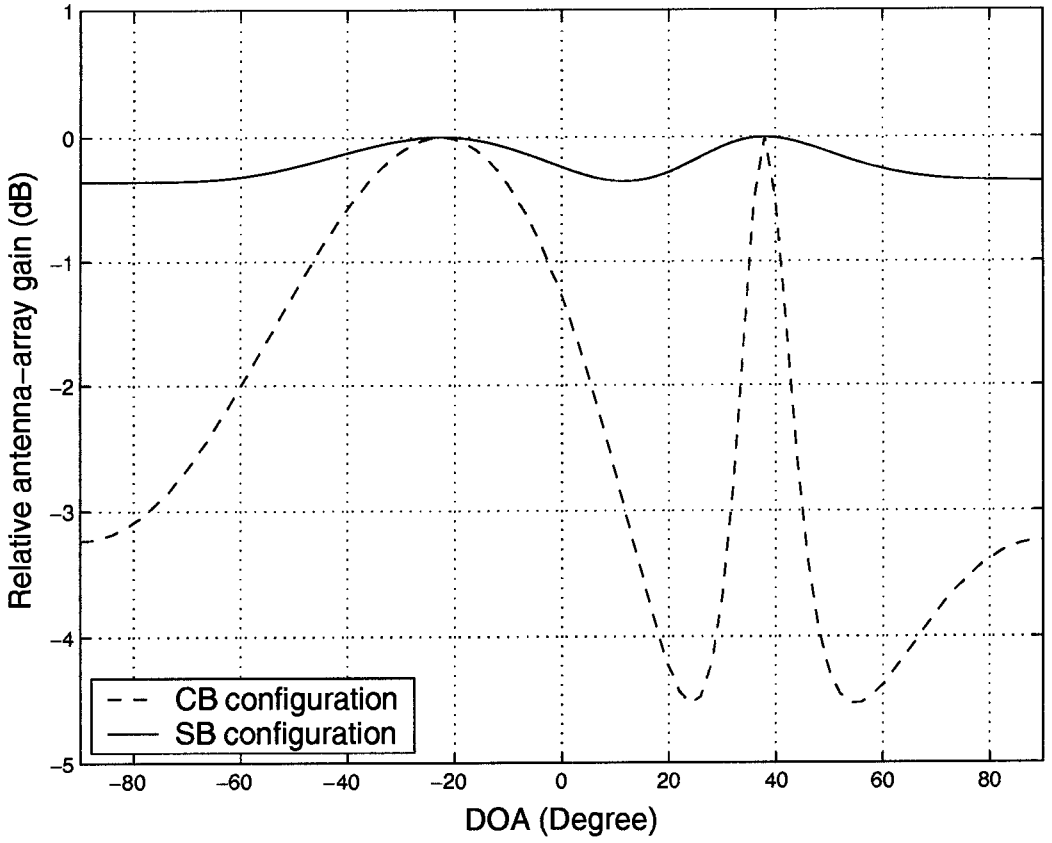

Figure 3.5. *Relative antenna-array gain versus DOA of the SOI for Example 1.*

the SINR obtained using the CB configuration is close to that in the SB configuration only in two special cases in which the weight vectors of the CB and SB configurations are steered to the same direction as the DOA of the SOI. Except for these cases, the performance of the CB configuration ends up being inferior relative to that of the SB configuration in terms of the SINR at the output of the BF-MF unit.

3.5.2 Example 2

Example 2 deals with an asynchronous DS-CDMA system as described in Sec. 3.4. A 2-element antenna array with the spacing set to $d = \lambda/2$ and Gold codes of length 31

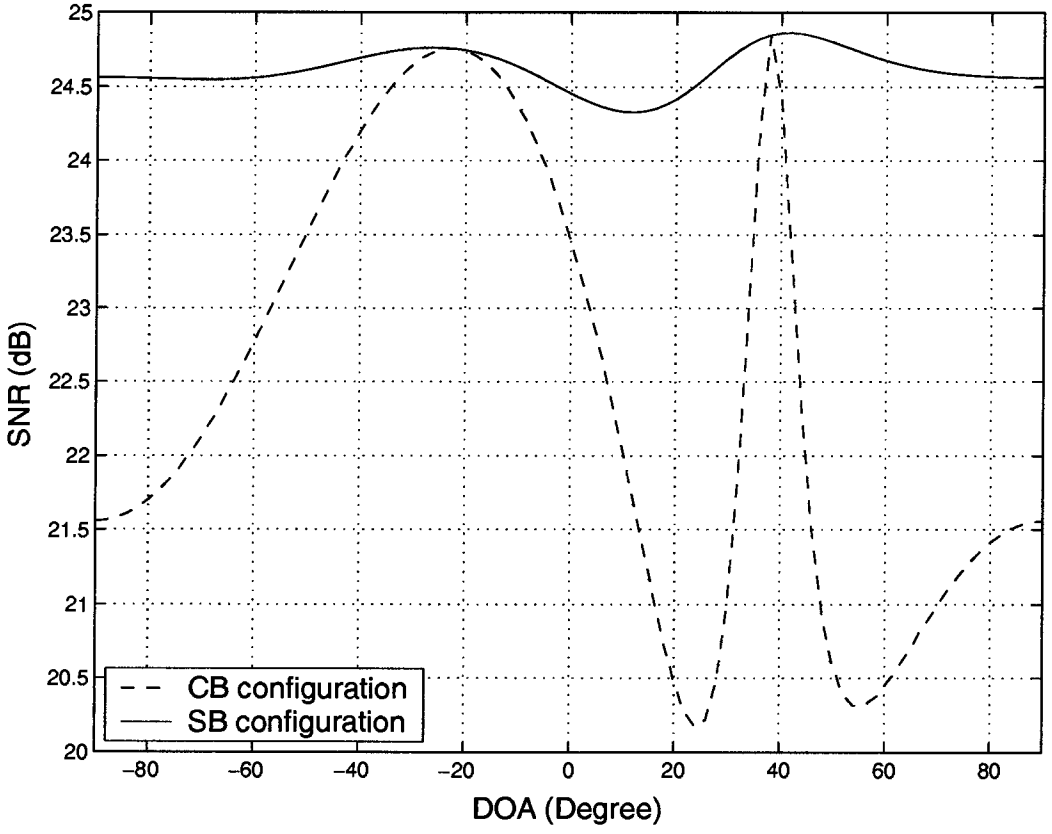

Figure 3.6. *SNR versus DOA of the SOI for Example 1.*

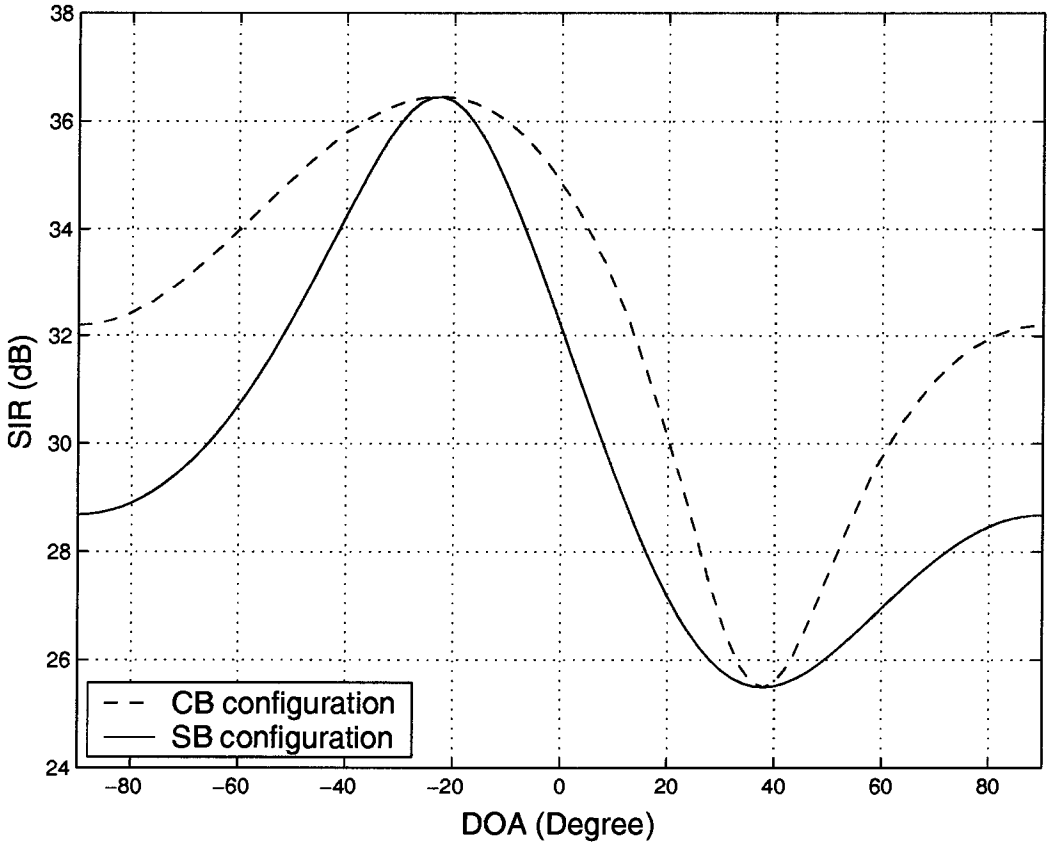

Figure 3.7. *SIR versus DOA of the SOI for Example 1.*

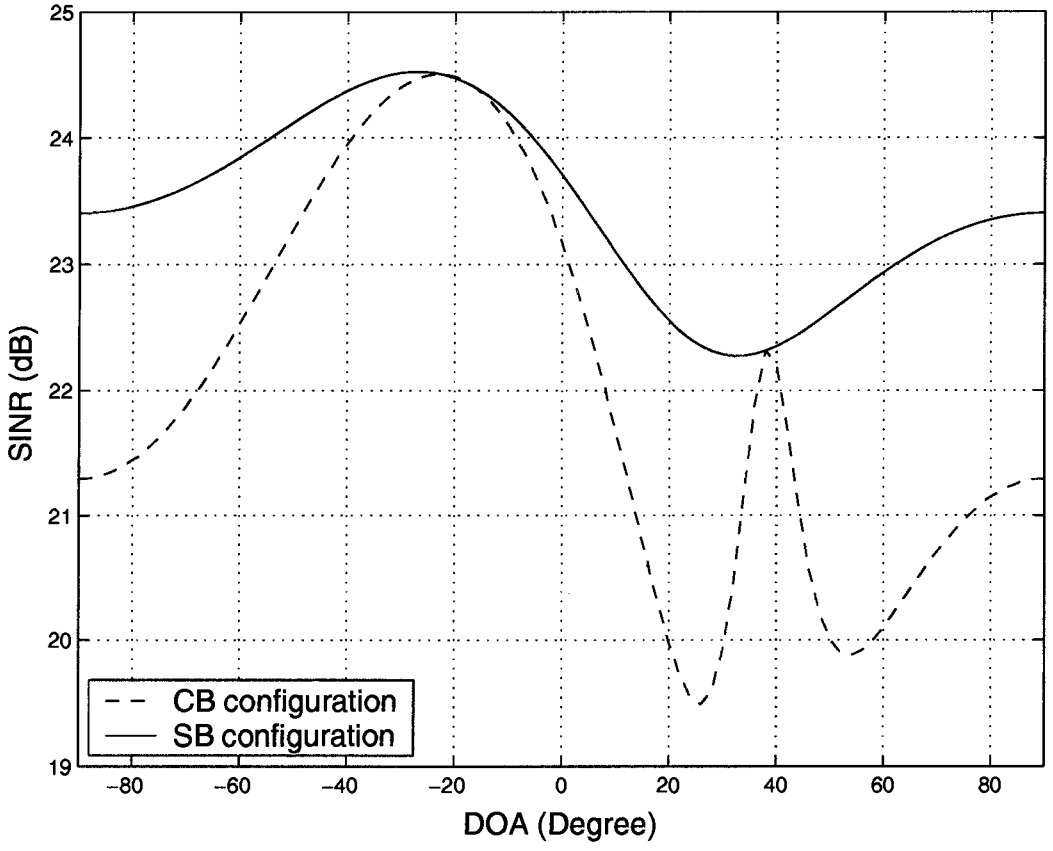

Figure 3.8. *SINR versus DOA of the SOI for Example 1.*

were assumed as in the previous case. A single path with a static channel was assumed and the asynchronous code correlation between the interfering component from MS C and the SOI from MS A was 8.99 times the code correlation between the interfering component from MS B and the SOI from MS A. The power of the signal received at the antenna array from MSs A and C was half of the power from MS B. The DOAs for the signal from MSs A, B, and C were fixed at 0^o, -45^o, and 45^o, respectively. Fig. 3.9 shows that using the SB configuration, the beam pattern obtained leads to rejecting the strong interfering component from MS C more effectively than the interfering component from MS B. Conversely, the beam pattern obtained using the CB configuration leads to more rejection for the interfering signal from MS B due to the higher power received at the antenna array. Simulations were carried out with the DOA of the SOI from MS A varying from -90^o to 90^o and the DOAs of the interfering components from MSs B and C were kept constant at -45^o and 45^o as before. The SIR for both beamforming configurations is illustrated in Fig. 3.10 and as can be seen the SB configuration is more effective in rejecting interference. Fig. 3.11 depicts the SNR versus the DOA and as can be seen for some DOAs, it is higher in the CB configuration, and for some DOAs, it is higher in the SB configuration. However, the SINR is always higher in the SB configuration as can be seen in Fig. 3.12.

3.5.3 Example 3

In this Example, the difference in the spatial selectivity of the CB and SB configurations will be further illustrated through simulations of an asynchronous DS-CDMA system with a 6-element ULA deployed at the BS. As in the previous cases, a static channel was assumed and the spacing of the antennas was $d = \lambda/2$ and Gold codes of length 31 were used. Five MSs, A, the MS of interest, B, C, D, and E, and 3 paths for each MS were assumed. It was further assumed that signal components from different MSs and paths have equal power when received at the antenna array. The SOI originates from path 1 of MS A and all other paths of MS A and other MSs are considered

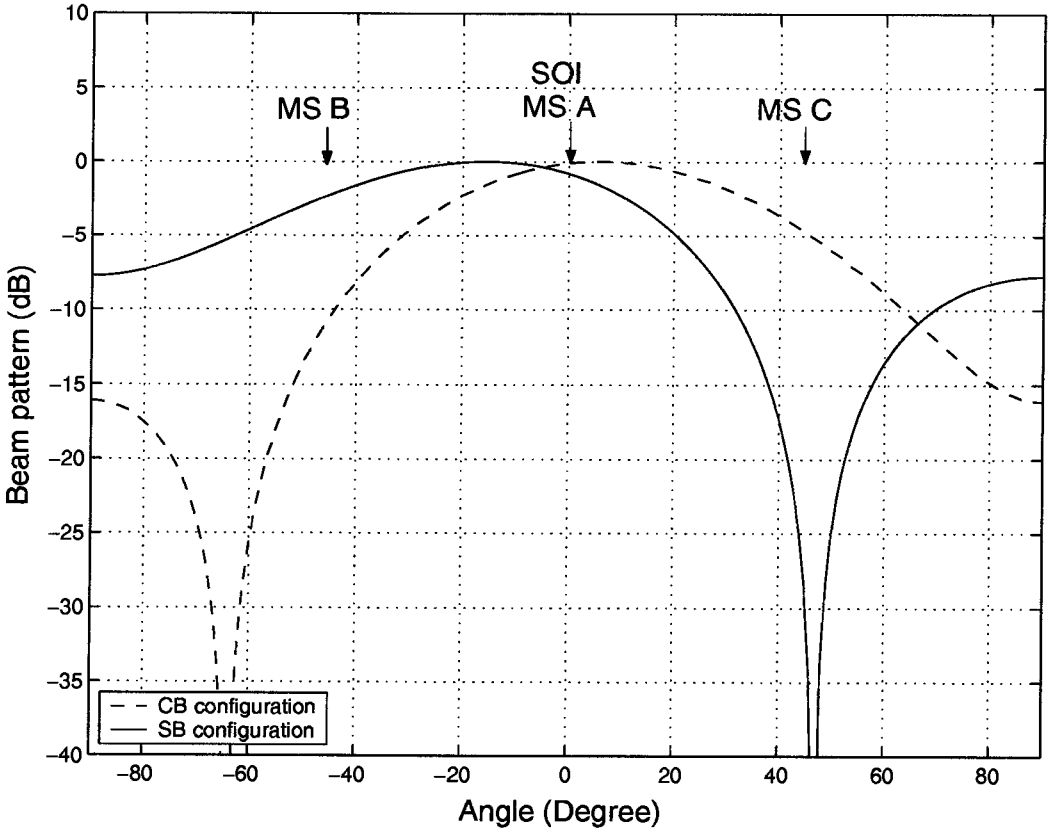

Figure 3.9. *Beam pattern for Example 2.*

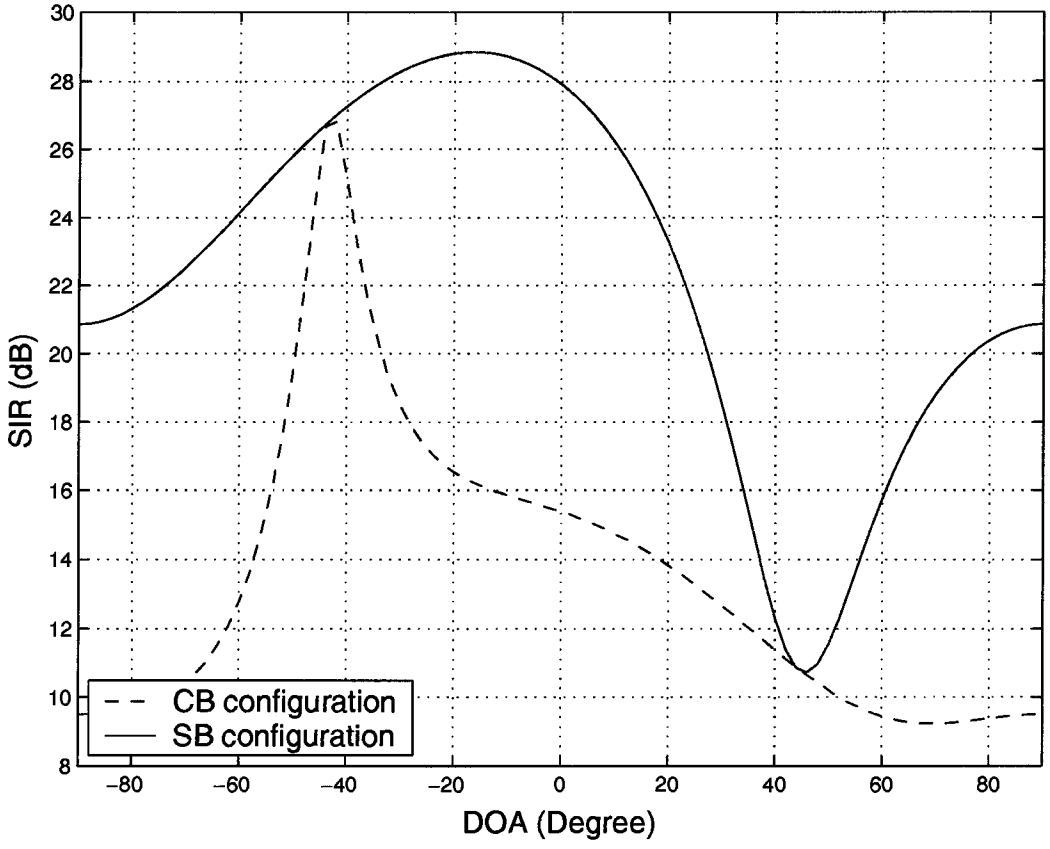

Figure 3.10. *SIR versus DOA of the SOI for Example 2.*

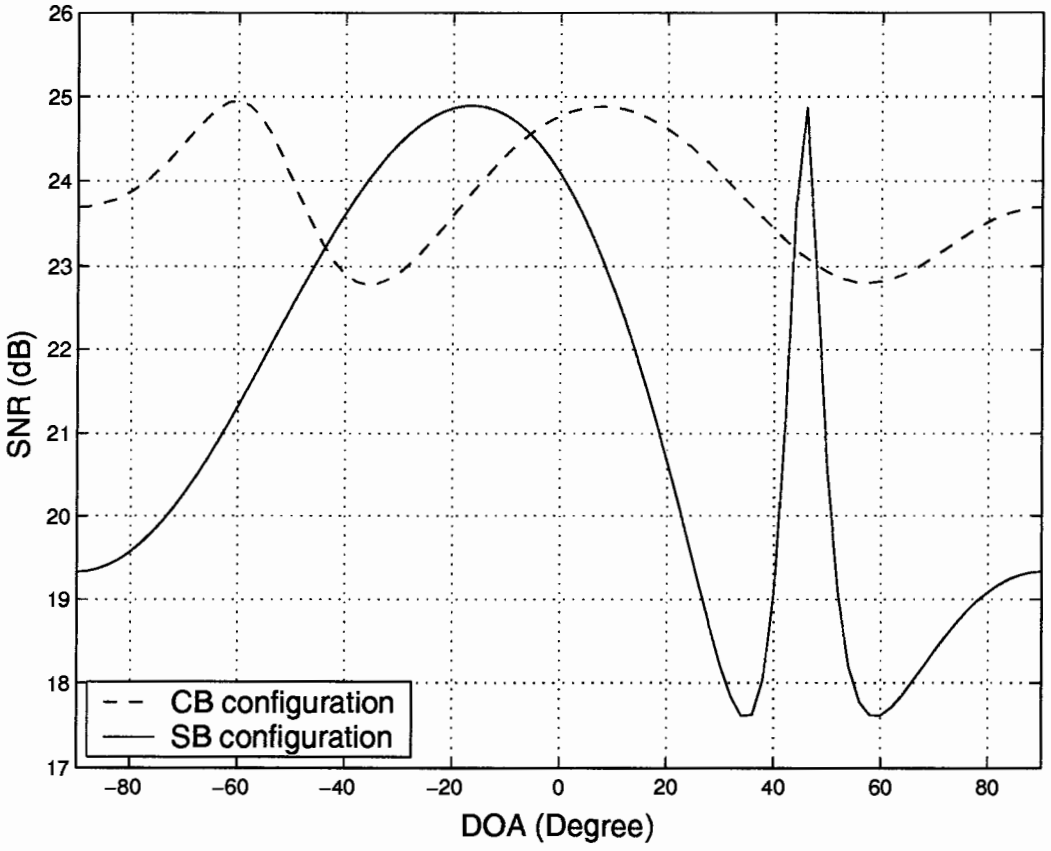

Figure 3.11. *SNR versus DOA of the SOI for Example 2.*

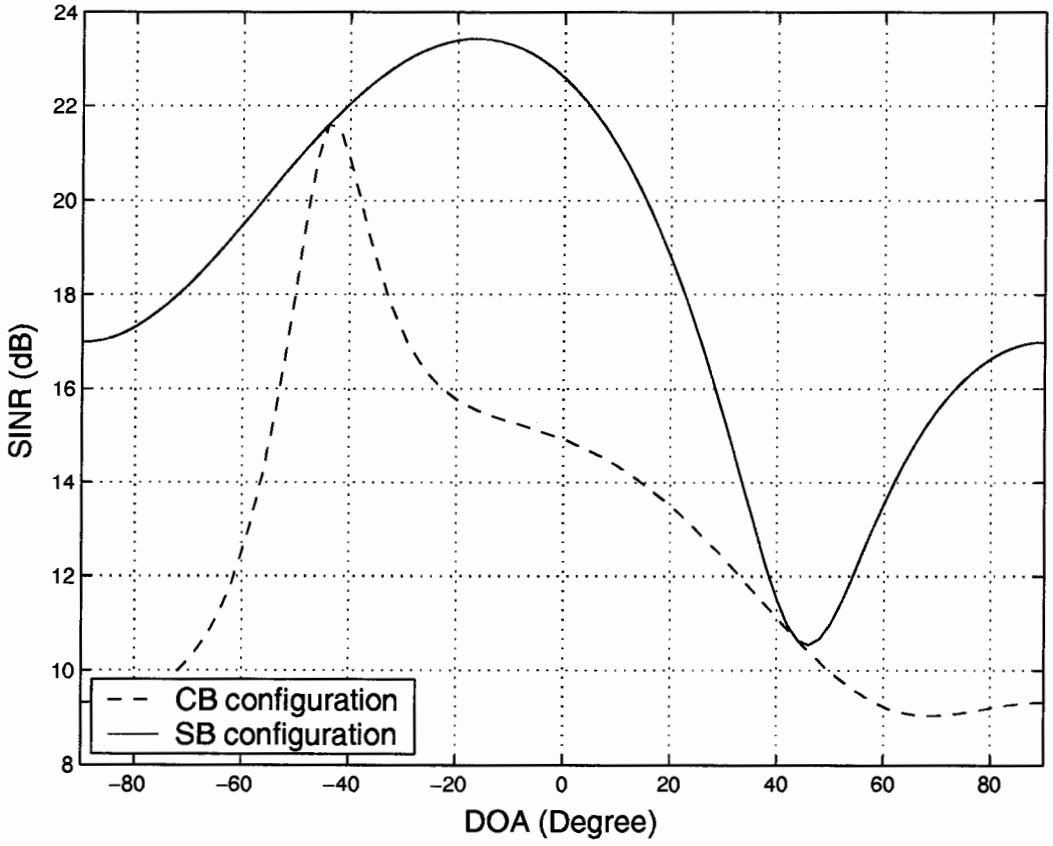

Figure 3.12. *SINR versus DOA of the SOI for Example 2.*

as interference. The DOAs and ISs normalized by the power of the SOI of different interfering components are presented with vertical bars in Fig. 3.13. A more negative IS means an interfering component interfering less with the SOI. The beam patterns obtained using the CB and SB configurations for the SOI, the first path of MS A, are also shown in Fig. 3.13. It can be observed that the SB configuration is more selective than the CB configuration in that a lower gain is obtained in the direction of an interference with stronger IS such as C-1, C-2, C-3, D-1, D-3, E-1, and E-2 in Fig. 3.13. The output signals at the BF-MF units for different paths in Fig. 3.1 were summed by a RAKE combiner. Using the SB configuration, the corresponding SINR of the signal at the RAKE combiner output was 4.89 dB higher than that obtained by using the CB configuration. As expected, the SB outperforms the CB configuration in terms of SINR.

3.5.4 Example 4

In Example 4, two DS-CDMA systems, one with 6-element and another with 8-element ULAs deployed at the BS were considered assuming multipath Rayleigh fading channels. The spacing of the antennas was $d = \lambda/2$ and 3 paths for each MS were assumed. The angle of spread was assumed to be $\pi/6$ and DOAs of signals from different MSs were evenly distributed from $-\pi/2$ to $\pi/2$. Simulations were carried out with the number of MSs varying from 10 to 30. The average received power at the BS of signals from different MSs was assumed to be log-normally distributed with standard deviation of 4 dB. The maximum Doppler frequency f_d was set to 100 Hz and the channel coherence time T_{co} was given by $0.423/f_d = 0.00423$s [54]. A data rate of 64 kbps was assumed in the uplink. Gold codes of length 63 were used. It was assumed that the exact fading coefficients are known at the receiver. The bit error rate (BER) versus the number of MSs using the CB and SB configurations are plotted in Fig. 3.14. It can be observed from Fig. 3.14 that the SB configuration leads to a lower BER relative to that in the CB configuration.

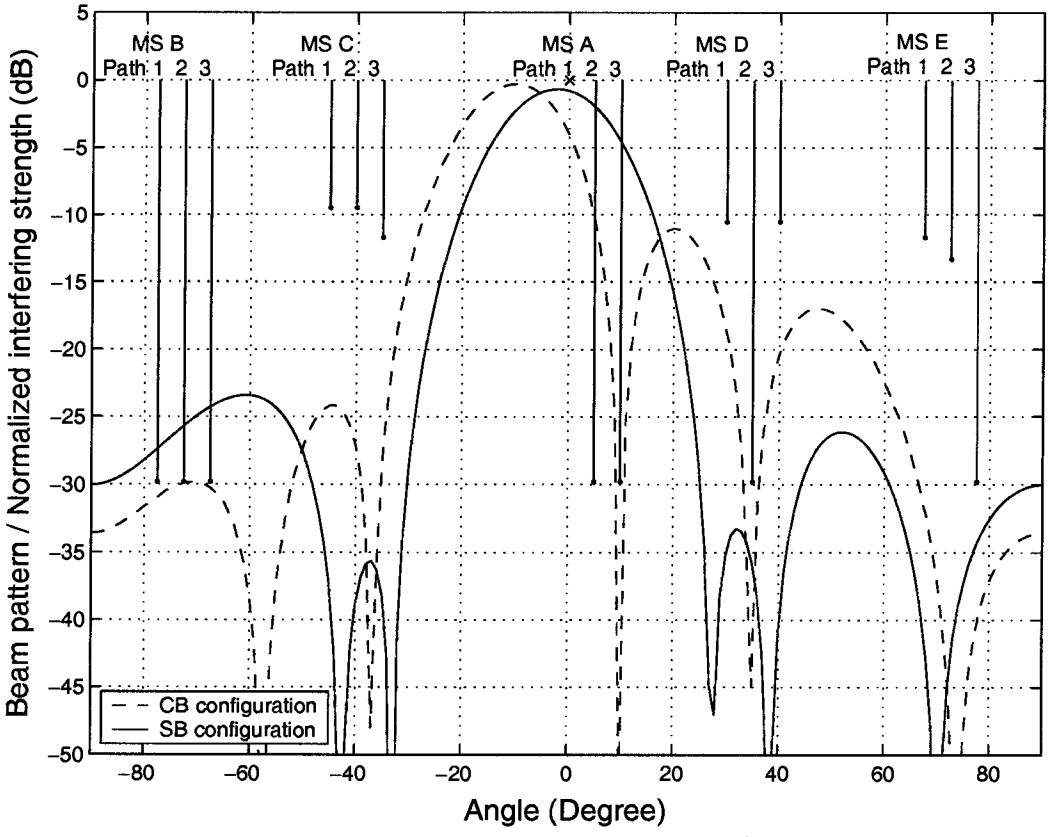

Figure 3.13. *Relative antenna-array gain for Example 3.*

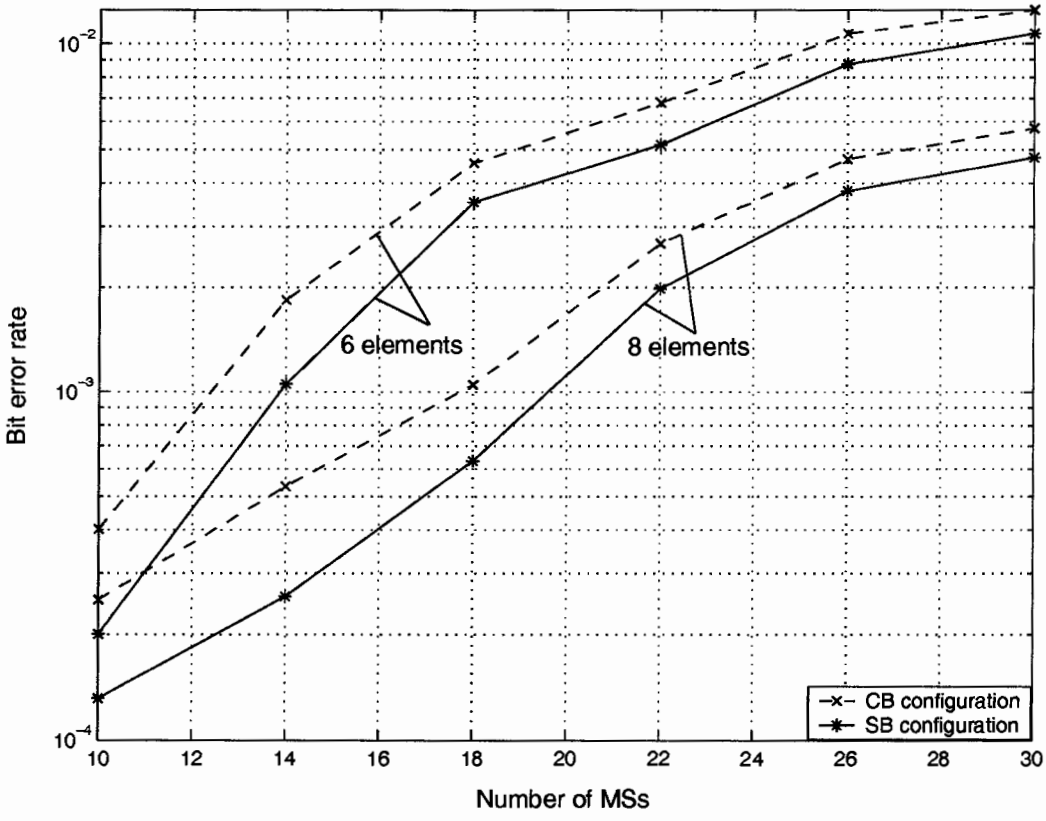

Figure 3.14. *BER versus number of MSs for Example 4.*

3.6 Conclusions

CB and SB beamformer configurations for DS-CDMA systems were studied through analysis and simulations. Using the CB configuration, different interfering components are spatially rejected in terms of the spatial distribution of their power regardless of their code correlation with the SOI. On the other hand, using the SB configuration, they are rejected on the basis of their IS which depends on both the power and the code correlation with the SOI. Thus, interference that has a more significant impact on system performance can be more efficiently rejected. As a consequence, the SB configuration leads to a better trade-off between SNR and SIR and a higher SINR can be achieved. In effect, the SB is superior relative to the CB configuration in the presence of MAI.

Chapter 4

A New DOA Estimation Technique Based on Subarray Beamforming

4.1 Introduction

The use of antenna arrays in a wireless communication system makes it possible to track the DOA of each signal and locate the position of an MS. This is required in most of interference cancellation techniques which transmit and receive signals in a directional manner. As will be shown in the subsequent chapters, the performance of most beamforming techniques relies heavily on the accurate estimation of the DOA of each signal.

In this chapter, a new DOA estimation technique, the SBDOA technique, which uses a reference signal (pilot or decision-directed signal) is proposed. In the proposed technique, the target DOA is estimated from the phase shift introduced in the target signal by subarray beamforming, which is a function of the target DOA. Since the phase shift is estimated after subarray beamforming, all signals and interference other than the target one can be efficiently rejected before DOA estimation. Thus their interference on DOA estimation is reduced. The major difference between the proposed SBDOA estimation technique and existing techniques is that in the SBDOA estimation technique, the target DOA is estimated after interference rejection using beamforming. In existing techniques, DOA estimation is based on either computing

the spatial signatures (or antenna response vectors) or the signal subspace spanned by the spatial signatures. Since the information pertaining to spatial signatures exists only in the received signals before beamforming, none of the existing techniques can estimate a DOA after beamforming. As a result, a DOA is estimated in the presence of many other signals from sources other than the target one and, therefore, the performance of DOA estimation algorithms is significantly degraded by the interference. Due to subarray beamforming, the estimation resolution and accuracy of the proposed SBDOA technique are better than those of existing techniques. The capacity of DOA estimation using the proposed SBDOA technique can be far larger than the number of antenna elements. Since subspace estimation, eigendecomposition, and multidimensional nonlinear optimization are not required in the SBDOA technique as is the case in other DOA estimation techniques, the SBDOA technique is computationally simpler and can be easily implemented on hardware. Further, the use of a reference signal which can be either a pilot or a decision-directed signal enables the proposed SBDOA technique to identify which signal source corresponds to which estimated DOA.

The organization of this chapter is as follows: in Sec. 4.2, the signal model considered is described. The subarray signal formation, subarray beamforming and DOA computation of the proposed SBDOA technique are presented in Sec. 4.3. A performance analysis of the new DOA estimation technique is provided in Sec. 4.4. The application of the SBDOA estimator in CDMA communication systems is discussed in Sec. 4.6. In Sec. 4.6.2, numerical results pertaining to the resolution, capacity, and accuracy for the SBDOA technique and existing techniques are presented. Conclusions are drawn in Sec. 4.7.

4.2 Signal Model

The SBDOA technique uses the same antenna array geometry as that used in ESPRIT-class techniques. The antenna array is decomposed into two equal-sized subarrays such that for each element in one subarray there is a corresponding element in the other subarray displaced by a fixed translational distance. Below, we discuss only the commonly used ULA since the SBDOA technique can be easily applied to other kinds of antenna arrays.

Consider an M-element ULA with adjacent element spacing D deployed at a BS. Let angle θ_k in rad denote the DOA of the signal from source k. The M-dimension antenna-array response vector $\mathbf{a}(\theta_k)$ is given by

$$\mathbf{a}(\theta_k) = [1 \; z(\theta_k) \; \cdots \; z(\theta_k)^{M-1}]^T \tag{4.1}$$

where $z(\theta_k) = e^{-j2\pi D \sin\theta_k/\lambda}$ and λ is the wavelength.

In this dissertation, we assume that signals from different sources are uncorrelated or have negligible correlation with each other. If there are K signal sources and J unknown interference sources, the received signal at the antenna array after down-converting to baseband can be represented by the M-dimensional vector

$$\mathbf{u}(t) = \sum_{k=1}^{K+J} s_k(t)\mathbf{a}(\theta_k) + \mathbf{n}(t) \tag{4.2}$$

where $s_k(t)$ for $k = 1, 2, \ldots, K$ is a target signal component, $s_k(t)$ for $k = K + 1, 2, \ldots, K + J$ is an unknown interference component, and $\mathbf{n}(t)$ is a spatially stationary background noise vector with zero mean and cross-covariance

$$E[\mathbf{n}(t_1)\mathbf{n}^H(t_2)] = \sigma^2\delta(t_1 - t_2)\mathbf{I}_M \tag{4.3}$$

where $\mathbf{I}_M$ is the identity matrix.

4.3 Subarray Beamforming-Based DOA Estimation

The block diagram of the proposed SBDOA system is illustrated in Fig. 4.1. Two virtual subarrays are used in conjunction with two subarray beamformers to obtain an optimum estimation of a phase-shifted reference signal whose phase relative to that of the reference signal is a function of the target DOA. The target DOA is then computed from the estimated phase shift between the phase-shifted reference signal and the reference signal. Consider the case where θ_k for $k = 1, 2, \ldots, K$ is the target DOA to be estimated. The function of the proposed DOA estimator is as follows. Two subarray signal vectors $\mathbf{y}_A$ and $\mathbf{y}_B$ are formed such that the phase shift between each signal component in $\mathbf{y}_A$ and its corresponding signal component from the same source in $\mathbf{y}_B$ is a function of the DOA. The two subarray signals are then fed into beamformers A and B. The weight vector $\mathbf{w}_k$ is obtained by minimizing the mean-square error (MSE), e_k, between the output signal of beamformer A and the reference signal r_k. Using the weight vector $\mathbf{w}_k$ obtained from beamformer A, the subarray signal $\mathbf{y}_B$ is weighted and combined in beamformer B. It will be shown that the output of beamformer B, i.e., $\hat{r}_k$, is an optimum estimation of the phase-shifted reference signal and, further, the phase of $\hat{r}_k$ relative to that of the reference signal r_k is a function of the target DOA, θ_k. Finally, the estimation $\hat{\theta}_k$ of the target θ_k is obtained based on the computation of the phase shift between the phase-shifted reference signal $\hat{r}_k$ and the reference signal r_k.

The proposed DOA estimator is described in detail in Sec. 4.3.1-4.3.3 below.

4.3.1 Subarray Signal Formation

As mentioned in Sec. 4.2, the SBDOA technique requires that each pair of elements in the two subarrays be displaced by a fixed translational distance. In the case where a ULA is deployed at the receiver, two kinds of antenna element multiplexing geometries

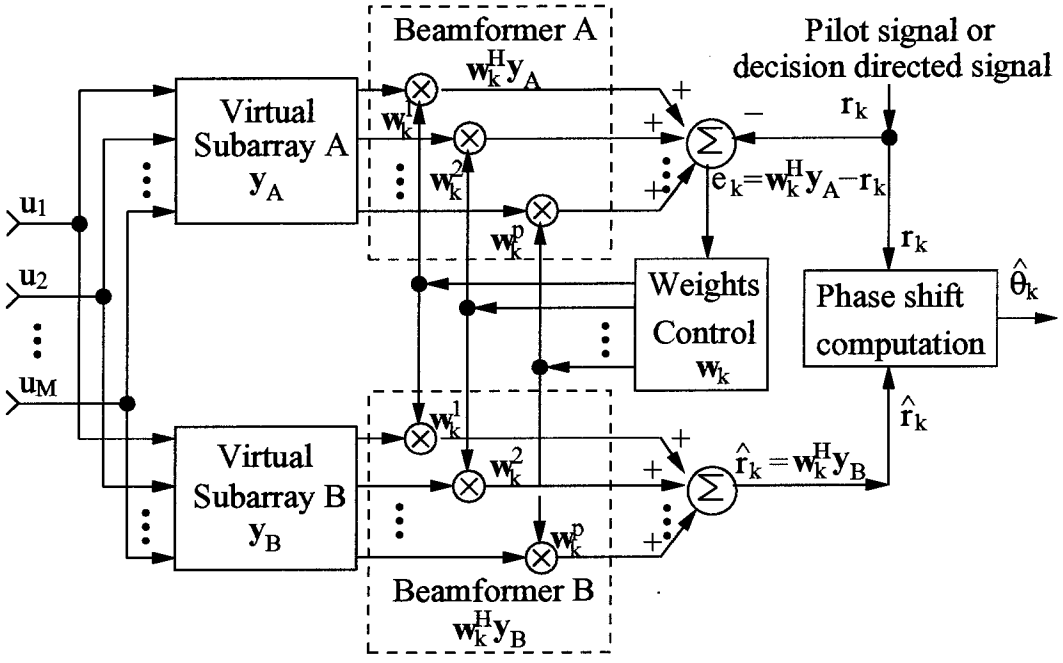

Figure 4.1. *Block diagram of the SBDOA system.*

can be used to obtain two virtual subarrays, namely, maximum overlapping subarrays (MOSs) [77] or conjugate subarrays (CSs) [15].

4.3.1.1 Use of Maximum Overlapping Subarrays

Consider an M-element ULA deployed at a receiver. MOSs have two sets of $(M-1)$-element virtual subarrays, A and B. Subarray A consists of the first $M-1$ elements of the M-element antenna array deployed at the receiver and subarray B consists of the last $M-1$ elements. If

$$u_m(t) = \sum_{k=1}^{K+J} z(\theta_k)^{m-1} s_k(t) \tag{4.4}$$

represents the down-converted baseband signals received by the mth element of the antenna array for $m = 1, 2, \ldots, M$, then the two $(M-1)$-dimension signal vectors of subarrays A and B are given by

$$\mathbf{y}_A(t) = [u_1(t)\ u_2(t)\ \cdots\ u_{M-1}(t)]^T \tag{4.5}$$

and

$$\mathbf{y}_B(t) = [u_2(t)\ u_3(t)\ \cdots\ u_M(t)]^T \tag{4.6}$$

respectively. If we let $\mathbf{b}(\theta_k) = [1\ z(\theta_k)\ \cdots\ z(\theta_k)^{M-2}]^T$, subarray signals $\mathbf{y}_A(t)$ and $\mathbf{y}_B(t)$ can be written as

$$\mathbf{y}_A(t) = \sum_{k=1}^{K+J} s_k(t)\mathbf{b}(\theta_k) + \mathbf{n}_A(t) \tag{4.7}$$

and

$$\mathbf{y}_B(t) = \sum_{k=1}^{K+J} z(\theta_k) s_k(t)\mathbf{b}(\theta_k) + \mathbf{n}_B(t) \tag{4.8}$$

where vectors $\mathbf{n}_A(t)$ and $\mathbf{n}_B(t)$ are the background noise at subarrays A and B, respectively. It can be seen from (4.7) and (4.8) that using MOSs, the phase shift between the kth signal components of $\mathbf{y}_B(t)$ and $\mathbf{y}_A(t)$ is an angle $\phi_k = \arg[z(\theta_k)]$ which is a function of the DOA, θ_k, of the kth component.

4.3.1.2 Use of Conjugate Subarrays

The use of CSs was originally proposed in conjugate ESPRIT (C-SPRIT) in [15]. In CSs, each virtual subarray has the same number of elements as the antenna array deployed. It has been shown in [15] that by using CSs, C-SPRIT can provide higher resolution and can estimate one more DOA than conventional ESPRIT using MOSs. This is due to the fact that CSs have one more antenna element in each subarray than MOSs. Similarly, as will be shown, using the SBDOA technique, CSs lead to more efficient subarray beamforming and provide higher estimation accuracy of the DOA than MOSs. However, CSs have limited applications due to the fact that the phase-shift relationship between each pair of signal components in the two signals $\mathbf{y}_A$ and $\mathbf{y}_B$ exists only when $s_k(t)$ is real.

Consider an M-element ULA deployed at a receiver. CSs have two sets of M-element virtual subarrays. The M-dimension signal vectors $\mathbf{y}_A$ of subarray A and $\mathbf{y}_B$ of subarray B are

$$\begin{aligned}\mathbf{y}_A(t) &= [u_1(t)\ u_2(t)\ u_3(t)\ \cdots\ u_M(t)]^T \\ &= \sum_{k=1}^{K+J} s_k(t)\mathbf{a}(\theta_k) + \mathbf{n}_A(t).\end{aligned} \tag{4.9}$$

and

$$\mathbf{y}_B(t) = [u_2(t)^*\ u_1(t)\ u_2(t)\ \cdots\ u_{M-1}(t)]^T \tag{4.10}$$

respectively. If $s_k(t)$ is real, then

$$\mathbf{y}_B(t) = \sum_{k=1}^{K+J} [z(\theta_k)]^* s_k(t)\mathbf{a}(\theta_k) + \mathbf{n}_B(t). \tag{4.11}$$

From (4.9) and (4.11), it can be seen that using CSs, the phase shift between the kth signal components of $\mathbf{y}_A(t)$ and $\mathbf{y}_B(t)$ is an angle $\phi_k = \arg\{[z(\theta_k)]^*\}$ which is a function of the DOA, θ_k, of the kth component.

4.3.1.3 Unifying Signal Models for MOSs and CSs

If we let the number of subarray elements in the above analysis be P, then a unified description of the SBDOA technique is obtained which applies to the MOSs geometry if $P = M - 1$ or to the CSs geometry if $P = M$. Thus we can write

$$\mathbf{y}_A(t) = \sum_{k=1}^{K+J} s_k(t)\tilde{\mathbf{a}}(\theta_k) + \mathbf{n}_A(t) \tag{4.12}$$

$$\mathbf{y}_B(t) = \sum_{k=1}^{K+J} e^{j\phi_k} s_k(t)\tilde{\mathbf{a}}(\theta_k) + \mathbf{n}_B(t) \tag{4.13}$$

where $\tilde{\mathbf{a}}(\theta_k) = [1 \; z(\theta_k) \; \cdots \; z(\theta_k)^P]^T$ is the subarray antenna response vector. The phase-shift factor between the kth components of signals $\mathbf{y}_A(t)$ and $\mathbf{y}_B(t)$ which originate from the kth signal is given by

$$e^{j\phi_k} = \begin{cases} z(\theta_k) = e^{-j2\pi D \sin\theta_k/\lambda} & \text{for MOSs} \\ [z(\theta_k)]^* = e^{j2\pi D \sin\theta_k/\lambda} & \text{for CSs} \end{cases}. \tag{4.14}$$

4.3.2 Subarray Beamforming

In the previous subsection, it has been shown that the phase of each signal component of $\mathbf{y}_B(t)$ is shifted relative to its corresponding signal component from the same source in $\mathbf{y}_A(t)$ by an angle ϕ_k. In this subsection, we will show that the optimum estimation of the phase-shifted reference signal at the output of beamformer B in the minimum mean-square error (MMSE) sense can be obtained by using beamforming weights obtained from beamformer A.

Consider the case where θ_k for $k = 1, 2, \ldots, K$ is the target DOA to be estimated. The purpose of beamformer B is to reject all the signal and interference components from sources other than source k and obtain an optimum estimation of the phase-shifted reference signal at the output of beamformer B. This can be achieved by solving the optimization problem

$$\underset{\mathbf{w}_k^B}{\text{minimize}} \; E\left[\left| (\mathbf{w}_k^B)^H \mathbf{y}_B(t) - e^{j\phi_k} r_k(t) \right|^2\right]. \tag{4.15}$$

In (4.15), r_k is the reference signal for signal k. It can be the pilot signal in the pilot channel-aided beamforming [78][79] or the decision-directed signal in the decision-directed signal-based beamforming techniques [80][26]. Since the phase-shift factor $e^{j\phi_k}$ is unknown, the phase-shifted reference signal $e^{j\phi_k}r_k(t)$ is not available. Thus, the weight vector $\mathbf{w}_k^B$ cannot be obtained directly from (4.15), but it can be obtained from the optimum weights of beamformer A as shown in Proposition 1 below.

Proposition 1: The weight vector $\mathbf{w}_k^B$ that solves the problem in (4.15) is the same as the weight vector $\mathbf{w}_k^A$ that solves the optimization problem

$$\underset{\mathbf{w}_k^A}{\text{minimize}}\ E\left[\mid (\mathbf{w}_k^A)^H \mathbf{y}_A(t) - r_k(t) \mid^2\right] \tag{4.16}$$

i.e., finding the optimum weight vector for beamformer A where the MSE, e_k, between the output signal of beamformer A and the known reference signal r_k is minimized.

Proof: The optimal weight vector $\mathbf{w}_k^A$ in (4.16) can be readily obtained in closed form as

$$\mathbf{w}_k^A = \mathbf{R}_A^{-1}\mathbf{h}_k^A \tag{4.17}$$

where

$$\mathbf{R}_A = E[\mathbf{y}_A(t)\mathbf{y}_A^H(t)] \tag{4.18}$$

$$\mathbf{h}_k^A = E\left\{[r_k(t)]^*\mathbf{y}_A(t)\right\} \tag{4.19}$$

are the autocorrelation matrix of the input signal $\mathbf{y}_A(t)$ and the cross-correlation vector between the input signal and the reference signal $r_k(t)$, respectively.

The optimum weight vector $\mathbf{w}_k^B$ in (4.15) can be obtained in closed form as

$$\mathbf{w}_k^B = \mathbf{R}_B^{-1}\mathbf{h}_k^B \tag{4.20}$$

where

$$\mathbf{R}_B = E[\mathbf{y}_B(t)\mathbf{y}_B^H(t)] \tag{4.21}$$

$$\mathbf{h}_k^B = E\left\{e^{-j\phi_k}[r_k(t)]^*\mathbf{y}_B(t)\right\}. \tag{4.22}$$

Substituting (4.12) and (4.13) into (4.18) and (4.21), respectively, yields

$$\mathbf{R}_A = \sum_{k=1}^{K+J} \sigma_k^2 \tilde{\mathbf{a}}(\theta_k)\tilde{\mathbf{a}}(\theta_k)^H + \sigma_A^2 \mathbf{I} \tag{4.23}$$

$$\mathbf{R}_B = \sum_{k=1}^{K+J} \sigma_k^2 \tilde{\mathbf{a}}(\theta_k)\tilde{\mathbf{a}}(\theta_k)^H + \sigma_B^2 \mathbf{I} \tag{4.24}$$

where $\sigma_k^2 = |s_k|^2$ is the power of a target signal component for $k = 1, 2, \ldots, K$ and is the power of an interference component for $k = K + J, 2, \ldots, K + J$, $\mathbf{I}$ is an identity matrix, and σ_A^2 and σ_B^2 are the variances of background noise vectors $\mathbf{n}_A$ and $\mathbf{n}_B$ in subarrays A and B, respectively. Based on the assumption that the background noise is spatially stationary, we have

$$\sigma_A^2 = \sigma_B^2 = \sigma^2 \tag{4.25}$$

and hence it follows that

$$\mathbf{R}_A = \mathbf{R}_B = \sum_{k=1}^{K+J} \sigma_k^2 \tilde{\mathbf{a}}(\theta_k)\tilde{\mathbf{a}}(\theta_k)^H + \sigma^2 \mathbf{I}. \tag{4.26}$$

Substituting (4.12) and (4.13) into (4.19) and (4.22), respectively, it can be shown that

$$\mathbf{h}_k^B = \mathbf{h}_k^A = \sigma_k \sigma_r \tilde{\mathbf{a}}(\theta_k) \tag{4.27}$$

where $\sigma_r^2 = |r_k|^2$ is the power of the reference signal r_k. From (4.26) and (4.27), we have

$$\mathbf{w}_k^B = \mathbf{w}_k^A. \tag{4.28}$$

Thus, Proposition 1 is proved.

Since $\mathbf{w}_k^B = \mathbf{w}_k^A$, the weight vector $\mathbf{w}_k^B$ can then be obtained by solving the problem in (4.16) using existing algorithms such as the direct approach [78] using (4.17) or the least-mean-square (LMS) algorithm [79][26].

4.3.3 Computation of DOA

Let $\hat{r}_k(t) = (\mathbf{w}_k^B)^H \mathbf{y}_B(t)$ denote the output signal of beamformer B. Since $\hat{r}_k(t)$ is an optimum estimation of the phase-shifted reference signal $e^{j\phi_k} r_k(t)$ in the MMSE sense, it can be written as

$$\hat{r}_k(t) = e^{j\phi_k} r_k(t) + n_k(t) \tag{4.29}$$

which represents the reference signal shifted by ϕ_k plus an estimation error. Let

$$\mathbf{r}_k = [r_k(1)\ r_k(2)\ \cdots\ r_k(L)]^T \tag{4.30}$$

$$\hat{\mathbf{r}}_k = [\hat{r}_k(1)\ \hat{r}_k(2)\ \cdots\ \hat{r}_k(L)]^T \tag{4.31}$$

denote vectors with samples of the reference signal and the estimated phase-shifted reference signal in a snapshot interval, respectively. If $\hat{\phi}_k$ denotes an estimate of ϕ_k, it can be computed using the least-square method such that the square error between the two signal vectors $\hat{\mathbf{r}}_k$ and $\mathbf{r}_k$ is minimized, i.e.,

$$\underset{\hat{\phi}_k}{\text{minimize}} \parallel \hat{\mathbf{r}}_k - e^{j\hat{\phi}_k} \mathbf{r}_k \parallel_2 \tag{4.32}$$

If $e^{j\hat{\phi}_k} = p + jq$ where $p^2 + q^2 = 1$, the optimization problem in (4.32) can be written as

$$\begin{aligned} \underset{p,q}{\text{minimize}}\ & f(p,q) = \parallel \hat{\mathbf{r}}_k - (p + jq)\mathbf{r}_k \parallel_2 \\ & \text{subject to}\ \ p^2 + q^2 = 1 \end{aligned} \tag{4.33}$$

This optimization problem can be easily solved using the Lagrange multipliers method and the solutions p and q can be obtained as

$$p = \left\{ \frac{[\mathrm{Re}(\hat{\mathbf{r}}_k^H \mathbf{r}_k)]^2}{[\mathrm{Re}(\hat{\mathbf{r}}_k^H \mathbf{r}_k)]^2 + [\mathrm{Im}(\hat{\mathbf{r}}_k^H \mathbf{r}_k)]^2} \right\}^{\frac{1}{2}} \tag{4.34}$$

and

$$q = -p \frac{\mathrm{Im}(\hat{\mathbf{r}}_k^H \mathbf{r}_k)}{\mathrm{Re}(\hat{\mathbf{r}}_k^H \mathbf{r}_k)}. \tag{4.35}$$

respectively. Hence

$$\hat{\phi}_k = \arg(\mathbf{r}_k^H \hat{\mathbf{r}}_k) \tag{4.36}$$

which is the angle of the complex inner product of the reference signal vector and its phase-shifted version. In light of (4.14), an estimation of the target DOA can then be obtained as

$$\hat{\theta}_k = \begin{cases} \arcsin\left(\dfrac{-\lambda\hat{\phi}_k}{2\pi D}\right) & \text{for MOSs} \\ \arcsin\left(\dfrac{\lambda\hat{\phi}_k}{2\pi D}\right) & \text{for CSs} \end{cases} . \tag{4.37}$$

In the proposed technique, the DOA is estimated from the phase shift between the reference signal and its phase-shifted version. Thus, the capacity of DOA estimation is no longer bounded by the number of antenna elements as in existing techniques. Most importantly, the DOAs are estimated after interference rejection through subarray beamforming and, therefore, the effect of co-channel interference on DOA estimation is reduced as will be verified through performance analysis and simulations in the next two sections.

4.4 Performance Analysis

In this section, the performance of the SBDOA technique will be analyzed. Proposition 2 below shows that the SBDOA estimator is an asymptotically consistent estimator. In Proposition 3, the probability-density function and the variance of the estimated DOA using the SBDOA technique are derived. Based on Proposition 3, the effects of snapshot length and signal-to-interference-plus-noise ratio (SINR) on DOA estimation can be investigated.

Proposition 2: The SBDOA estimator is an asymptotically consistent estimator, i.e.,

$$\lim_{L\to\infty} \triangle\theta_k = 0. \tag{4.38}$$

Proof: Let

$$\mathbf{n}_k = [n_k(1)\ n_k(2)\ \cdots\ n_k(L)]^T \tag{4.39}$$

denote the estimation error vector between the output of beamformer B and its desired response in a snapshot interval, L. Using (4.29), we have

$$\hat{\mathbf{r}}_k = e^{j\phi_k}\mathbf{r}_k + \mathbf{n}_k \tag{4.40}$$

and hence

$$\mathbf{r}_k = e^{-j\phi_k}(\hat{\mathbf{r}}_k - \mathbf{n}_k). \tag{4.41}$$

Substituting (4.41) into (4.36), the estimated phase shift $\hat{\phi}_k$ can be written as

$$\hat{\phi}_k = \phi_k + \arg(\hat{\mathbf{r}}_k^H\hat{\mathbf{r}}_k - \mathbf{n}_k^H\hat{\mathbf{r}}_k) \tag{4.42}$$

If

$$\triangle\phi_k = \hat{\phi}_k - \phi_k \tag{4.43}$$

denotes the estimation error of the phase shift of target source k, then we have

$$\begin{aligned}\triangle\phi_k &= \arg(\hat{\mathbf{r}}_k^H\hat{\mathbf{r}}_k - \mathbf{n}_k^H\hat{\mathbf{r}}_k) \\ &= \arg\left(\frac{\hat{\mathbf{r}}_k^H\hat{\mathbf{r}}_k - \mathbf{n}_k^H\hat{\mathbf{r}}_k}{L}\right).\end{aligned} \tag{4.44}$$

When $L \to \infty$, we have

$$\lim_{L\to\infty}\frac{\hat{\mathbf{r}}_k^H\hat{\mathbf{r}}_k}{L} = \lim_{L\to\infty}\frac{1}{L}\sum_{l=1}^{L}|\ \hat{r}_k(l)\ |^2 = E[|\ \hat{r}_k(t)\ |^2] \tag{4.45}$$

and

$$\lim_{L\to\infty}\frac{\mathbf{n}_k^H\hat{\mathbf{r}}_k}{L} = \lim_{L\to\infty}\frac{1}{L}\sum_{l=1}^{L}n_k^*(l)\hat{r}(l) = E[n_k^*(t)\hat{r}_k(t)] \tag{4.46}$$

where $E[\cdot]$ denotes expectation. Substituting (4.45) and (4.46) into (4.44) yields

$$\lim_{L\to\infty}\triangle\phi_k = \arg\left\{E\left[|\ \hat{r}_k(t)\ |^2\right] - E\left[n_k^*(t)\hat{r}_k(t)\right]\right\}. \tag{4.47}$$

It has been shown in Sec. 4.3.2 that $\mathbf{w}_k^B = \mathbf{w}_k^A$ and that the weight vector obtained from beamformer A is the optimal solution in the sense of minimizing (4.15). In light of the corollary to the principle of orthogonality of Wiener filters [63], the estimate of the desired response $\hat{r}_k(t)$ at the output of beamformer B and the corresponding estimation error $n_k(t)$ (4.29) are orthogonal to each other. Thus, we have

$$E[n_k^*(t)\hat{r}_k(t)] = 0. \tag{4.48}$$

Substituting (4.48) into (4.47) yields

$$\lim_{L\to\infty} \triangle\phi_k = \arg\{E[|\ \hat{r}_k(t)\ |^2]\} = 0. \tag{4.49}$$

From (4.37), we have

$$\triangle\theta_k = \begin{cases} \arcsin\left[\sin(\theta_k) - \dfrac{\lambda\triangle\phi_k}{2\pi D}\right] - \theta_k & \text{for MOSs} \\ \arcsin\left[\sin(\theta_k) + \dfrac{\lambda\triangle\phi_k}{2\pi D}\right] - \theta_k & \text{for CSs} \end{cases} \tag{4.50}$$

and by using (4.49)

$$\lim_{L\to\infty} \triangle\theta_k = \begin{cases} 0 & \text{for MOSs} \\ 0 & \text{for CSs} \end{cases}. \tag{4.51}$$

Thus, proposition 2 is proved.

Proposition 2 shows that the SBDOA estimator is an asymptotically consistent estimator such that the DOA estimation error will approach zero as the snapshot length approaches infinity. In many applications, a long snapshot length may be impractical and it is, therefore, important that a DOA estimator be able to track fast-changing DOAs based on limited signal samples. Proposition 3 below gives the probability-density function and variance of the estimated DOA, which will be used to evaluate the effect of snapshot length on the estimation accuracy and capacity of the proposed technique.

Proposition 3: The probability-density function and the variance of the estimated DOA using the SBDOA technique are given by

$$P_{\hat{\theta}_k}(\hat{\theta}_k) = \frac{2\pi D \mid \cos\hat{\theta}_k \mid}{\lambda} \int_0^\infty \int_0^\infty \rho P_v \left\{\rho \sin[\triangle\phi_k(\hat{\theta}_k)]\right\} \times P_\alpha(\alpha) P_\beta \left\{\rho\cos[\triangle\phi_k(\hat{\theta}_k)] - \alpha\right\} \, d\alpha d\rho \tag{4.52}$$

and

$$\mathrm{var}(\hat{\theta}_k) = \int_{-\pi/2}^{\pi/2} (\hat{\theta}_k - \theta_k)^2 P_{\hat{\theta}_k}(\hat{\theta}_k) \, d\hat{\theta}_k \tag{4.53}$$

respectively, where

$$\triangle\phi_k(\hat{\theta}_k) = \begin{cases} -\dfrac{2\pi D[\sin(\hat{\theta}_k) - \sin(\theta_k)]}{\lambda} & \text{for MOSs} \\ \dfrac{2\pi D[\sin(\hat{\theta}_k) - \sin(\theta_k)]}{\lambda} & \text{for CSs} \end{cases} \tag{4.54}$$

and P_α is the probability-density function of a chi-squared distributed random process whose degrees of freedom are equal to the snapshot length L, P_β and P_v are probability-density functions of two zero-mean Gaussian random processes. They are given by

$$P_\alpha(\alpha) = \frac{\alpha^{\frac{L}{2}-1} e^{-\frac{\alpha}{2}}}{\Gamma(\frac{L}{2}) 2^{\frac{L}{2}}} \tag{4.55}$$

$$P_\beta(\beta) = \frac{1}{\sigma_\beta\sqrt{2\pi}} e^{-\beta^2/(2\sigma_\beta^2)} \tag{4.56}$$

$$P_v(v) = \frac{1}{\sigma_v\sqrt{2\pi}} e^{-v^2/(2\sigma_v^2)} \tag{4.57}$$

where

$$\sigma_\beta^2 = \sigma_v^2 = \frac{L}{2}\left(\frac{\sigma_r^2}{\sigma_e^2} - 1\right)^{-1} = \frac{L}{2}\left(10^{\gamma_{SINR}/10} - 1\right)^{-1} \tag{4.58}$$

and σ_r^2 is the power of the reference signal $r_k(t)$, σ_e^2 is the power of the error signal $e_k(t)$ at the output of beamformer A, and γ_{SINR} is the SINR at the output of beamformer A.

Proof: From (4.44), we have

$$\triangle\phi_k = \arg\left[\sum_{l=1}^{L} \mid \hat{r}_k(l) \mid^2 - \sum_{l=1}^{L} n_k^*(l)\hat{r}_k(l)\right]. \tag{4.59}$$

If we let

$$\delta_{re}(l) = \mathrm{Re}[-n_k^*(l)\hat{r}_k(l)] \tag{4.60}$$

$$\delta_{im}(l) = \mathrm{Im}[-n_k^*(l)\hat{r}_k(l)] \tag{4.61}$$

be the real and imaginary components of $-n_k^*(l)\hat{r}_k(l)$, respectively, the estimation error of the phase shift in (4.59) can be written as

$$\triangle\phi_k = \arg\left[\sum_{l=1}^{L} \mid \hat{r}_k(l) \mid^2 + \sum_{l=1}^{L} \delta_{re}(l) + j\sum_{l=1}^{L} \delta_{im}(l)\right]. \tag{4.62}$$

Assuming that $\hat{r}_k$ is a complex Gaussian process with zero mean, it can be derived from (4.41) and (4.48) that

$$\mathrm{var}[\hat{r}_k(t)] = E[\hat{r}_k^*(t)\hat{r}_k(t)] = \sigma_r^2 - \sigma_n^2 \tag{4.63}$$

(see Appendix B) where

$$\sigma_r^2 = E[r_k^*(t)r_k(t)] \tag{4.64}$$

$$\sigma_n^2 = E[n_k^*(t)n_k(t)] \tag{4.65}$$

denote the powers of the reference signal and the estimation error, respectively.

From (4.48), we have

$$E[-n_k^*(t)\hat{r}_k(t)] = E[\delta_{re}(t)] + jE[\delta_{im}(t)] = 0. \tag{4.66}$$

Hence

$$E[\delta_{re}(t)] = E[\delta_{im}(t)] = 0 \tag{4.67}$$

i.e., random processes $\delta_{re}(t)$ and $\delta_{im}(t)$ have zero means. Assuming that $\delta_{re}(t)$ and $\delta_{im}(t)$ are two independent Gaussian processes with equal variances, it can be shown that

$$\mathrm{var}[\delta_{re}(t)] = \mathrm{var}[\delta_{im}(t)] = \sigma_n^2(\sigma_r^2 - \sigma_n^2)/2 \tag{4.68}$$

(see Appendix C). If we let

$$\alpha = \sum_{l=1}^{L} \frac{|\hat{r}_k(l)|^2}{\sigma_r^2 - \sigma_n^2} \tag{4.69}$$

$$\beta = \sum_{l=1}^{L} \frac{\delta_{re}(l)}{\sigma_r^2 - \sigma_n^2} \tag{4.70}$$

$$v = \sum_{l=1}^{L} \frac{\delta_{im}(l)}{\sigma_r^2 - \sigma_n^2} \tag{4.71}$$

the estimation error of the phase shift in (4.62) assumes the form

$$\Delta\phi_k = \arg(\alpha + \beta + jv). \tag{4.72}$$

Since $\hat{r}_k/\sqrt{\sigma_r^2 - \sigma_n^2}$ is also a Gaussian process with

$$E\left(\frac{\hat{r}_k}{\sqrt{\sigma_r^2 - \sigma_n^2}}\right) = 0 \tag{4.73}$$

$$\text{var}\left(\frac{\hat{r}_k}{\sqrt{\sigma_r^2 - \sigma_n^2}}\right) = 1 \tag{4.74}$$

random process α is chi-squared distributed with L degrees of freedom. Its probability-density function is given by (4.55). The random variables β and v are the sums of Gaussian variables and thus they are still Gaussian distributed. It can be shown that

$$E(\beta) = E(v) = 0 \tag{4.75}$$

i.e., β and v have zero means. The variances of β and v can be readily derived as

$$\sigma_\beta^2 = \sigma_v^2 = \frac{L\sigma_n^2}{2(\sigma_r^2 - \sigma_n^2)}. \tag{4.76}$$

It can be shown that

$$\sigma_e^2 = \sigma_n^2 \tag{4.77}$$

(see Appendix A), i.e., the error signal $e_k(t)$ at the output of beamformer A has the same power as error signal $n_k(t)$ at the output of beamformer B. If we let

$$\gamma_{SINR} = 10\log_{10}^{\sigma_r^2/\sigma_e^2} \tag{4.78}$$

be the SINR of the signal at the output of beamformer A, substituting (4.77) and (4.78) into (4.76) yields

$$\sigma_\beta^2 = \sigma_v^2 = \frac{L}{2}\left(\frac{\sigma_r^2}{\sigma_e^2} - 1\right)^{-1} = \frac{L}{2}\left(10^{\gamma_{SINR}/10} - 1\right)^{-1} \tag{4.79}$$

and the probability-density functions of β and v are given by (4.56) and (4.57), respectively.

The probability-density function of $\triangle\phi_k$ can now be derived as (see Appendix B for details)

$$\begin{aligned} P_{\triangle\phi_k}(\triangle\phi_k) = &\int_0^\infty \int_0^\infty \rho P_v[\rho \sin(\triangle\phi_k)] \\ &\times P_\alpha(\alpha) P_\beta[\rho\cos(\triangle\phi_k) - \alpha]\, d\alpha d\rho. \end{aligned} \tag{4.80}$$

and from (4.50), we have

$$\triangle\phi_k(\hat{\theta}_k) = \begin{cases} -\dfrac{2\pi D[\sin(\hat{\theta}_k) - \sin(\theta_k)]}{\lambda} & \text{for MOSs} \\ \dfrac{2\pi D[\sin(\hat{\theta}_k) - \sin(\theta_k)]}{\lambda} & \text{for CSs} \end{cases}. \tag{4.81}$$

The probability-density function of $\hat{\theta}_k$ is thus obtained as

$$P_{\hat{\theta}_k}(\hat{\theta}_k) = \left|\triangle\phi_k'(\hat{\theta}_k)\right| P_{\hat{\phi}_k}[\triangle\phi_k(\hat{\theta}_k)] \tag{4.82}$$

where $\triangle\phi_k'(\hat{\theta}_k)$ is the derivative of function $\triangle\phi_k(\hat{\theta}_k)$ with respect to $\hat{\theta}_k$. It can be written as

$$\begin{aligned} P_{\hat{\theta}_k}(\hat{\theta}_k) = &\frac{2\pi D \mid \cos\hat{\theta}_k \mid}{\lambda} \int_0^\infty \int_0^\infty \rho P_v \left\{\rho \sin[\triangle\phi_k(\hat{\theta}_k)]\right\} \\ &\times P_\alpha(\alpha) P_\beta \left\{\rho\cos[\triangle\phi_k(\hat{\theta}_k)] - \alpha\right\} d\alpha d\rho. \end{aligned} \tag{4.83}$$

The variance of the estimated $\hat{\theta}_k$ can then be obtained as

$$\mathrm{var}(\hat{\theta}_k) = \int_{-\pi/2}^{\pi/2} (\hat{\theta}_k - \theta_k)^2 P_{\hat{\theta}_k}(\hat{\theta}_k)\, d\hat{\theta}_k. \tag{4.84}$$

Thus, Proposition 3 is proved.

Plots of the probability-density function of the estimated DOA in degrees for different snapshot lengths and SINRs at the output of beamformer B are illustrated in Figs. 4.2 and 4.3. It can be seen from Fig. 4.2 that a higher estimation accuracy can be obtained using a longer snapshot length. This is consistent with Proposition 1. Similarly, Fig. 4.3 shows that the a higher SINR will lead to a better estimation accuracy. Thus, the number of sources detectable using the SBDOA technique is not limited by the number of antenna elements and the accuracy of DOA estimation can be improved by an efficient interference rejection through subarray beamforming. Therefore, high capacity and improved resolution of DOA estimation can be achieved using the SBDOA technique.

4.5 Simulation Results

In this section, the resolution, capacity, and accuracy of the SBDOA technique will be evaluated and compared with those of existing techniques through simulations. The term resolution of DOA estimation is used to denote the minimum angle difference between two DOAs that can be resolved by the estimation technique. The term capacity is used to denote the maximum number of signal sources that a DOA estimation technique is capable of detecting. In Examples 1 and 2, the resolution and capacity of the DOA estimation using the SBDOA technique and existing techniques will be compared and illustrated. In Example 3, the effects of snapshot length and strength of interference on the estimation capacity and accuracy will be investigated.

4.5.1 Example 1: Resolution of DOA Estimation

Example 1 deals with a case where the DOAs of five signal and interference sources are closely distributed. A 6-element ULA with a spacing of $D = \lambda/2$ deployed at the receiver was considered. Three target signal components with a pilot signal and two unknown interference components were assumed to be received at the antenna

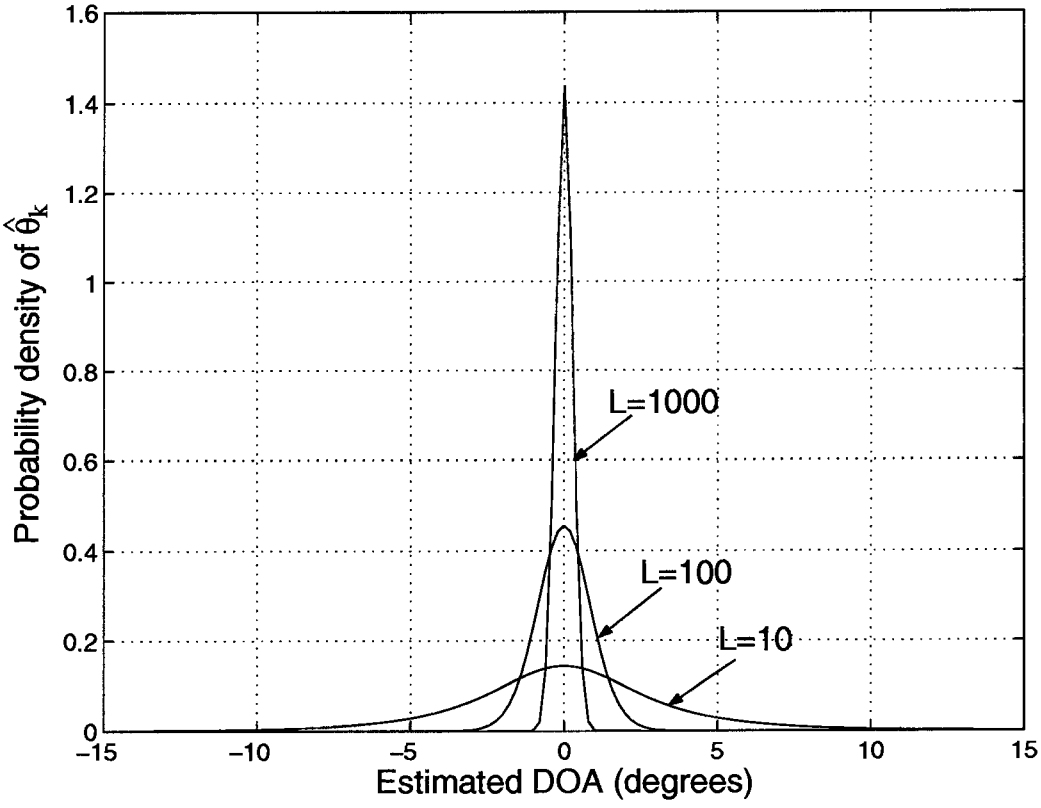

Figure 4.2. *Effect of the snapshot length L on the estimated DOA (plots of probability-density function for $\gamma_{SINR} = 5dB$, $L = 10, 100, 1000$ and the target DOA $\theta_k^o = 0^o$).*

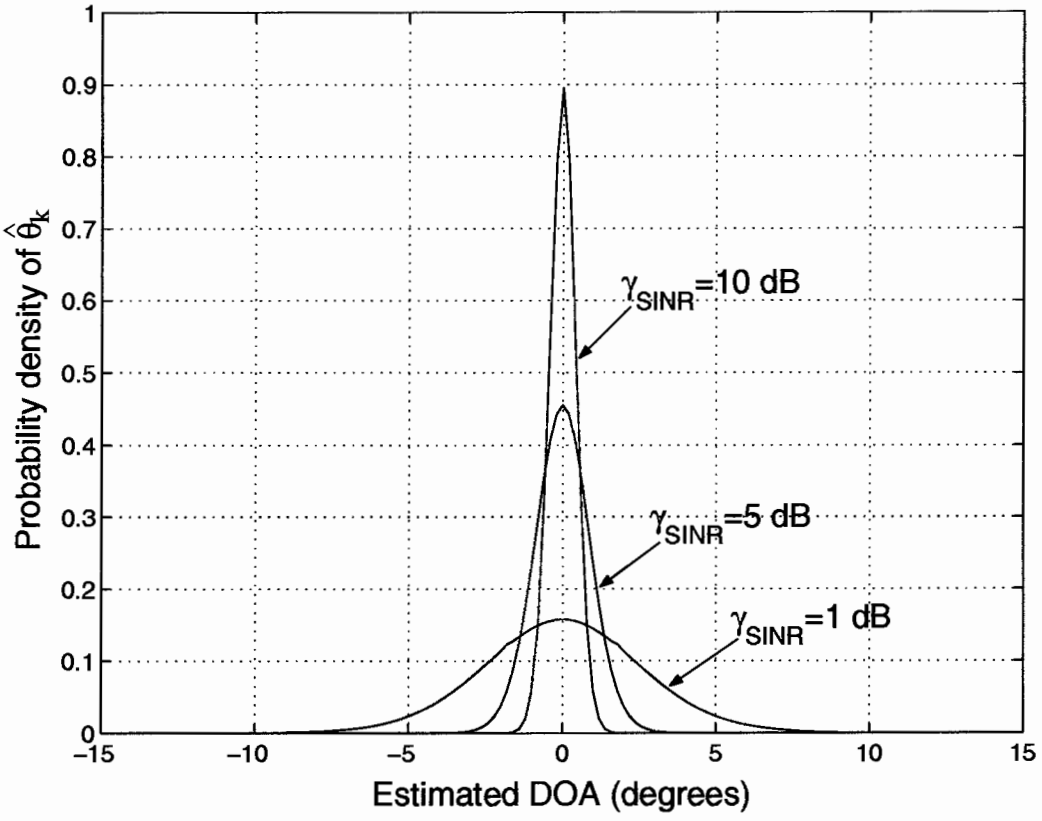

Figure 4.3. *Effect of the SINR γ_{SINR} at the output of beamformer B on the estimated DOA (plots of probability-density function for $\gamma_{SINR} = 1dB,\ 5dB,\ 10dB$, $L = 100$ and the target DOA $\theta_k^o = 0^o$).*

array with equal power. It was further assumed that the DOAs of the target signal components were at -2^o, 0^o and 2^o. The DOAs of the interference components were at -4^o and 4^o. The information bit-to-background noise (not including interference components) power spectral density ratio (E_b/N_0) of the received signal was set to 15 dB. Ten thousand simulation runs were performed. For each run, the DOA was obtained using MUSIC [10], ESPRIT [12] using MOSs, ESPRIT using CSs (C-SPRIT) [15], Capon [7], the decoupled ML (DEML) algorithm [17], the spatial signature based ML (SSBML) estimation technique [18] with the assumption that the delays are known, and the proposed SBDOA technique using MOSs or CSs were used to obtain the DOAs. A snapshot length of 200 samples was used for all techniques to assure a fair comparison. The subarray beamforming weights for the SBDOA technique were obtained by applying the direct approach using (17). The histograms obtained for the various techniques are shown in Fig. 4. Each histogram depicts the number of occurrences of each estimated DOA as a function of DOA in degrees. The actual DOAs of different signals are marked at the top of each figure by triangles. In Fig. 4.4(a-d), only one or two peaks can be seen in the histogram plots indicating that existing techniques do not lead to satisfactory results when the signals' DOAs are very close. In contrast, the histogram plots in Fig. 4.4(e-f) show three peak values indicating that using the proposed SBDOA technique all the three DOAs are successfully estimated. This confirms that the SBDOA technique leads to a better resolution than existing techniques. Further, it can be seen by comparing Figs. 4.4(e) and 4.4(f) that the resolution of the SBDOA technique using CSs is better than that obtained using MOSs. This is due to the fact that CSs have one more element than MOSs in each subarray which will lead to higher SINR at the beamformer output for CSs. This is consistent with Proposition 3 where it was shown that an increase in SINR leads to better estimation accuracy.

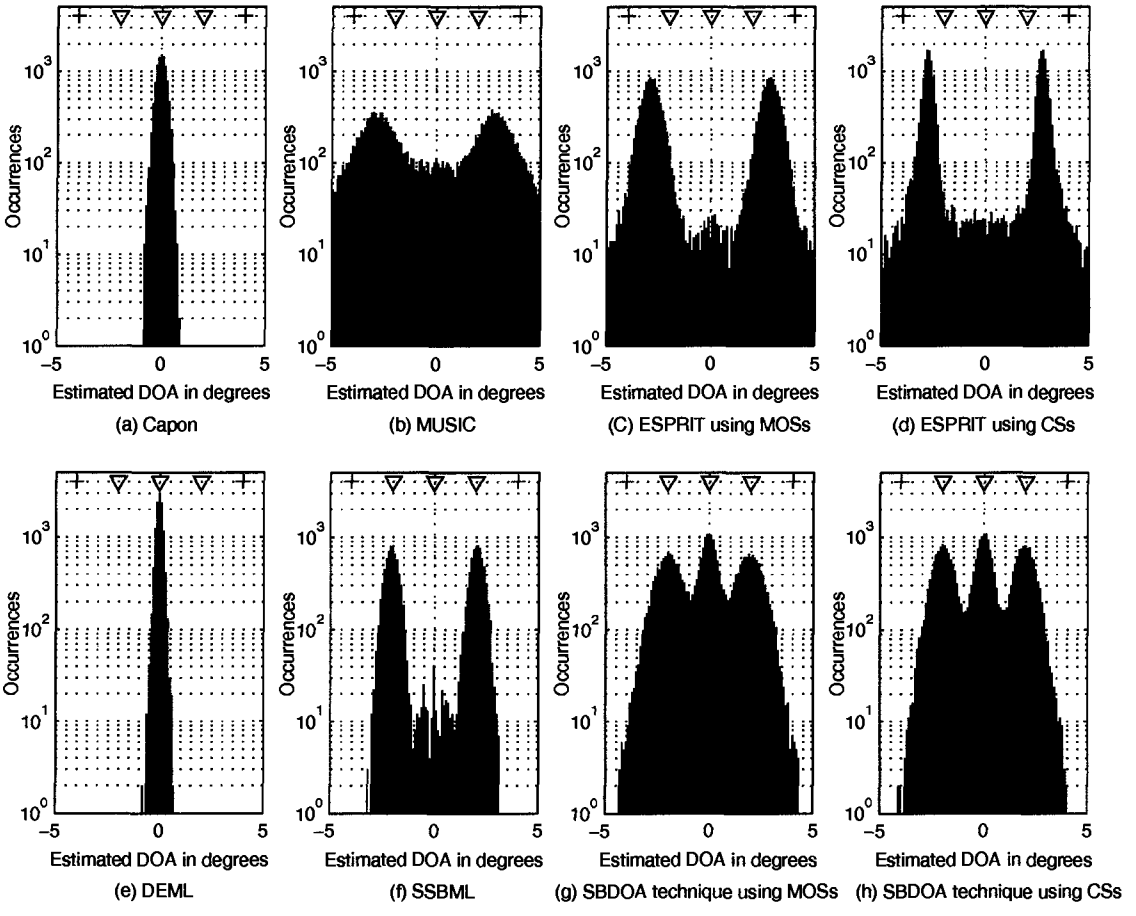

Figure 4.4. *Example 1: Comparison of the resolution of DOA estimation for signal sources which are closely distributed. A snapshot length of 200 samples was used for all techniques. The vertical axis represents the number of times that a certain value of estimated DOA was obtained. The triangles at the top indicate the actual DOAs of 3 target signal components at -2^o, 0^o, and 2^o. The pluses at the top indicate the DOAs of 2 interference components at 4^o and -4^o.*

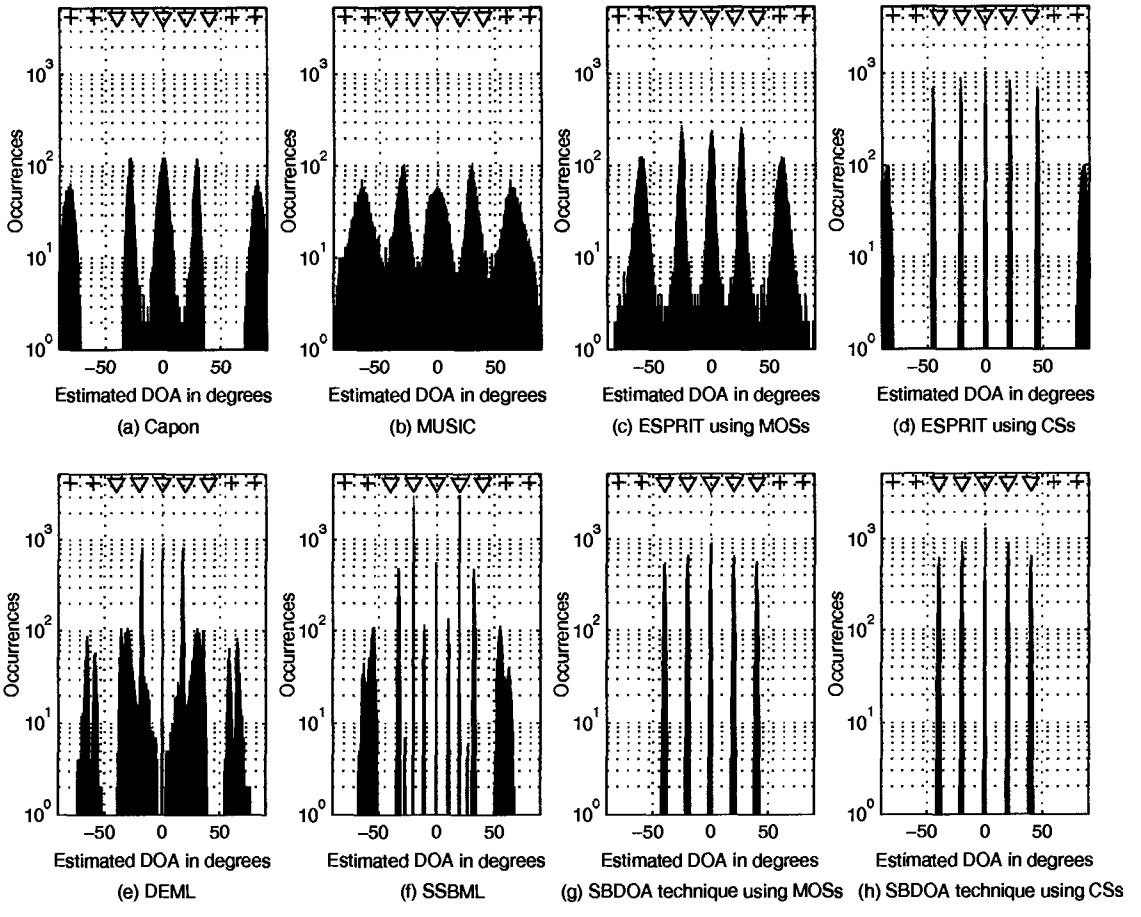

Figure 4.5. *Example 2: Example 2: Comparison of the capacity of DOA estimation when the number of signal and interference sources is larger than the number of antenna elements. A snapshot length of 200 samples was used for all techniques. The vertical axis represents the number of times that a certain value of estimated DOA was obtained. The triangles at the top indicate the actual DOAs of 5 target signal components at* -40^o, -20^o, 0^o, 20^o, *and* 40^o. *The pluses at the top indicate the DOAs of 4 interference components at* -80^o, -60^o, 60^o, *and* 80^o.

4.5.2 Example 2: Capacity and Accuracy of DOA Estimation

Example 2 deals with a case where the number of signal and interference sources is larger than the number of antenna elements. All simulation conditions were kept the same as in Example 1 except the number of signal sources considered. Five target signal components with pilot and four unknown interference components were assumed to be received at the antenna array with equal power. The DOAs of the five target signal components were set to -40^o, -20^o, 0^o, 20^o, and 40^o. The DOAs of the four interference components were at -80^o, -60^o, 60^o, and 80^o. Histograms of the estimated DOAs obtained are shown in Fig. 4.5. As expected, Fig. 4.5 (a-d) demonstrates that the subspace-based techniques investigated do not provide an acceptable DOA estimation if the total number of interference and signal components is larger than the number of antenna elements. Fig. 4.5 (e-f) shows that the DEML and SSBML techniques lead to several local suboptimal solutions and are sensitive to the interference. In contrast, all the 5 target DOAs were successfully estimated when the proposed SBDOA technique was used. This confirms that the proposed technique has a higher estimation capacity and accuracy than existing techniques. This improvement will be further illustrated by means of simulations considering more signal sources in Example 3. The capacity of DOA estimation for different techniques is summarized in Table 4.1.

4.5.3 Example 3: Effects of Snapshot Length and Interference on Estimation Capacity and Accuracy

In Example 3, the snapshot length for subarray beamforming and DOA computation was set to different values, i.e., 20, 30, 50, 100 and 1000, and the number of signal sources varied from 4 to 20. The DOA of the target signal with pilot was fixed at 0^o and the DOAs of unknown signals from other sources were randomly distributed from -90^o to 90^o in each simulation run. All other simulation conditions were kept

Table 4.1. *Capacity of DOA Estimation for Different Techniques*

	subarrays	capacity
Capon	N/A	$M-1$
MUSIC	N/A	$M-1$
ESPRIT	MOSs	$M-1$
	CSs	M
DEML	N/A	$> M$
SSBML	N/A	$\gg M$
SBDOA	MOSs	$\gg M$
	CSs	$\gg M$

the same as in Example 1. The root-mean-square error (RMSE) of the estimated target DOA averaged over 10000 simulation runs versus the number of signal sources and the snapshot length are illustrated in Fig. 4.6. As can be seen, using a small snapshot length such as 50, the proposed SBDOA technique leads to an RMSE of less than 4 degrees in the presence of 20 equal-powered signals. This demonstrates the fast DOA tracking capability of the SBDOA technique and further confirms that its estimation capacity can be larger than the number of antenna elements. It can also be seen in Fig. 4.6 that the RMSE decreases as the snapshot length increases. This confirms the performance analysis in Sec. 4.4 that the capacity and accuracy of the DOA estimation can be improved by increasing the snapshot length.

4.6 SBDOA for CDMA Communication Systems

4.6.1 DOA Estimation in CDMA Communication Systems

In CDMA communication systems, the number of signal sources is generally much larger than the number of antenna elements. In order to overcome the limitation

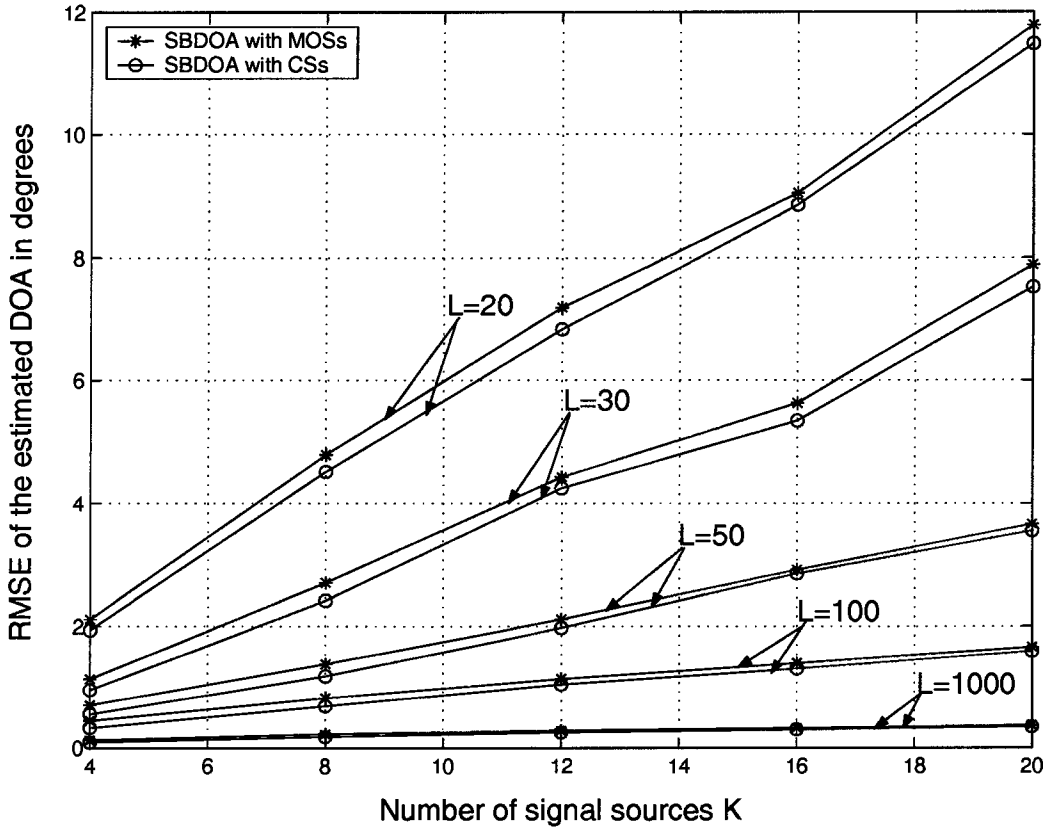

Figure 4.6. *Example 3: Root-mean-square error of the estimated DOA for different snapshot length L and number of signal sources K.*

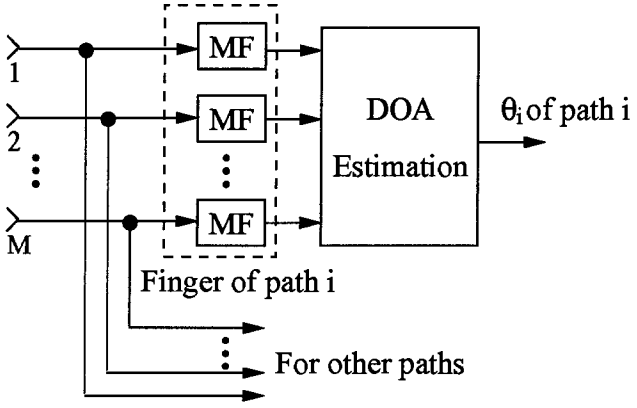

Figure 4.7. *DOA estimation for CDMA communication systems.*

of capacity and improve the accuracy of DOA estimation, the code-matched filter and parallel MUSIC algorithm for asynchronous DS-CDMA system is proposed in [19]. In [20], the ESPRIT is implemented on received signals after despreading. The block diagram of DOA estimation using these techniques is illustrated in Fig. 4.7. The down-converted baseband signals received from M antenna elements are firstly passed through a set of symbol-rate MFs (or code correlators) which are matched to the delay of the target path and then fed into the DOA estimator. Since the power of the interference can be significantly reduced after despreading, it can be assumed that the signals at the output of the symbol-rate MFs can be approximately modeled as the signal received from the target DOA plus white noise. In such a case, the target DOA can be successfully estimated using existing techniques. However, this assumption may not be hold in 3G and future wireless communication systems due to the increasing multiple-bit-rate service and multiple QoSs. In these systems, the despreaded signal may consist of many interfering components with high strength and the signal from target DOA may not be dominant. As a result, the performance of a DOA estimator using existing techniques will be significantly affected by interference even though it operates on the despreaded signals.

Pilot signals, particularly user-specific pilot signals, which can be used as reference

signal in the DOA estimation, make the SBDOA estimator more suitable for 3G mobile communication systems. In the uplink of UMTS, a DPCCH is used to transmit pilot symbols at each MS [4]. In the downlink, S-CPICHs are supported so that the MSs can use it to detect the signal coherently. In the CDMA2000 systems, dedicated pilot channels are provided in the uplink. In the downlink, code multiplexed auxiliary pilots are supported by assigning a different orthogonal code to each pilot when adaptive beamforming is used [23].

In mobile communication systems, the SBDOA estimator operates also on the despreaded signals if there is a large number of MSs in a service area. Since the DOA is estimated from the despreaded signals after subarray beamforming, the effect of interference on the DOA estimation is further reduced relative to that in existing techniques where the interference is rejected by despreading alone. As will be shown, this leads to a significant performance improvement relative to that of using existing techniques.

4.6.2 Simulation Results

4.6.2.1 Example 4: Capacity and accuracy of DOA estimation

Example 4 deals with asynchronous DS-CDMA systems with a 6-element linear antenna array deployed at the BS. Mobile stations ranging from 10 to 30 were considered in the simulation. Three uplink signal paths with 10^o spacing and Rayleigh fading channels with maximum Doppler frequency $f_d = 50$ Hz for each mobile station were assumed. The spacing of the antenna elements was set to $d = \lambda/2$. The information bit-to-background power spectral density ratio (E_b/N_0) of the received signal was set to 15 dB. A data rate of 64 kbps was assumed in the uplink. Gold codes of length 63 were used as the spreading codes. Ten thousand simulation runs were evaluated. In each simulation run, the DOA of the target signal was fixed at 0^o and the DOAs of other mobile stations were randomly distributed from -90^o to 90^o. MUSIC [19],

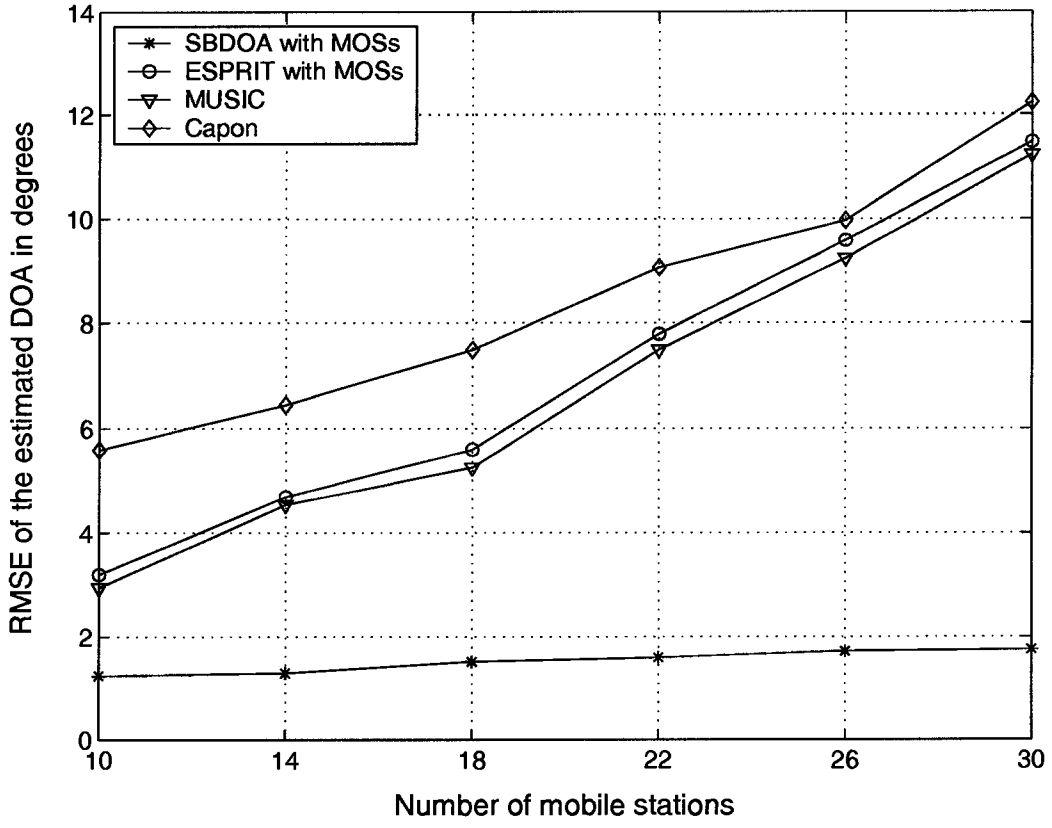

Figure 4.8. *Example 4: RMSE of the estimated DOA versus the number of MSs.*

ESPRIT [20] with maximum overlapped subarrays, Capon [7], and the proposed SBDOA were implemented using the despreaded signals to obtain the DOAs at the BS. The snapshot length was set to 50 samples for all these techniques. The root-mean-square error (RMSE) of the target DOA averaged over 10000 runs versus the number of mobile stations is illustrated in Fig. 4.8. As can be seen, the SBDOA technique leads to better estimation accuracy than the existing technique investigated. In addition, it leads to acceptable accuracy in the case of a large number of mobile stations. This further verifies that it has significantly higher estimation capacity than existing techniques.

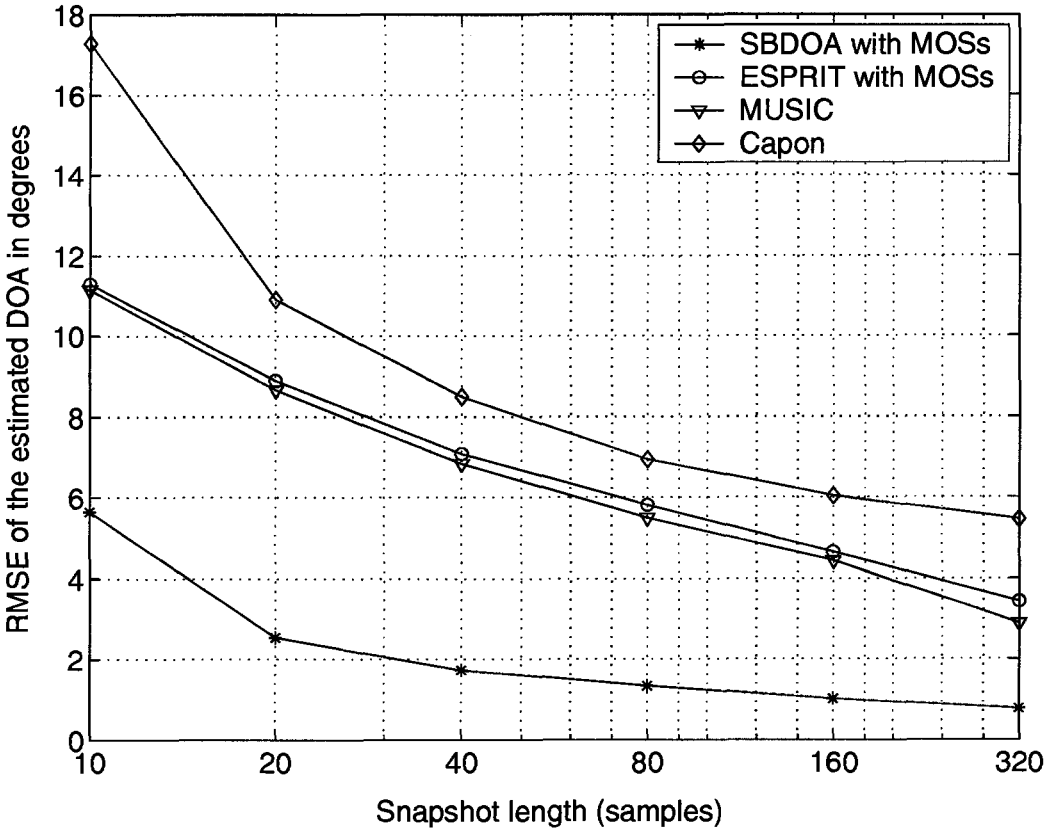

Figure 4.9. *Example 5: RMSE of the estimated DOA versus snapshot length.*

4.6.2.2 Example 5: Tracking capability and effect of snapshot length

Example 5 deals with the case of 20 mobile stations and different snapshot lengths ranging from 10 to 320 for DOA estimation. All other simulation conditions were kept the same as in Example 1. The RMSE of the target DOA averaged over 10000 simulation runs versus the snapshot length is illustrated in Fig. 4.9. As can be seen, the proposed SBDOA technique requires a significantly shorter snapshot for a given estimation accuracy than existing techniques. This demonstrates the fast DOA tracking capability of the proposed technique.

4.7 Conclusions

A new DOA estimation technique based on subarray beamforming has been proposed. In the new technique, two subarray beamformers are used to obtain an optimum estimation of the phase-shifted reference signal whose phase relative to the reference signal is a function of the target DOA. The target DOA is estimated from the phase shift between the reference signal and its phase-shifted version. In this way, the effect of interference on DOA estimation is reduced and the number of signal sources detectable can exceed the number of antenna elements. Performance analysis as well as extensive simulations have shown that the proposed technique leads to increased resolution, capacity, tracking capability, and improved accuracy of DOA estimation relative to those achieved with existing techniques.

Chapter 5

Weighted Downlink Beamforming Algorithm for Wireless Communications

5.1 Introduction

In the previous chapter, the SBDOA estimator was developed and the performance of different DOA estimators was evaluated with respect to their estimation capacity, resolution, tracking capability, and accuracy. In this chapter, a new weighted downlink SUB algorithm is proposed based on the estimated DOAs, and the performance of the new SUB algorithm is compared with that of some conventional ones [36]-[40].

As discussed in Chapter 2, the objective of conventional generalized eigenvalue-based SUB algorithms is to adaptively adjust the beamforming weights so that the transmitted power from the BS is concentrated towards the direction of the target MS and its interference on the downlink signals to other MSs is reduced. In wireless communication systems, particularly 3G and future wireless communication systems, downlink signals to different MSs have different power levers due to power control, multiple-bit-rate service requirements, and multiple QoSs constraints. Thus, they have different resistance to the co-channel interference caused by the downlink signals to other MSs. In conventional SUB algorithms, this difference is not taken into

consideration in the determination of beamforming weights and, therefore, a system using these algorithms suffers from, what is called, the near-far problem. This means that a low-power signal is significantly affected by the high-power signals. Based on this observation, a new downlink SUB algorithm will now be proposed. The objective is to improve the overall system performance by reducing the power of co-channel interference in the direction of an MS whose downlink signal has low power. The power of the downlink signal to a target MS radiated in the direction of other MSs is weighted by the relative interfering strength of the downlink signal to the target MS on the downlink signals to other MSs. Thus, less power is radiated in the direction of MSs whose downlink signals are sensitive to interference. Numerical results have shown that the proposed SUB algorithm leads to a lower system outage probability relative to conventional SUB algorithms.

The organization of the chapter is as follows: The proposed weighted downlink SUB algorithm is presented in Sec. 5.2. In Sec. 5.3, numerical results pertaining to the beam pattern and outage probability for the proposed SUB algorithm and conventional SUB algorithms are presented. Conclusions are drawn in Sec. 5.4.

5.2 Downlink SUB

5.2.1 Conventional Downlink SUB Algorithms

In chapter 2, conventional downlink SUB algorithms [36]-[40] was introduced. In this section, the performance of these algorithms will be further discussed. Assuming that MS u is the target user, the optimization problem in (2.30) can be rewritten as

$$\underset{\mathbf{w}_u}{\text{maximize}} \left\{ \frac{p_{u,u}}{\sum_{\substack{j=1 \\ j\neq u}}^{K} p_{j,u}} \right\} \tag{5.1}$$

where $p_{u,u}$ and $p_{j,u}$ depend on the information available about the downlink channel gain. If the BS operates in 'open-loop' [84][85], full information about the downlink

channel may not be available. The downlink SUB is based on the DOAs obtained from the uplink. In such a case, $p_{u,u}$ is the BS transmitted signal power in the direction of MS u, and $p_{j,u}$ is the power of the co-channel interference radiated in the direction of MS j caused by the downlink signal to MS u. If the BS operates in 'closed-loop' [43][86], the downlink channel gain and direction of departure will be estimated. In such a case, $p_{u,u}$ is the received downlink signal power at MS u, and $p_{j,u}$ is the received power of the co-channel interference at MS j caused by the downlink signal to MS u.

It should be noted that using (5.1), the beamforming weight vector is derived independently of the required downlink signal power and, therefore, it provides only the direction of the optimal weight vector. The optimization problem in (5.1) can be combined with the required downlink signal power p_u, determined from the downlink power control, to obtain the beamforming weight vector $\mathbf{w}_u$. Based on the above discussion, the optimization problem for the conventional generalized eigenvalue-based beamforming algorithms can be formulated as

$$\begin{aligned} &\underset{\mathbf{w}_u}{\text{maximize}} \left\{ \frac{p_{u,u}}{\sum_{\substack{j=1 \\ j \neq u}}^{K} p_{j,u}} \right\} \\ &\text{subject to } p_{u,u} = p_u \end{aligned} \tag{5.2}$$

5.2.2 New Weighted Downlink SUB Algorithm

Consider the situation where the power of signals transmitted from the BS to the MS vary due to power control or multiple-bit-rate services. Downlink signals to different MSs have different resistance to the co-channel interference caused by the downlink signals to other MSs. Conventional generalized eigenvalue-based beamforming algorithms [36]-[40], as formulated in (5.2), are equivalent to minimizing the power of the interference to other MSs for a given power level p_u by solving the optimization

problem

$$\begin{aligned} &\underset{\mathbf{w}_u}{\text{minimize}} \left\{ \sum_{\substack{j=1 \\ j \neq u}}^{K} p_{j,u} \right\} \\ &\text{subject to } p_{u,u} = p_u \end{aligned} \tag{5.3}$$

The fact that downlink signals to different MSs have different resistance to co-channel interference is not taken into consideration in these algorithms. When the power of the downlink signal to the target MS u $p_{u,u}$ is high, the signal will interfere with the downlink signals to other MSs, in particular with those that have low power. Using the conventional algorithms, an MS whose downlink signal has low power may receive the same amount of interference as an MS whose downlink signal has high power. As a result, the received SIR of an MS whose downlink signal has low power may be far less than that of an MS whose downlink signal has high power.

To take into consideration the difference in the resistance to the co-channel interference, a weighted downlink SUB algorithm is proposed for obtaining the beamforming weight vector $\mathbf{w}_u$ for the target MS u.

Given a power level p_u, the objective of the algorithm is to minimize the relative power of the interference caused by the downlink signal to the target MS u. The optimization problem is thus formulated as

$$\begin{aligned} &\underset{\mathbf{w}_u}{\text{minimize}} \left\{ \sum_{\substack{j=1 \\ j \neq u}}^{K} \frac{p_{j,u}}{p_j} \right\} \\ &\text{subject to } p_{u,u} = p_u \end{aligned} \tag{5.4}$$

Eq. (5.4) can be rewritten as

$$\begin{aligned} &\underset{\mathbf{w}_u}{\text{minimize}} \left\{ \frac{p_{u,u}}{\sum_{\substack{j=1 \\ j \neq u}}^{K} \alpha_{j,u} p_{j,u}} \right\} \\ &\text{subject to } p_{u,u} = p_u \end{aligned} \tag{5.5}$$

where weighting coefficient $\alpha_{j,u}$ is given by

$$\alpha_{j,u} = \frac{p_u}{p_j} \tag{5.6}$$

and can be interpreted as the relative interference strength (RIS) of the downlink signal to MS u on the downlink signal to MS j.

As mentioned before, the expressions for p_j, $p_{u,u}$, and $p_{j,u}$ depend on information available about the downlink channel gain. If such information is not available and the downlink SUB is based on the DOAs obtained from the uplink, p_j is the BS transmitted signal power in the direction of MS j. In this case, $p_{u,u}$ is the BS transmitted signal power in the direction of the target MS u, and $p_{j,u}$ is the power of the co-channel interference radiated in the direction of MS j caused by the downlink signal to the target MS u. They are given by

$$p_{u,u} = \mathbf{w}_u^H \left(\sum_{l=1}^{L_u} \mathbf{R}_{u,l} \right) \mathbf{w}_u \tag{5.7}$$

and

$$p_{j,u} = \mathbf{w}_u^H \left(\sum_{l=1}^{L_j} \mathbf{R}_{j,l} \right) \mathbf{w}_u \tag{5.8}$$

respectively where matrices $\mathbf{R}_{u,l}$ and $\mathbf{R}_{j,l}$ are given by

$$\mathbf{R}_{u,l} = \mathbf{a}_{u,l}\mathbf{a}_{u,l}^H$$

and

$$\mathbf{R}_{j,l} = \mathbf{a}_{j,l}\mathbf{a}_{j,l}^H$$

respectively.

If information about the downlink channel gain is available, then p_j is the received downlink signal power at MS j. In this case, $p_{u,u}$ is the received downlink signal power

at the target MS u, and $p_{j,u}$ is the received power of the co-channel interference at MS j caused by the downlink signal to MS u. They are given by

$$p_{u,u} = \mathbf{w}_u^H \left(\sum_{l=1}^{L_u} \mathbf{R}_{u,l} \right) \mathbf{w}_u \tag{5.9}$$

and

$$p_{j,u} = \mathbf{w}_u^H \left(\sum_{l=1}^{L_j} \mathbf{R}_{j,l} \right) \mathbf{w}_u \tag{5.10}$$

respectively where matrices $\mathbf{R}_{u,l}$ and $\mathbf{R}_{j,l}$ are given by

$$\mathbf{R}_{u,l} = E[|\beta_{u,l}|^2]\mathbf{a}_{u,l}\mathbf{a}_{u,l}^H$$

and

$$\mathbf{R}_{j,l} = E[|\beta_{j,l}|^2]\mathbf{a}_{j,l}\mathbf{a}_{j,l}^H$$

respectively.

The optimization problem in (5.5) can be rewritten as

$$\begin{aligned} \underset{\mathbf{w}_u}{\text{maximize}} \quad & \frac{\mathbf{w}_u^H (\sum_{l=1}^{L_u} \mathbf{R}_{u,l}) \mathbf{w}_u}{\mathbf{w}_u^H \left[\sum_{\substack{j=1 \\ j \neq u}}^{K} (\alpha_{j,u} \sum_{l=1}^{L_j} \mathbf{R}_{j,l}) + \sigma^2 \mathbf{I} \right] \mathbf{w}_u} \\ \text{subject to} \quad & \mathbf{w}_u^H \left(\sum_{l=1}^{L_u} \mathbf{R}_{u,l} \right) \mathbf{w}_u = p_u \end{aligned} \tag{5.11}$$

where $\sigma^2\mathbf{I}$ is introduced to increase the algorithm robustness to channel uncertainties [35]. Let $\hat{\mathbf{w}}_u$ denote the normalized vector of $\mathbf{w}_u$. It can be obtained by maximizing the objective function in (5.11). The optimum solution is the eigenvector associated with the largest eigenvalue of the generalized eigenvalue problem [22] given by

$$\left(\sum_{l=1}^{L_u} \mathbf{R}_{u,l} \right) \hat{\mathbf{w}}_u = \lambda_{max} \left(\sum_{\substack{j=1 \\ j \neq u}}^{K} \alpha_{j,u} \sum_{l=1}^{L_j} \mathbf{R}_{j,l} + \sigma^2 \mathbf{I} \right) \hat{\mathbf{w}}_u$$

and $\mathbf{w}_u$ can be derived as

$$\mathbf{w}_u = \left[\frac{p_u}{\hat{\mathbf{w}}_u^H \left(\sum_{l=1}^{L_u} \mathbf{R}_{u,l} \right) \hat{\mathbf{w}}_u} \right]^{\frac{1}{2}} \hat{\mathbf{w}}_u \tag{5.12}$$

In this new weighted downlink SUB algorithm, the power of co-channel interference in the direction of other MSs is weighted by the corresponding RISs (5.6) of the downlink signal to the target MS. The larger the RIS of the downlink signal to the target MS u on the downlink signal to another MS, the less power is radiated in its direction. This results in smaller antenna-array gains in the directions of MSs whose downlink signals have lower power, than the gains obtained using the conventional algorithms. Thus, the power of co-channel interference in these directions is reduced and the SIR at these MSs is increased. This, in turn, reduces the system outage probability as will be illustrated in the next section.

5.3 Simulation Results

A first set of simulations was carried out to illustrate the difference between the proposed weighted beamforming algorithm and the conventional ones given by (5.2). A DS-CDMA system with an antenna array deployed at the BS was assumed. The spacing of a 3-element ULA was set to $d = \lambda/2$ and Gold codes of length 31 were used as the spreading codes. The information bit-to-background power spectral density ratio (E_b/N_0) of the received signal was set to 10 dB. Four MSs, namely, A, B, C, and D, and 2 paths for each MS were assumed. The BS beam pattern for the downlink signal to MS A is presented in Fig. 5.1. The RISs in (5.6) of the downlink signal to the target MS A on the downlink signals to the other MSs B, C, and D are also presented in Fig. 5.1 using vertical bars. They indicate that the downlink signal to MS D has the highest resistance to the co-channel interference caused by the downlink signal to MS A. It can be observed that by using the weighted beamforming algorithm, the antenna-array gains in the directions of MSs B and C are lower than those obtained

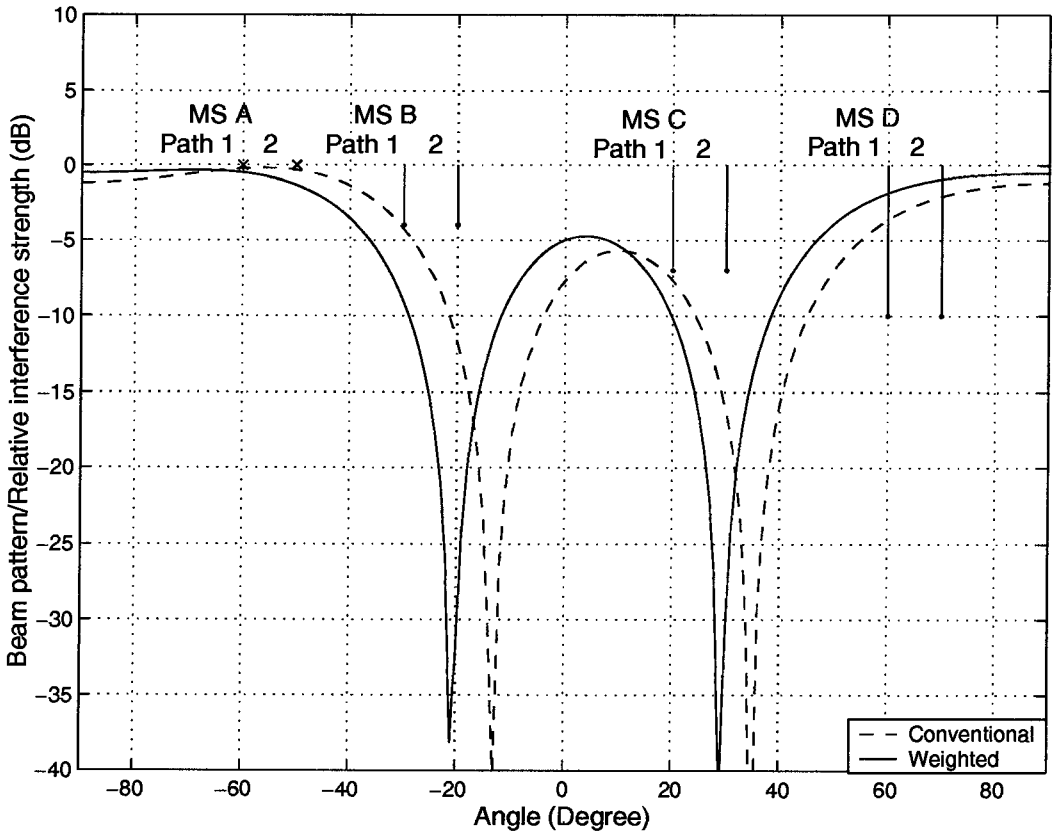

Figure 5.1. *Beam pattern and relative interference strength of MS A.*

using the conventional beamforming algorithm. As a result, the power of co-channel interference caused by the downlink signal to MS A radiated in the directions of MSs B and C is less than the power radiated using the conventional beamforming algorithms.

A second set of simulations was carried out based on a DS-CDMA system with 8-element linear antenna array deployed at the BS. Ten MSs and 2 paths for each MS were assumed. Perfect power control for the downlink was further assumed. Different BS transmitted power levels and the maximum RIS ranges from 10 dB to 30 dB were simulated. Plots of the system outage probability versus the threshold of

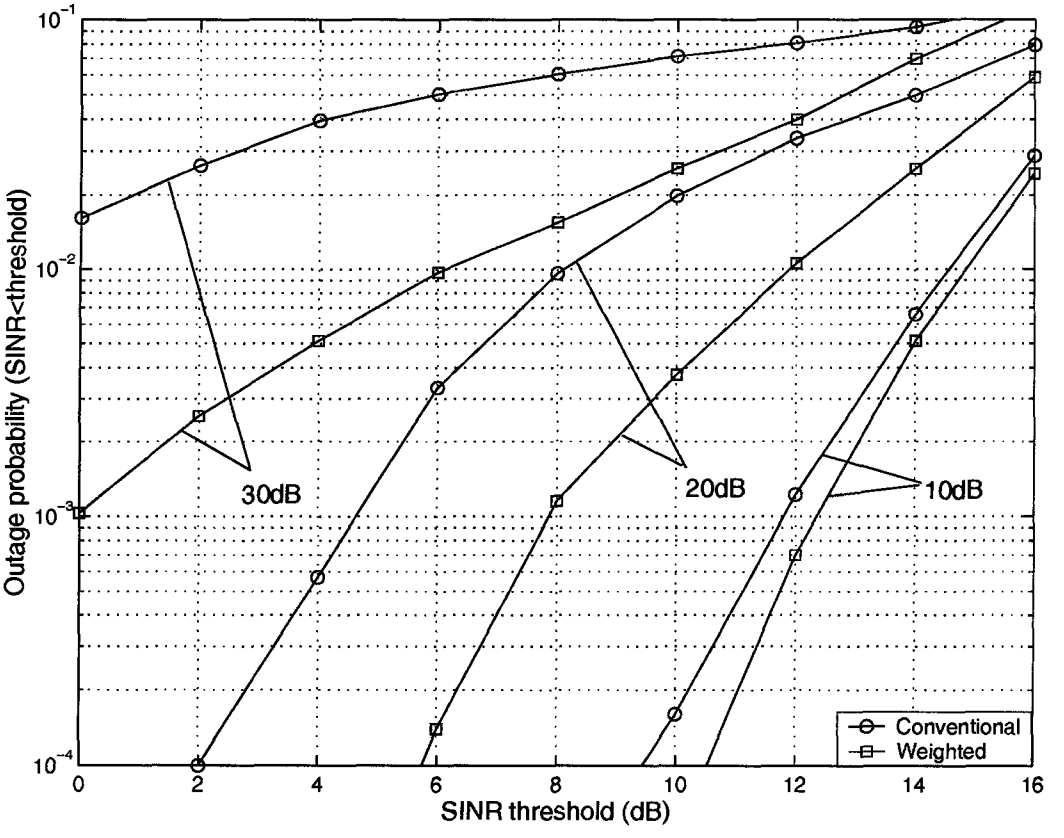

Figure 5.2. *Outage probability.*

SINR using conventional algorithms and the proposed weighted algorithm are shown in Fig. 5.2. It can be observed that the system outage probability obtained by using the weighted algorithm is significantly lower than that of using conventional downlink SUB algorithms.

5.4 Conclusions

A new weighted downlink SUB algorithm has been proposed. Using the proposed algorithm, the relative strength of the co-channel interference on the interfered signal is taken into consideration in the determination of beamforming weights. This leads to

a downlink beam pattern that less power of co-channel interference is radiated in the direction of an MS whose downlink signal has low power. Simulation results show that the proposed algorithm leads to lower system outage probability than conventional downlink SUB algorithms.

Chapter 6

A Subspace Multiuser Beamforming Algorithm

6.1 Introduction

The downlink SUB algorithm proposed in the previous chapter is intended for obtaining the BS beamforming weight vectors for each MS. Based on the BS weight vectors obtained, the BS transmitted power to each MS is computed to satisfy the SINR specification at the MS [41]. This downlink SUB algorithm is computationally simple due to the independent optimization of weight vectors for different MSs but provides a suboptimal solution to the problem of minimizing the BS transmitted power.

Another approach is to use the downlink MUB to jointly optimize all the beamforming weight vectors to satisfy given SINR specifications at each MS while at the same time minimize the total power transmitted from the BS. As we have discussed in chapter 2, the optimal MUB turns out to be an optimization problem with non-convex quadratic constraints. Two of the most commonly used algorithms to find the optimal solution are the duality-based MUB algorithm [41] and the SDP-based MUB algorithm [45]-[47]. The duality-based MUB algorithm tends to converge more slowly as the SINR requirements become more stringent and the SDP-based MUB algorithm entails high computational complexity and it increases rapidly as the number of antenna elements increases.

In this chapter, a new downlink MUB technique for wireless communications is developed. The MUB optimization problem in [45] is reformulated by modifying the SINR constraints so as to obtain a feasible region for the solution which is a subset of the region of the original optimization problem. The BS weight vectors of different MSs are then jointly optimized in their corresponding subspaces instead of the entire parameter space. Simulations of CDMA systems with various numbers of antenna elements show that the modified optimization problem leads to a solution that satisfies the SINR specification at each MS while the total power transmitted from the BS is very close to the optimal one. In addition, the solution requires significantly less computation than the optimal MUB algorithms.

The organization of the chapter is as follows: The proposed subspace downlink MUB algorithm is presented in Sec. 6.2. In Sec. 6.3, numerical results pertaining to the BS transmitted power and computational complexity for the proposed MUB algorithm and existing MUB algorithms are presented. Conclusions are drawn in Sec. 6.4.

6.2 New downlink MUB algorithm

In this section, a subspace MUB algorithm is proposed. If p_k^t denotes the L_2-norm $\| \mathbf{w}_k \|^2$ of the BS beamforming weight vector $\mathbf{w}_k$ for MS k, the downlink MUB optimization problem in (2.39) can be rewritten as

$$\begin{aligned} &\min \left[\sum_{k=1}^{K} p_k^t \right] \\ &\text{subject to } f_k(\mathbf{w}_1, \mathbf{w}_2, \ \ldots, \ \mathbf{w}_K) \geq \gamma_k \\ &\text{for } k = 1, \ 2, \ \ldots, \ K \end{aligned} \tag{6.1}$$

where

$$f_k(\mathbf{w}_1, \mathbf{w}_2, \ \ldots, \ \mathbf{w}_K) = \frac{p_{k,k}^r}{\sum_{\substack{j=1 \\ j \neq i}}^{K} p_{k,j}^r + \sigma_k^2}. \tag{6.2}$$

In the above equation, σ_k is the noise variance at MS k, γ_k is the required minimum SINR at MS k,

$$p_{k,k}^r = \sum_{l=1}^{L_k} E\left|x_{k,l}^s\right|^2 = \mathbf{w}_k^H \mathbf{R}_k \mathbf{w}_k \tag{6.3}$$

is the received downlink signal power at MS k, and

$$p_{k,j}^r = \sum_{l=1}^{L_k} E\left|x_{k,l}^{I_j}\right|^2 = \mathbf{w}_j^H \mathbf{R}_k \mathbf{w}_j \tag{6.4}$$

is the received power of the co-channel interference at MS k caused by the downlink signal to MS j.

Considering the MUB optimization problem in (6.1), the proposed approach is based on the decomposition of the range space of $\mathbf{R}_k$. Matrix $\mathbf{R}_k$ in (2.34) is Hermitian and positive semidefinite and, hence, it has real and nonnegative eigenvalues. It can be decomposed as

$$\mathbf{R}_k = \mathbf{U}_k \Lambda_k \mathbf{U}_k^H \tag{6.5}$$

where

$$\Lambda_k = \text{diag}\{\lambda_1,\ \lambda_2,\ \ldots,\ \lambda_p\}$$

and

$$\mathbf{U}_k = [\mathbf{v}_k^1\ \mathbf{v}_k^2\ \cdots\ \mathbf{v}_k^p].$$

Since $\{\mathbf{v}_k^1,\ \mathbf{v}_k^2,\ \ldots,\ \mathbf{v}_k^p\}$ is a set of orthonormal eigenvectors of matrix $\mathbf{R}_k$ which is a basis of vector space C, the weight vector $\mathbf{w}_k$ can be expressed as

$$\mathbf{w}_k = \mathbf{U}_k \mathbf{x}_k. \tag{6.6}$$

Generally, the rank of the spatial correlation matrix $\mathbf{R}_k$ is less than p. In such a case, the span of $\{\mathbf{v}_k^1,\ \mathbf{v}_k^2,\ \ldots,\ \mathbf{v}_k^{s_k}\}$, which is the set of the eigenvectors associated with the

s_k nonzero eigenvalues $\lambda_1, \lambda_2, \ldots, \lambda_{s_k}$, is the subspace $\hat{C}_k$ of the downlink signal to MS k. The subspace $\hat{C}_k$ can also be selected as the set of the eigenvectors associated with the largest s_k eigenvalues due to the presence of noise component. The span of the remaining eigenvectors $\mathbf{v}_k^{s_k+1}, \mathbf{v}_k^{s_k+2}, \ldots, \mathbf{v}_k^p$ is the orthogonal complement $\bar{C}_k$ of the subspace $\hat{C}_k$. If we let

$$\hat{\mathbf{U}}_k = \left[\begin{array}{cccc} \mathbf{v}_k^1 & \mathbf{v}_k^2 & \cdots & \mathbf{v}_k^{s_k} \end{array} \right]$$

and

$$\bar{\mathbf{U}}_k = \left[\begin{array}{cccc} \mathbf{v}_k^{s_k+1} & \mathbf{v}_k^{s_k+2} & \cdots & \mathbf{v}_k^p \end{array} \right]$$

matrix $\mathbf{R}_k$ can be rewritten as

$$\mathbf{R}_k = \hat{\mathbf{U}}_k \hat{\Lambda}_k \hat{\mathbf{U}}_k^H \tag{6.7}$$

where $\hat{\Lambda}_k = \text{diag}\{\lambda_1, \lambda_2, \ldots, \lambda_{s_k}\}$. Vector $\mathbf{x}_k$ can now be partitioned as

$$\mathbf{x}_k = \left[\begin{array}{c} \hat{\mathbf{x}}_k \\ \bar{\mathbf{x}}_k \end{array} \right] \tag{6.8}$$

where the s_k components of vector $\hat{\mathbf{x}}_k$ and the $p - s_k$ components of vector $\bar{\mathbf{x}}_k$ are the components of $\mathbf{x}_k$ in subspace $\hat{C}_k$ and its orthogonal complement $\bar{C}_k$, respectively. Thus the weight vector $\mathbf{w}_k$ can be rewritten as

$$\mathbf{w}_k = \left[\begin{array}{cc} \hat{\mathbf{U}}_k & \bar{\mathbf{U}}_k \end{array} \right] \left[\begin{array}{c} \hat{\mathbf{x}}_k \\ \bar{\mathbf{x}}_k \end{array} \right] = \hat{\mathbf{U}}_k \hat{\mathbf{x}}_k + \bar{\mathbf{U}}_k \bar{\mathbf{x}}_k. \tag{6.9}$$

Since

$$\hat{\mathbf{U}}_k^H \hat{\mathbf{U}}_k = \mathbf{I}_{s_k} \tag{6.10}$$

$$\bar{\mathbf{U}}_k^H \bar{\mathbf{U}}_k = \mathbf{I}_{p-s_k} \tag{6.11}$$

$$\hat{\mathbf{U}}_k^H \bar{\mathbf{U}}_k = 0 \tag{6.12}$$

the BS transmitted power p_k^t for MS k can be derived as

$$p_k^t = \| \mathbf{w}_k \|^2 = \| \hat{\mathbf{U}}_k \hat{\mathbf{x}}_k + \bar{\mathbf{U}}_k \bar{\mathbf{x}}_k \|^2 = \hat{p}_k^t + \bar{p}_k^t \tag{6.13}$$

where $\hat{p}_k^t = \| \hat{\mathbf{x}}_k \|^2$ and $\bar{p}_k^t = \| \bar{\mathbf{x}}_k \|^2$ are the power in the subspace $\hat{C}_k$ and its orthogonal complement $\bar{C}_k$, respectively. If we substitute (6.9) into (6.3), the received signal power $p_{k,k}^r$ at MS k can be expressed as

$$\begin{aligned} p_{k,k}^r =& \begin{bmatrix} \hat{\mathbf{x}}_k^H & \bar{\mathbf{x}}_k^H \end{bmatrix} \begin{bmatrix} \hat{\mathbf{U}}_k^H \\ \bar{\mathbf{U}}_k^H \end{bmatrix} \hat{\mathbf{U}}_k \hat{\Lambda}_k \hat{\mathbf{U}}_k^H \begin{bmatrix} \hat{\mathbf{U}}_k & \bar{\mathbf{U}}_k \end{bmatrix} \begin{bmatrix} \hat{\mathbf{x}}_k \\ \bar{\mathbf{x}}_k \end{bmatrix} \\ =& \hat{\mathbf{x}}_k^H \hat{\mathbf{U}}_k^H \hat{\mathbf{U}}_k \hat{\Lambda}_k \hat{\mathbf{U}}_k^H \hat{\mathbf{U}}_k \hat{\mathbf{x}}_k. \end{aligned} \tag{6.14}$$

If we define $\mathbf{R}_k^{\frac{1}{2}} = \hat{\Lambda}_k^{\frac{1}{2}} \hat{\mathbf{U}}_k^H$ where $\hat{\Lambda}_k^{\frac{1}{2}} = \text{diag}\{\lambda_1^{\frac{1}{2}}, \lambda_2^{\frac{1}{2}}, \ldots, \lambda_{s_k}^{\frac{1}{2}}\}$, the received signal power $p_{k,k}^r$ in (6.14) can be rewritten as

$$p_{k,k}^r = \| \mathbf{R}_k^{\frac{1}{2}} \hat{\mathbf{U}}_k \hat{\mathbf{x}}_k \|^2. \tag{6.15}$$

Similarly, the received power of co-channel interference $p_{k,j}^r$ at MS k caused by downlink signal to MS j can be expressed as

$$p_{k,j}^r = \| \mathbf{R}_k^{\frac{1}{2}} \hat{\mathbf{U}}_j \hat{\mathbf{x}}_j + \mathbf{R}_k^{\frac{1}{2}} \bar{\mathbf{U}}_j \bar{\mathbf{x}}_j \|^2. \tag{6.16}$$

Applying the triangle inequality to (6.16), we have

$$p_{k,j}^r \leq \hat{p}_{k,j}^r + \bar{p}_{k,j}^r \tag{6.17}$$

where

$$\hat{p}_{k,j}^r = \| \mathbf{R}_k^{\frac{1}{2}} \hat{\mathbf{U}}_j \hat{\mathbf{x}}_j \|^2 \tag{6.18}$$

$$\bar{p}_{k,j}^r = \| \mathbf{R}_k^{\frac{1}{2}} \bar{\mathbf{U}}_j \bar{\mathbf{x}}_j \|^2 + 2 \| \mathbf{R}_k^{\frac{1}{2}} \hat{\mathbf{U}}_j \hat{\mathbf{x}}_j \| \| \mathbf{R}_k^{\frac{1}{2}} \bar{\mathbf{U}}_j \bar{\mathbf{x}}_j \|. \tag{6.19}$$

Let us now consider a modified optimization problem that has the same objective function as the optimization problem in (6.1) but different constraints from those in (6.2), i.e.,

$$\begin{aligned} &\min \left[\sum_{k=1}^{K} (\hat{p}_k^t + \bar{p}_k^t) \right] \\ &\text{subject to } g_k(\mathbf{x}_1, \mathbf{x}_2, \ldots, \mathbf{x}_K) \geq \gamma_k \\ &\text{for } k = 1, 2, \ldots, K \end{aligned} \tag{6.20}$$

where

$$g_k(\mathbf{x}_1, \mathbf{x}_2, \ \ldots, \ \mathbf{x}_K) = \frac{p^r_{k,k}}{\sum_{\substack{j=1 \\ j \neq i}}^{K} (\hat{p}^r_{k,j} + \bar{p}^r_{k,j}) + \sigma_k^2}. \tag{6.21}$$

Proposition 1: The feasible solution of the modified optimization problem in (6.20) satisfies the SINR specification at each MS.

Proof: Let $\Re^f$ and $\Re^g$ denote the feasible regions of the original optimization problems in (6.1), (6.2) and the modified optimization problem in (6.20), (6.21), respectively. Consider a feasible solution $(\mathbf{x}_1, \mathbf{x}_2, \ \ldots, \ \mathbf{x}_K)$ in $\Re^g$ such that

$$g_k(\mathbf{x}_1, \mathbf{x}_2, \ \ldots, \ \mathbf{x}_K) \geq \gamma_k, \text{ for } k = 1, \ 2, \ \ldots, \ K.$$

From (6.17), it can be readily shown that

$$f_k(\mathbf{x}_1, \mathbf{x}_2, \ \ldots, \ \mathbf{x}_K) \geq g_k(\mathbf{x}_1, \mathbf{x}_2, \ \ldots, \ \mathbf{x}_K)$$
$$\text{for } k = 1, \ 2, \ \ldots, \ K.$$

and hence it follows that

$$f_k(\mathbf{x}_1, \mathbf{x}_2, \ \ldots, \ \mathbf{x}_K) \geq \gamma_k, \text{ for } k = 1, \ 2, \ \ldots, \ K.$$

Therefore, $\Re^g \subseteq \Re^f$ and any feasible solution in $\Re^g$ is also a feasible solution in $\Re^f$. Thus, the modified optimization problem leads to a solution that satisfies the SINR specification at each MS.

Proposition 2: The optimal solution of the modified optimization problem in (6.20) is obtained when $\bar{\mathbf{x}}_k = 0$, for $i = 1, \ 2, \ \ldots, \ K$.

Proof: The proposition will be proved by contradiction. Assume that the optimal solution of the problem in (6.20) has the form

$$\mathbf{w}_k^A = \hat{\mathbf{U}}_k \hat{\mathbf{x}}_k^a + \bar{\mathbf{U}}_k \bar{\mathbf{x}}_k^a \ \text{ for } k = 1, \ 2, \ \ldots, \ K \tag{6.22}$$

and $\| \ \bar{\mathbf{x}}_k^a \ \|^2 \neq 0$ for at least one MS. Consider a non-optimal solution

$$\mathbf{w}_k^B = \hat{\mathbf{U}}_k \hat{\mathbf{x}}_k^a \ \text{ for } k = 1, \ 2, \ \ldots, \ K. \tag{6.23}$$

Quantities $g_k(\mathbf{x}_1^A, \mathbf{x}_2^A, \ldots, \mathbf{x}_K^A)$ and $g_k(\mathbf{x}_1^B, \mathbf{x}_2^B, \ldots, \mathbf{x}_K^B)$ for $k = 1, 2, \ldots, K$ can then be obtained by substituting (6.22) and (6.23) into (6.21) which leads to

$$g_k(\mathbf{x}_1^B, \mathbf{x}_2^B, \ldots, \mathbf{x}_K^B) \geq g_k(\mathbf{x}_1^A, \mathbf{x}_2^A, \ldots, \mathbf{x}_K^A) \geq \gamma_k$$
$$\text{for } k = 1, 2, \ldots, K.$$

All the constraints in (6.20) are satisfied using the weights $\mathbf{w}_1^B, \mathbf{w}_2^B, \ldots, \mathbf{w}_K^B$ and, therefore, $\mathbf{x}_1^B, \mathbf{x}_2^B, \ldots, \mathbf{x}_K^B$ is a set of feasible solutions. Substituting (6.22) and (6.23) into the objective function in (6.20), we obtain the total BS transmitted powers as

$$p^t(\mathbf{x}_1^A, \mathbf{x}_2^A, \cdots, \mathbf{x}_K^A) = \sum_{k=1}^{K} (\hat{\mathbf{x}}_k^H \hat{\mathbf{x}}_k + \bar{\mathbf{x}}_k^H \bar{\mathbf{x}}_k) \tag{6.24}$$

and

$$p^t(\mathbf{x}_1^B, \mathbf{x}_2^B, \cdots, \mathbf{x}_K^B) = \sum_{k=1}^{K} \hat{\mathbf{x}}_k^H \hat{\mathbf{x}}_k \tag{6.25}$$

respectively. Hence from (6.24) and (6.25) it follows that

$$p^t(\mathbf{x}_1^B, \mathbf{x}_2^B, \ldots, \mathbf{x}_K^B) < p^t(\mathbf{x}_1^A, \mathbf{x}_2^A, \ldots, \mathbf{x}_K^A). \tag{6.26}$$

This leads to the contradiction that the non-optimal beamforming weights $\mathbf{w}_1^B$, $\mathbf{w}_2^B$, ..., $\mathbf{w}_K^B$ are better than the optimal beamforming weights $\mathbf{w}_1^A, \mathbf{w}_2^A, \ldots, \mathbf{w}_K^A$. This contradiction implies that the optimal beamforming weight vectors of the modified optimization problem in (6.20) are obtained when $\bar{\mathbf{x}}_k = 0$, for $k = 1, 2, \ldots, K$.

Since only the s_k components of vector $\hat{\mathbf{x}}_k$, for $k = 1, 2, \ldots, K$, need to be considered, the optimization problem in (6.20) can be reformulated as

$$\min \left[\sum_{k=1}^{K} \| \hat{\mathbf{x}}_k \|^2 \right] \tag{6.27}$$
$$\text{subject to } \frac{\| \mathbf{R}_k^{\frac{1}{2}} \hat{\mathbf{U}}_k \hat{\mathbf{x}}_k \|^2}{\sum_{\substack{j=1 \\ j \neq i}}^{K} \| \mathbf{R}_k^{\frac{1}{2}} \hat{\mathbf{U}}_j \hat{\mathbf{x}}_j \|^2 + \sigma_k^2} \geq \gamma_k$$
$$\text{for } k = 1, 2, \ldots, K.$$

Further, if we define $\hat{\mathbf{X}}_k = \hat{\mathbf{x}}_k \hat{\mathbf{x}}_k^H$ for $k = 1, 2, \ldots, K$ and relax the constraint $\text{Rank}(\hat{\mathbf{X}}_k) = 1$, then the optimization problem in (6.27) can be rewritten as an SDP problem of the form

$$\min_{\hat{\mathbf{X}}} \sum_{k=1}^{K} \text{tr}\left[\hat{\mathbf{X}}_k\right] \tag{6.28}$$

subject to

$$\text{tr}\left[\hat{\mathbf{U}}_k^H \mathbf{R}_k \hat{\mathbf{U}}_k \hat{\mathbf{X}}_k\right] - \gamma_k \sum_{\substack{j=1 \\ j \neq k}}^{K} \text{tr}\left[\hat{\mathbf{U}}_j^H \mathbf{R}_k \hat{\mathbf{U}}_j \hat{\mathbf{X}}_j\right] - \sigma_k^2 \gamma_k \geq 0$$

$$\hat{\mathbf{X}}_k = \hat{\mathbf{X}}_k^H$$

$$\hat{\mathbf{X}}_k \succeq 0$$

for $k = 1, 2, \ldots, K$.

Based on the solution $\hat{\mathbf{X}}_k$ for $k = 1, 2, \ldots, K$ of the optimization problem in (6.28), $\hat{\mathbf{x}}_k$ can be calculated as

$$\hat{\mathbf{x}}_k = \sqrt{\mu_k}\mathbf{q}_k \quad \text{for } k = 1, 2, \ldots, K \tag{6.29}$$

where $\mathbf{q}_k$ is the eigenvector associated with the nonzero eigenvalue μ_k of matrix $\hat{\mathbf{X}}_k$. Hence, from (6.9), the weight vectors can be obtained as

$$\mathbf{w}_k = \hat{\mathbf{U}}_k \hat{\mathbf{x}}_k \quad \text{for } k = 1, 2, \ldots, K. \tag{6.30}$$

An algorithm based on the method described is summarized in Table 6.1.

The proposed MUB algorithm solves the modified optimization problem in (6.28) instead of the original optimization problem in (6.1). Because of proposition 1, the solution of the former will satisfy the SINR specifications of the original optimization problem. Furthermore, the solution can be obtained in a subspace of the optimization parameter space of the original problem due to proposition 2. The number of variables to be considered in the modified optimization problem and the original optimization

Table 6.1. *Proposed subspace MUB algorithm*

Step 1: Computation of the subspaces

- Eigenvalue decomposition of matrix $\mathbf{R}_k$, for $k = 1,\ 2,\ \ldots,\ K$.
- Obtain the subspace $\hat{C}_k$ by finding the eigenvectors associated with the largest s_k eigenvalues.
- Obtain $\hat{\mathbf{U}}_k = \left[\ \mathbf{v}_k^1\ \mathbf{v}_k^2\ \cdots\ \mathbf{v}_k^{s_k}\ \right]$, for $k = 1,\ 2,\ \ldots,\ K$.

Step 2: Computation of the downlink weight vectors

- Compute $\hat{\mathbf{X}}_k$ by solving the optimization problem in (6.28).
- Compute $\hat{\mathbf{x}}_k$ by solving by finding the eigenvector $\hat{\mathbf{w}}_k$ associated with the nonzero eigenvalue of matrix $\hat{\mathbf{X}}_k$.
- Set $\mathbf{w}_k = \hat{\mathbf{U}}_k\hat{\mathbf{x}}_k$, for $k = 1,\ 2,\ \ldots,\ K$.

problem, n^s and n^o, respectively, can be readily obtained as

$$n^s = \sum_{k=1}^{K}(s_k + 1)s_k/2 \tag{6.31}$$

$$n^o = K(p+1)p/2. \tag{6.32}$$

The use of more antenna elements is an effective way to reduce the transmitted power, improve the quality of service, and increase the capacity of a wireless communication system. However, it can be shown from (6.32) that the number of variables required in the original optimization problem is of order $O(p^2)$ and thus its computational complexity increases rapidly with the number of antenna elements. This tends to render the problem less tractable for real-time applications. In contrast, the number of variables in the modified optimization problem depends only on the downlink channels. Since $s_k \leq p$ and in most cases $s_k < p$ for $k = 1,\ 2,\ \ldots,\ K$, n^s is much smaller than n^o. Thus the solution of the modified optimization problem requires significantly less computation than the optimal MUB. In addition, as will be illustrated in the next section, the power transmitted by the BS is close to that of the optimal MUB. In the extreme case where $s_k = p$ for $k = 1,\ 2,\ \ldots,\ K$, the modified optimization problem

is equivalent to the original optimization problem and thus the two problems have the same computational complexity.

6.3 Simulation Results

Direct-sequence code-division multiple access systems with 3 to 8 ULA elements in the BS array were simulated. The information bit-to-background power spectral density ratio (E_b/N_0) of the received signal was set to 10 dB and γ_k was set to -10 dB for $k = 1, 2, \ldots, K$. Twenty MSs and an angle of path spread of $\pi/3$ for each MS were assumed. The spacing of the antenna array was set to $d = \lambda/2$. The performance measures in the simulation were the total power transmitted from the BS and the computational complexity in terms of CPU time averaged over 1000 runs. In each run, the SUB [41], the proposed MUB, the optimal MUB using SDP [45], and the optimal MUB exploiting the duality between the uplink and the downlink [41] were simulated. As can be seen in Fig. 6.1, the computational complexity of the proposed MUB algorithm is significantly reduced relative to that of the optimal MUB. The MUB is insensitive to the increase of antenna elements since the number of variables in the SDP depends only on the downlink channels whereas the number of variables and, in turn, the computational complexity of the optimal MUB using SDP increases rapidly with the number of antenna elements. This confirms the discussion in Sec. 6.2. It can also be observed that when the number of antenna elements is small, the optimal MUB algorithm that exploits the duality between the uplink and the downlink requires high computational complexity due to its low rate of convergence in the case of a stringent SINR specification. The relative power transmitted from the BS versus the number of antenna elements is shown in Fig. 6.2. It can be observed that the total transmitted power using the proposed MUB algorithm approaches that achieved by the optimal MUB. Furthermore, the SUB leads to a much higher BS transmitted power than the proposed MUB algorithm though it is computationally

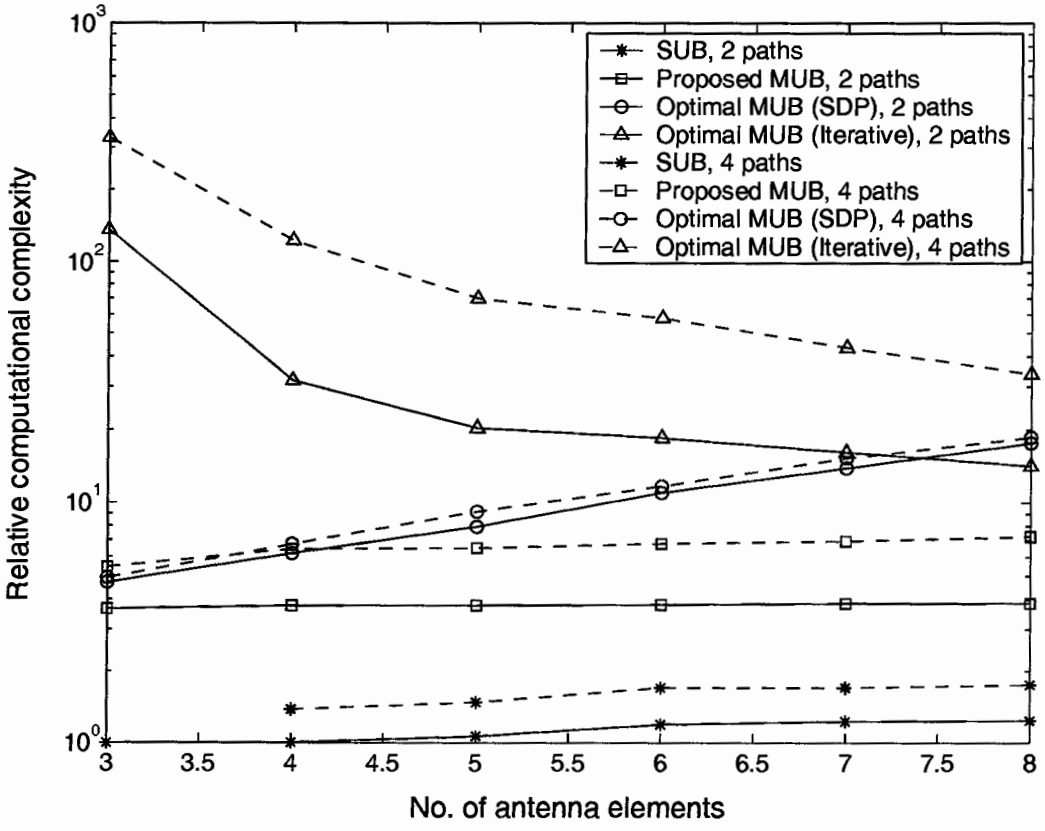

Figure 6.1. *Comparison of computational complexity in terms of CPU time.*

simpler.

6.4 Conclusions

A new downlink MUB algorithm for wireless communications has been developed. In the new algorithm, the weight vectors of different MSs are jointly optimized in their corresponding subspaces instead of searching in the entire parameter space. Using the proposed algorithm, the number of variables considered in SDP problem is reduced and its computational complexity is significantly reduced relative to that of the optimal MUB algorithms. In addition, the proposed algorithm leads to solutions

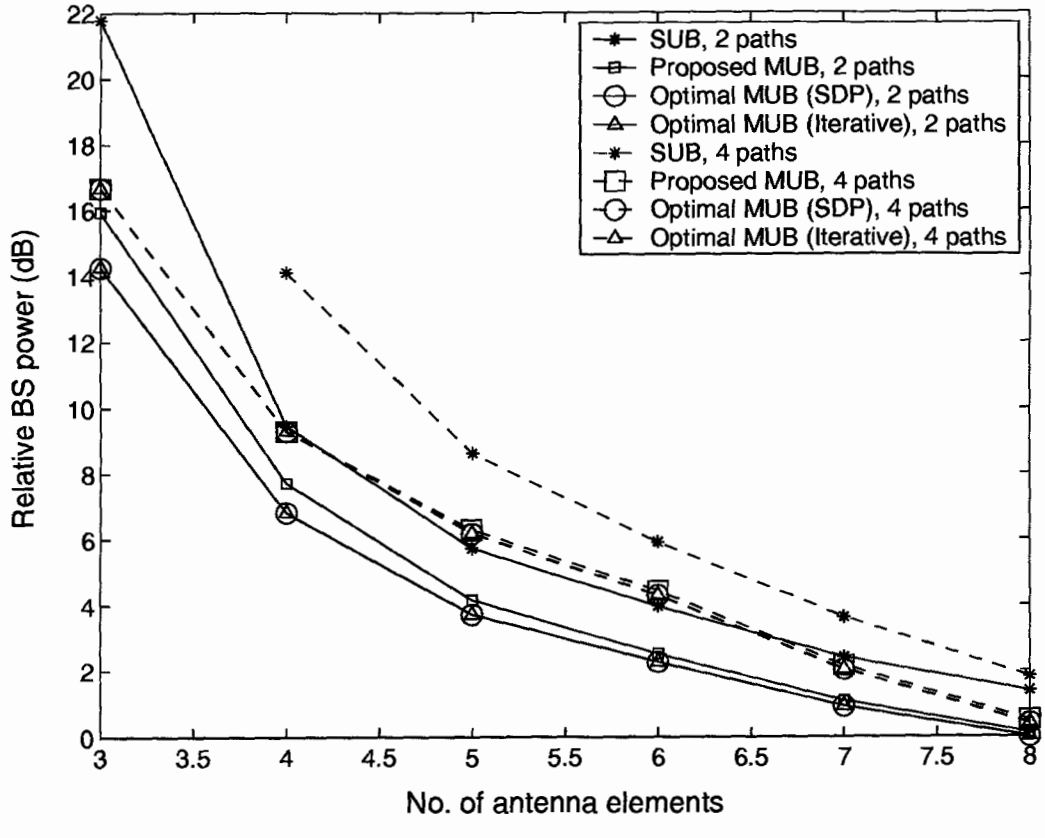

Figure 6.2. *Comparison of BS transmitted power.*

that satisfy the SINR specification at each MS and at a total BS transmitted power which is close to the optimal one.

Chapter 7

Conclusions and Future Work

7.1 Conclusions

The main focus of this dissertation has been the development of beamforming and DOA estimation techniques for wireless communication systems. In Chapter 3, two different beamformer configurations for the uplink in DS-CDMA systems, the CB and SB configurations, have been studied. In Chapter 4, the SBDOA estimator was developed to provide DOA estimation with fast tracking capability, high capacity and resolution. In Chapter 5, the weighted SUB algorithm in the downlink of wireless communication systems was designed to obtain beamforming weights at BS so as to reduce the effect of co-channel interference caused by downlink signals. In Chapter 6, the subspace MUB algorithm for the downlink of wireless communication systems was developed to jointly optimize the weight vectors and transmitted power at BS and achieve low computational complexity relative to the optimum MUB.

7.1.1 Comparison of Beamformer Configurations

Our attention in Chapter 3 was focused on the analysis of beamformer configurations for the BS receiver in DS-CDMA systems. The performance of the CB and SB configurations in rejecting interference was investigated through theoretical analysis on the basis of closed-form solutions for the beamforming weights. It has been shown that in the SB configuration different interfering components are rejected based on their

interfering strength which depends on both their power and code correlation with the SOI, whereas in the chip-based configuration they are rejected based on only their power. This difference between the CB and SB configurations leads to different performance. We have shown through theoretical analysis that the SB configuration offers a better performance with respect to SINR and MMSE than the CB configuration but the improvement comes with an increased hardware complexity relative to that for the CB configuration.

Two aspects of the difference in the performance of the two configurations were investigated through two simple examples, one corresponding to the mismatch loss in a synchronous DS-CDMA system and the other corresponding to the spatial selectivity in an asynchronous DS-CDMA system. It has been shown that in a synchronous DS-CDMA system the impact of interference on the system performance is overvalued using the CB configuration and it leads to more mismatch loss than the SB configuration. In an asynchronous DS-CDMA system, the power of an interfering component may not reflect its actual impact on system performance. Using the CB configuration, an interfering component which has low power but high correlation with the signal of interest cannot be effectively rejected. In contrast, different interfering components are rejected in terms of their interfering strength using the SB configuration. More effort is applied to rejecting the interfering components with higher interfering strength and thus a more selective and efficient system is achieved.

Computer simulations have been presented to demonstrate the performance of the two configurations. It has been shown that in a synchronous DS-CDMA system, the SB configuration leads to less mismatch loss and higher SINR. In an asynchronous DS-CDMA system, the SB configuration leads to a better trade-off between SNR and SIR and a higher SINR can be achieved than the CB configuration. As a result, the SB is superior relative to the CB configuration in the presence of MAI.

7.1.2 SBDOA Estimator

In Chapter 4, we have proposed a DOA estimator to estimate the DOA of signals in the presence of interference. It is based on subarray beamforming and is called SBDOA estimator. In this estimator, a phase-shifted reference signal whose phase relative to that of the reference signal is a function of the target DOA is formed through subarray beamforming. The target DOA is estimated from the phase shift between the reference signal and the phase-shifted reference signal. It has been shown that through the use of subarray beamforming, the signals from sources which severely interfere with the target signal can be efficiently rejected. Thus their interference on the DOA estimation is reduced. The DOA estimation using the SBDOA estimator is not based on subspace estimation and, therefore, its estimation capacity is no longer bounded by the number of antenna elements. In addition, it is computationally simpler and can be easily implemented on hardware.

The performance of the SBDOA estimator has been evaluated through a theoretical analysis and the probability-density function and the variance of the estimated DOA were derived. It was shown that the SBDOA estimator is an asymptotically consistent estimator and its performance was compared with that of existing estimators. The result obtained show that the SBDOA estimator is superior relative to existing DOA estimators with respect to estimation capacity, resolution, accuracy, and tracking capability.

7.1.3 Weighted SUB

In Chapter 5, we have developed a new weighted downlink SUB algorithm. In this algorithm, the fact that downlink signals to different MSs have different resistance to co-channel interference is not taken into consideration in the beamforming. The power of co-channel interference in the direction of MSs other than the target one is weighted by the corresponding RIS of the downlink signal to the target MS. The

larger the RIS of the downlink signal to the target MS on the downlink signal to another MS, the less power is radiated in its direction. It has been shown that this results in smaller antenna-array gains in the directions of MSs whose downlink signals have lower power, than the gains obtained using the conventional algorithms. In this way, the power of co-channel interference in these directions is reduced and the SIR at these MSs is increased. This, in turn, reduces the system outage probability, particularly, for the 3G communication systems where the power transmitted by the BS to different MSs can vary over a wide range.

The performance of the proposed algorithm has been evaluated and compared with the conventional downlink SUB algorithm through computer simulations. It has been shown that when using the proposed SUB algorithm, less power of co-channel interference is radiated in the direction of an MS that has less resistance to the co-channel interference. In cases where the BS transmitted power to different MSs varies in a wide range, the proposed algorithm leads to significantly lower system outage probability than that of using conventional SUB algorithms.

7.1.4 Subspace MUB

The SUB algorithm proposed in Chapter 6 is computationally simple but provides suboptimal solutions to the problem of minimizing the BS transmitted power. In Chapter 6, our attention was focused on the development of a low-complexity MUB technique for the downlink in wireless communications. It has been shown that the use of more antenna elements is an effective way of reducing the BS transmitted power and increasing the capacity of wireless communication systems. However, the computational complexity of the optimal MUB using SDP increases rapidly with the number of antenna elements, which prevents its use in the real-time applications. In the proposed subspace MUB, the optimization problem of optimal MUB is reformulated by modifying the SINR constraints so as to obtain a feasible region for the solution which is a subset of the region of the original optimization problem. The

BS weight vectors of different MSs are then jointly optimized in their corresponding subspaces instead of the entire parameter space. It has been shown through theoretical analysis that the computational complexity of the subspace MUB depends on downlink channels other than the number of antenna elements. When the number of antenna elements is larger than the dominant signal paths, this leads to a solution of the modified optimization problem with significantly less computation than that in the optimal MUB.

Computer simulations have been presented to demonstrate that the computational complexity of the proposed MUB algorithm is insensitive to an increase of antenna elements since the number of variables considered in the optimization problem of subspace MUB depends only on downlink channels. The solution of the optimization problem of subspace MUB requires significantly less computation than that of the optimal MUB. It has also been shown that the proposed subspace MUB leads to solutions that satisfy the signal-to-noise-plus-interference ratio specification at each MS and that the total power transmitted from the BS is very close to the optimal one.

7.2 Future Work

In what follows, two research topics are suggested as a continuation of the work in this dissertation.

7.2.1 Broadband DOA Estimation

The DOA estimation and beamforming techniques discussed are based on the assumption of bandlimited signals. In some applications such as ultra wideband communications and speech detection using sensor arrays, there are no carriers and thus the antenna response of signal received at antenna array is frequency-dependent. In this regard, it is worthwhile to extend the current work to design a broadband SBDOA

estimator. The extension could include the development of a broadband subarray beamforming algorithm to form two signals at the outputs of two subarray beamfomers such that the phase of one signal relative to the other one is a function of the target DOA. Together with the current work, the proposed extension will constitute a feasible solution for DOA estimation in wireless communication systems.

7.2.2 Uplink MUB for CDMA Systems

In the existing uplink MUB approaches, the uplink MUB problem is formulated as an optimization problem where the weight vectors at the BS for different MSs are jointly optimized so as to satisfy given SINR specifications at the BS and, at the same time, the total power transmitted from all the users in the service area is minimized. Since the optimization problem is formulated to satisfy given SINR specifications before despreading, the code correlation between an interfering component and the SOI is not considered in uplink MUB. Different interfering component are rejected based on only their power in the case of uplink MUB. In chapter 4, it has been shown that the SB configuration leads to better performance than the CB configuration because in the SB configuration the beamforming weights are computed by taking both the power of the interference and its code correlation with the SOI into consideration. Although the discussion of SB and CB configurations was based on uplink SUB, it would be natural to extend it to uplink MUB and develop a more efficient MUB algorithm. This extension could involve

1. Developing approaches to estimate the code correlation (or alternatively, the relative path delay) between two co-channel signals.
2. Reformulating the SINR constraints of the optimization problem for uplink MUB so that the code correlation is taken into account.
3. Developing adaptive algorithms for the above systems to improve the implementation efficiency.

Together with the current work, the proposed extensions will constitute a feasible solution for MUB in DS-CDMA systems.

Bibliography

[1] S. Heeralall, "Discussion of spectrum efficiency and the factors that affect it," in *Proc. IEEE International Conference on Selected Topics in Wireless Communications*, pp. 413-416, June 1992.

[2] V. M. Jovanovic and J. Gazzola, "Capacity of present narrowband cellular systems: interference-limited or blocking-limited," *IEEE Trans. Personal Communications*, vol. 4, pp. 42-51, Dec. 1997.

[3] M. Chryssomallis, "Smart antennas," *IEEE Antennas and Propagation Magazine*, vol. 3, pp. 129-136, Jun. 2000.

[4] K. I. Pedersen, P. E. Mogensen, and J. Ramiro-Moreno, "Application and performance of downlink beamforming techniques in UMTS," *IEEE Communications Magazine*, vol. 41, pp. 134-143, Oct. 2003.

[5] S. H. Lim, J. Lee, and J. Park, "Performance evaluation of adaptive beamforming using pilot and traffic channel in CDMA2000 reverse link," in *Proc. IEEE VTC 2002-Fall*, Vol. 4, pp. 2154-2157, Sept. 2002.

[6] R. A. Soni, R. M. Buehrer, and R. D. Benning, "Intelligent antenna system for CDMA2000," *IEEE Signal Processing Magazine*, vol. 19, pp. 54-67, July 2002.

[7] J. C. Liberti and T. S. Rappaport, *Smart Antennas for Wireless Communications: IS-95 and Third Generation CDMA Applications*, Prentice Hall, 1999.

[8] L. C. Godara, "Application of antenna arrays to mobile communications. II. Beam-forming and direction-of-arrival considerations," *Proc. IEEE*, vol. 85, no. 8, pp. 1195-1245, Aug. 1997.

[9] A. J. Barabell, "Improving the resolution performance of eigenstructure-based direction-finding algorithms," *Proc. ICASSP 1983*, vol. AP-34, pp. 336-339, Mar. 1983.

[10] R. O. Schmidt, "Multiple emitter location and signal parameter estimation," *IEEE Trans. Antennas Propagation*, vol. AP-34, pp. 276-280, Mar. 1986.

[11] R. Roy, A. Paulrajand and T. Kailath, "Direction-of-arrival estimation by subspace rotation methods - ESPRIT," *Proc. ICASSP 1986*, vol. AP-34, pp. 2495-2498, Apr. 1986.

[12] R. Roy and T. Kailath, "ESPRIT-estimation of signal parameters via rotational invariance techniques," *IEEE Trans. Acoustics, Speech, and Signal Processing*, vol. 37, pp. 984-995, July 1989.

[13] G. Xu, S. D. Silverstein, R. H. Roy and T. Kailath, "Beamspace ESPRIT," *IEEE. Trans. Signal Processing*, vol. 42, pp. 349-356, Feb. 1994.

[14] M. L. McCloud and L. L. Scharf, "A new subspace identification algorithm for high-resolution DOA estimation," *IEEE Trans. Antennas Propagation*, vol. 50, pp. 1382-1390, Oct. 2002.

[15] N. Tayem and H. M. Kwon, "Conjugate ESPRIT (C-SPRIT)," *IEEE Trans. Antennas Propagation*, vol. 52, pp. 2618-2624, Oct. 2004.

[16] J. Li and R. T. Compton "Maximum likelihood angle estimation for signals with known waveforms," *IEEE. Trans. Signal Processing*, vol. 41, pp. 2850-2862, Sept. 1993.

[17] J. Li, B. Halder, P. Stoica, and M. Viberg "Computationally efficient angle estimation for signals with known waveforms," *IEEE. Trans. Signal Processing*, vol. 43, pp. 2154-2163, Sept. 1995.

[18] A. L. Swindlehurst, "Time delay and spatial signature estimation using known asynchronous signals," *IEEE. Trans. Signal Processing*, vol. 46, pp. 449-461, Feb. 1998.

[19] Ching-Tai Chiang and Ann-Chen Chang, "DOA estimation in the asynchronous DS-CDMA system," *IEEE Trans. Antennas Propagation*, vol. 51, pp. 40-47, Jan. 2003.

[20] Y. Wang and J. R. Cruz, "Adaptive antenna arrays for cellular CDMA communication systems," *Proc. IEEE International Conference on Acoustics, Speech, and Signal Processing*, vol. 3, pp. 1725-1728, Apr. 1995.

[21] P. Comon and G. H. Golub, "Tracking a few extreme singular values and vectors in signal processing," *Proc. IEEE*, vol. 78, no. 8, pp. 1327-1343, Aug. 1990.

[22] G. H. Golub and C. F. V. Loan, *Matrix Computation*, Johns Hopkins, 1996.

[23] T. Ojanpera and R. Prasad, *Wideband CDMA for Third Generation Mobile Communications*, Artech House, 1998.

[24] L. C. Godara, "Application of antenna arrays to mobile communications, part II: beam-forming and direction-of-arrival considerations," *Proc. IEEE*, vol. 85, no. 8, pp. 1195-1245, Aug. 1997.

[25] H. Cox, R. M. Zeskind, and M. M. Owen, "Robust adaptive beamforming,"

IEEE Trans. Acoustics, Speech, and Signal Processing, vol. ASSP-35, no. 10, pp. 1365-1375, Aug. 2000.

[26] S. Tanaka, M. Sawahashi, and F. Adachi, "Pilot symbol-assisted decision-directed coherent adaptive array diversity for DS-CDMA mobile radio reverse link," *IEICE. Trans. Fundamentals*, vol. E80-A, no. 12, Dec. 1997.

[27] Y. S. Song, H. M. Kwon, and B. J. Min, "Computationally efficient smart antennas for CDMA wireless communications," *IEEE Trans. Veh. Tech.*, vol. 50, pp. 1613-1628, Nov. 2001.

[28] J. H. Winters. "Optimum combining in digital mobile radio with co-channel interference," *IEEE Trans. Veh. Tech.*, vol. 33, pp. 181-188, Aug. 1984.

[29] A. Souloumiac, "Improved estimation of minimum variance beamformer with small number of samples," *Proc. IEEE International Conference on Acoustics, Speech, and Signal Processing*, vol. 5, pp. 2872-2875, May 1996.

[30] A. F. Naguib, *Adaptive Antenna for CDMA Wireless Networks*, Dissertation for the degree of Doctor of Philosophy, Stanford University, Aug. 1996.

[31] M. D. Anna and A. H. Aghvami, "Performance of optimum and suboptimum combining at the antenna array of a W-CDMA system," *IEEE J. Slect. Areas Commun.*, vol. 17, no. 12, pp. 2123-2137, Dec. 1999.

[32] L. C. Godara, "Applications of antenna arrays to mobile communications. I. Performance improvement, feasibility, and system considerations," *Proc. IEEE*, vol. 85, no. 7, pp. 1030-1061, July. 1997.

[33] J. J. Park, J. H. Lee and H. S. Oh, "Performance of chip-/symbol-level beamforming algorithm for WCDMA-TDD system," *Proc. IEEE Vehicular Technology Conference*, pp. 365-369, May 2002.

[34] J. Litva and T. K. Lo, *Digital Beamforming in Wireless Communications*, Artech House, 1996.

[35] R. Stridh, M. Bengtsson, and B. Ottersten, "System evaluation of optimal downlink beamforming in wireless communication," *Proc. IEEE Vehicular Technology Conference*, vol. 5, pp. 1441-1445, 2001.

[36] P. Zetterberg and B. Ottersten, "The spectrum efficiency of a base station antenna array system for spatially selective transmission," *IEEE Trans. Veh. Tech.*, vol. 44, pp. 651-660, Aug. 1995.

[37] H. Asakura and T. Matsumoto, "Cooperative signal reception and down-link beam forming in cellular mobile communications," *IEEE Trans. Veh. Tech.*, vol. 48, pp. 333-341, Mar. 1999.

[38] A. Czylwik, "Downlink beamforming for mobile radio systems with frequency division duplex," *Proc. PIMRC 2000*, vol. 1, pp. 72-76, 2001.

[39] G. G. Raleigh, S. N. Diggavi, and A. Paulraj, "A blind adaptive transmit antenna algorithm for wireless communication," *Proc. ICC 95*, vol. 3, pp. 1494-1499, 1995.

[40] J. Goldbery and J. R. Fonollosa, "Downlink beamforming for cellular mobile communications," *Proc. IEEE Vehicular Technology Conference*, vol. 2, pp. 632-636, 1997.

[41] F. Rashid-Farrokhi, K. J. R. Liu, and L. Tassiulas, "Transmit beamforming and power control for cellular wireless systems," *IEEE Journal on Selected Areas in Commun.*, vol. 16, no. 8, pp. 1437-1450, Oct. 1998.

[42] M. Schubert and H. Boche, "Solution of the multiuser downlink beamforming problem with individual SINR constraints," *IEEE Trans. Veh. Tech.*, vol. 53, pp. 18-28, Jan. 2004.

[43] D. Gerlach and A. Paulraj, "Adaptive transmitting antenna array with feedback," *IEEE Signal Processing Letter*, vol. 1, pp. 150-152, Oct. 1994.

[44] F. Rashid-Farrokhi, L. Tassiulas, and K. J. R. Liu, "Joint optimal power control and beamforming in wireless networks using antenna arrays," *IEEE Trans. Commun.*, vol. 46, no. 10, pp. 1313-1324, Oct. 1998.

[45] M. Bengtsson and B.Ottersten, "Optimal downlink beamforming using semidefinite optimization," *Proc. 37th Annual Allerton Conference on Communication, Control, and Computing*, pp. 987-996, Sept. 1999.

[46] M. Bengtsson and B. Ottersten, "Downlink beamformer design using semidefinite optimization," *Proc. Radiovetenskap och Kommunikation*, pp. 289-293, 1999.

[47] M. Bengtsson, "Jointly optimal downlink beamforming and base station assignment," *Proc. IEEE International Conference on Acoustics, Speech, and Signal Processing*, vol. 5, pp. 2961-2964, 2001.

[48] M. Schubert and H. Boche, "A unifying theory for uplink and downlink multi-user beamforming," *Proc. International Zurich Seminar on Broadband Communications*, pp. 27-1-27-6, Feb. 2002.

[49] M. Schubert and H. Boche, "Solvability of coupled downlink beamforming problems," *Proc. IEEE Global Telecommunications Conference*, vol. 1, pp. 614-618, 2001.

[50] L. Vandenberghe and S. Boyd, "Semidefinite programming," *SIAM Review*, vol. 38, pp. 49-95, Mar. 1996.

[51] B. Sklar, "Rayleigh fading channels in mobile digital communication systems

Part I: Characterization," *IEEE Communications Magazine*, vol. 35, pp. 136-146, Sep. 1997.

[52] M. Chryssomallis, "Simulation of mobile fading channels," *IEEE Antennas and Propagation Magazine*, vol. 44, pp. 172-183, Dec. 2002.

[53] M. D. Yacoub, "Fading distributions and co-channel interference in wireless systems," *IEEE Antennas and Propagation Magazine*, vol. 42, pp. 150-160, Feb. 2000.

[54] T. S. Rappaport, *Wireless Communications Principles and Practice*, Prentice Hall, 1996.

[55] U. Dersch and R. J. Ruegg, "Simulations of the time and frequency selective outdoor mobile radio channel," *IEEE Trans. Veh. Tech.*, vol. 42, pp. 338-344, Aug. 1993.

[56] X. Yang, H. Han, C. Huang, and J. Habermann, "Communication capacity of sectored CDMA systems," in *Proc. IEEE International Conference on Signal Processing*, vol. 2, pp. 1286-1290, Aug. 2002.

[57] A. R. Lopez, "Performance predictions for cellular switched-beam intelligent antenna systems," *IEEE Communications Magazine*, vol. 34, pp. 152-154, Oct. 1996.

[58] X. Yang, S. Ghaheri, and R. Tafazolli, Sectorization gain in CDMA cellular systems, in *Proc. IEE 3G Mobile Communication Technologies Conference*, pp. 70-75, Mar. 2000.

[59] B. Allen and M. Beach, "On the analysis of switched-beam antennas for the W-CDMA downlink," *IEEE Trans. Veh. Tech.*, vol. 53, pp. 569-578, May 2004.

[60] J. Ramiro-Moreno, K. I. Pedersen, and P. E. Mogensen, "Capacity gain of beamforming techniques in a WCDMA system under channelization code constraints," *IEEE Trans. Wireless Communications*, vol. 3, pp. 1199-1208, Jul. 2004.

[61] E. Viberg and U. Madhow, "Optimum beamforming using transmit antenna arrays," *Proc. VTC 1999*, vol. 1, pp. 851-856, May. 1999.

[62] M. Bengtsson, *Antenna Array Signal Processing for High Rank Data Models*, Dissertation for the degree of Doctor of Philosophy, Royal Institute of Technology, Stockholm, Sweden, 1999.

[63] S. Haykin, *Adaptive Filter Theory*, Prentice Hall, 1996.

[64] A. F. Naguib, "Space-time receivers for CDMA multipath signals," *Proc. IEEE International Conference on Communications*, vol. 1, pp. 304-308, Jun. 1997.

[65] A. F. Naguib and A. Paulraj, "Effects of multipath and base-station antenna

arrays on uplink capacity of cellular CDMA," *Proc. IEEE Global Telecommunications Conference*, vol. 1, pp. 395-399, Nov. 1994.

[66] M. G. Kyeong and J. J. Park, "3G-class space-time array transceiver for high data rate service WCDMA smart antenna system," *Proc. IEEE International Conference on Communications*, vol. 2, pp. 1025-1029, Jun. 2000.

[67] N. A. Mohamed and J. G. Dunham, "Adaptive beamforming for DS-CDMA using conjugate gradient algorithm in a multipath fading channel system," *Proc. IEEE Emerging Technologies Symposium on Wireless Communications and Systems*, vol. 1, pp. 1.1-1.5, 1999.

[68] S. Y. Miller and S. C. Schwartz, "Integrated spatial-temporal detectors for asynchronous Gaussian multiple-access channels," *IEEE Trans. Commun.*, vol. 43, no. 2/3/4, pp. 396-411, Feb./Mar./Apr. 1995.

[69] S. Tanaka, A. Harada, M. Sawahashi, and F. Adachi, "Experiments on coherent adaptive antenna array diversity for wideband DS-CDMA mobile radio," *IEEE J. Slect. Areas Commun.*, vol. 18, pp. 1495-1504, Aug. 2000.

[70] S. Choi, J. Choi, H. Im, and B. Choi, "A novel adaptive beamforming algorithm for antenna array CDMA systems with strong interferers," *IEEE Trans. Veh. Tech.*, vol. 51, pp. 808-816, Sept. 2002.

[71] W. Lee, J. Nam, and C. Ryu, "Joint beamformer-RAKE and decorrelating multiuser detector using matrix levinson polynomials," *IEICE Trans. Commun.*, vol. E83-b, no. 8, pp. 1640-1648, Aug. 2000.

[72] A. Paulraj and C. B. Papadias, "Space-time processing for wireless communications," *IEEE Signal Processing Mag.*, vol. 14, pp. 49-83, Nov. 1997.

[73] A. F. Naguib and A. Paulraj, "Performance of wireless CDMA with M-ary orthogonal modulation and cell site antenna arrays," *IEEE J. Slect. Areas Commun.*, vol. 14, no. 9, pp. 1770-1783, Dec. 1996.

[74] S. Verdú, *Multiuser Detection*, Cambridge University Press, 1998.

[75] S. Kim and S. L. Miller "An adaptive antenna array based propagation delay estimation for DS-CDMA communication systems," *Proc. Military Communications Conference*, vol. 1, pp. 333-337, Oct. 1998.

[76] J. H. Reed, K. J. Krizman, and B. D. Woerner, "An overview of the challenges and progress in meeting the E-911 requirement for location service," *IEEE Communications Magazine*, vol. 36, pp. 30-37, Apr. 1998.

[77] V. C. Soon and Y. F. Huang, "An analysis of ESPRIT under random sensor

uncertainties," *IEEE. Trans. Signal Processing*, vol. 40, pp. 2353-2358, Sept. 1992.

[78] J. Choi, "Pilot channel-aided techniques to compute the beamforming vector for CDMA systems with antenna array," *IEEE Trans. Veh. Tech.*, vol. 49, pp. 1760-1775, Sept. 2000.

[79] S. Lim, J. Lee, and J. Park, "Performance evaluation of adaptive beamforming using pilot and traffic channel in CDMA2000 reverse link," *Proc. IEEE Vehicular Technology Conference*, vol. 4, pp. 2154-2157, Sept. 2002.

[80] A. L. Swindlehurst, S. Daas, and J. Yang, "Analysis of a decision directed beamformer," *IEEE. Trans. Signal Processing*, vol. 43, pp. 2920-2927, Dec. 1995.

[81] A. Klouche-Djedid and M. Fujita, "Adaptive array sensor processing applications for mobile telephone communications," *IEEE Trans. Veh. Tech.*, vol. 45, pp. 405-416, Aug. 1996.

[82] O. Kempthorne and L. Folks, *Probability, Statistics, and Data Analysis*, The IOWA State University Press, 1971.

[83] H. Cox, R. M. Zeskind, and M. M. Owen, "Robust adaptive beamforming," *IEEE. Trans. Acoust., Speech, Signal Processing*, vol. ASSP-35, pp. 1365-1375, Oct. 1987.

[84] G. Xu and H. Lui, "An effective transmission beamforming scheme for frequency-division-duplex digital wireless communication systems," *Proc. ICASSP-95*, vol. 3, pp. 1729-1732, Aug. 1995.

[85] J. Panoff, S. Nagaraj, S. Gollamudi, Y. Huang, and J. A. Nossek, "A minimax approach to open-loop downlink beamforming," *Proc. ISCAS 2001*, vol. 2, pp. 73-76, 2001.

[86] R. T. Derryberry, S. D. Gray, D. M. Ionescu, G. Mandyam, and B. Raghothaman, "Transmit diversity in 3G CDMA systems," *IEEE Commun. Magazine*, vol. 40, pp. 68-75, Apr. 2002.

[87] A. Yener, R. D. Yates, and S. Ulukus, "Interference management for CDMA systems through power control, multiuser detection, and beamforming," *IEEE Trans. on Commun.*, vol. 49, pp. 1227-1239, July 2001.

[88] C., Farsakh and J. A. Nossek, "Channel allocation and downlink beamforming in an SDMA mobile radio system," *Proc. IEEE International Symposium on Personal, Indoor and Mobile Radio Communications Conference*, vol. 2, pp. 687-691, Sept. 1995.

Appendix A

Derivation of (3.13)

The optimum weight vector $\mathbf{w}_{u,v}^{s}$ in the MMSE sense for the SB beamformer can be obtained when the gradient of the cost function

$$J_s = E\left[\mid \mathbf{c}_u{}^H \mathbf{X}^H(nT)\mathbf{w}_{u,v} - \sqrt{p_u}\beta_{u,v}b_u(n) \mid^2\right] \tag{A.1}$$

is equal to zero. It follows that

$$\begin{aligned}\frac{\partial J_s}{\partial \mathbf{w}_{u,v}} &= E\left(\mathbf{X}\mathbf{c}_u\mathbf{c}_u{}^H\mathbf{X}^H\right)\mathbf{w}_{u,v} - E\left[\sqrt{p_u}\beta_{u,v}b_u(n)\mathbf{X}\mathbf{c}_u\right] \\ &= 0.\end{aligned} \tag{A.2}$$

Hence

$$\mathbf{w}_{u,v}^{s} = \mathbf{R}_s^{-1}\mathbf{q} \tag{A.3}$$

where $\mathbf{R}_s$ denotes the correlation matrix of the signal after passing through the MF. Its inverse is given by

$$\begin{aligned}\mathbf{R}_s^{-1} &= E(\mathbf{X}\mathbf{c}_u\mathbf{c}_u{}^H\mathbf{X}^H) \\ &= \rho_{(u,v)}^2\sigma_{u,v}^2\mathbf{a}_{u,v}\mathbf{a}_{u,v}^H + \sum_{\substack{l=1 \\ l\neq v}}^{L_u}\rho_{(u,l)}^2\sigma_{u,l}^2\mathbf{a}_{u,l}\mathbf{a}_{u,l}^H \\ &\quad + \sum_{\substack{k=1 \\ k\neq u}}^{K}\sum_{l=1}^{L_k}\rho_{(k,l)}^2\sigma_{k,l}^2\mathbf{a}_{k,l}\mathbf{a}_{k,l}^H + \sigma_n^2\mathbf{I}\end{aligned} \tag{A.4}$$

where

$$\begin{aligned}\mathbf{q} &= E\left[\sqrt{p_u}\beta_{u,v}b_u(n)\mathbf{X}\mathbf{c}_u\right] \\ &= E\left[\sqrt{p_u}\beta_{u,v}b_u(n)\sqrt{p_u}\beta_{u,v}b_u(n)\mathbf{a}_{u,v}\mathbf{c}_u^H\mathbf{c}_u\right].\end{aligned} \tag{A.5}$$

Since $\mathbf{c}_u^H\mathbf{c}_u = N \mid \mathbf{c}_u(k) \mid^2$, for $k = 0,\ 1,\ \ldots,\ N-1$, $\mathbf{q}$ can be rewritten as

$$\begin{aligned}\mathbf{q} &= E\left[N\mid \sqrt{p_u}\beta_{u,v}b_u(n)\mathbf{c}_u(k)\mid^2\mathbf{a}_{u,v}\right] \\ &= N\sigma_{u,v}^2\mathbf{a}_{u,v}.\end{aligned} \tag{A.6}$$

Hence

$$\mathbf{w}_{u,v}^s = N\sigma_{u,v}^2\mathbf{R}_s^{-1}\mathbf{a}_{u,v}. \tag{A.7}$$

Appendix B

Derivation of (4.63)

The variance of $\hat{r}_k(t)$ is given by

$$\text{var}[\hat{r}_k] = E\{[\hat{r}_k - E(\hat{r}_k)]^*[\hat{r}_k - E(\hat{r}_k)]\} = E(\hat{r}_k^*\hat{r}_k). \tag{B.1}$$

Using (4.29), it can be rewritten as

$$\begin{aligned}
\text{var}(\hat{r}_k) &= E[(e^{-j\phi}r_k^* + n_k^*)(e^{j\phi}r_k + n_k)] \\
&= E[r_k^*r_k] + E[n_k^*n_k] + 2Re[E(e^{-j\phi}r_k^*n_k)] \\
&= E[r_k^*r_k] + E[n_k^*n_k] + 2Re[E(\hat{r}_k^* - n_k^*)n_k] \\
&= E[r_k^*r_k] - E[n_k^*n_k] + 2Re[E(\hat{r}_k^*n_k)]
\end{aligned} \tag{B.2}$$

Substituting (4.48) into (B.2), we have

$$\text{var}[\hat{r}_k] = E[r_k^*r_k] - E[n_k^*n_k] = \sigma_r^2 - \sigma_n^2 \tag{B.3}$$

where σ_r^2 and σ_n^2 are the powers of the reference signal and the estimation error, respectively.

Appendix C

Derivation of (4.68)

It has been shown in (4.48) that

$$E(n_k^* \hat{r}_k) = 0. \tag{C.1}$$

Thus, the variance of $n_k^* \hat{r}_k$ is given by

$$\text{var}(n_k^* \hat{r}_k) = E(n_k^* \hat{r}_k n_k \hat{r}_k^*) = \sigma_n^2(\sigma_r^2 - \sigma_n^2) \tag{C.2}$$

It follows that

$$E[(c + jd)(c - jd)] = E(c^2) + E(d^2) = \sigma_n^2(\sigma_r^2 - \sigma_n^2) \tag{C.3}$$

Hence

$$\text{var}(c) = \text{var}(d) = \sigma_n^2(\sigma_r^2 - \sigma_n^2)/2. \tag{C.4}$$

Appendix D

Derivation of (4.77)

The power of error signal $e_k(t)$ at the output of beamformer A is given by

$$\sigma_e^2 = E[|\, e_k(t)\,|^2] = E\left[|\, (\mathbf{w}_k^A)^H \mathbf{y}_A(t) - r_k(t)\,|^2\right]. \tag{D.1}$$

Substituting (4.12) into (D.1) yields

$$\sigma_e^2 = (\mathbf{w}_k^A)^H \mathbf{R}_A \mathbf{w}_k^A + \sigma_r^2 - 2\mathrm{Re}[\sigma_r \sigma_k (\mathbf{w}_k^A)^H \tilde{\mathbf{a}}(\theta_k)]. \tag{D.2}$$

The power of the error signal $n_k(t)$ at the output of beamformer B is given by

$$\begin{aligned} \sigma_n^2 &= E[|\, n_k(t)\,|^2] = E\left[|\, \hat{r}_k - e^{j\phi_k} r_k\,|^2\right] \\ &= E\left[|\, (\mathbf{w}_k^B)^H \mathbf{y}_B(t) - e^{j\phi_k} r_k(t)\,|^2\right]. \end{aligned} \tag{D.3}$$

Substituting (4.13) into (D.3), we have

$$\sigma_n^2 = (\mathbf{w}_k^B)^H \mathbf{R}_B \mathbf{w}_k^B + \sigma_r^2 - 2\mathrm{Re}[\sigma_r \sigma_k (\mathbf{w}_k^B)^H \tilde{\mathbf{a}}(\theta_k)]. \tag{D.4}$$

From (4.26) and (4.28), it follows that

$$\sigma_e^2 = \sigma_n^2. \tag{D.5}$$

Appendix E

Derivation of (4.80)

By letting $u = \alpha + \beta$, it can be shown that u and v are statistically independent. Their joint probability density function $P_{u,\,v}(u,\,v)$ is given by

$$P_{u,\,v}(u,\,v) = P_v(v) \int_0^\infty P_\alpha(\alpha) P_\beta(u-\alpha) d\alpha \tag{E.1}$$

Assuming that

$$u = \rho \cos(\triangle\phi_k) \tag{E.2}$$

$$v = \rho \sin(\triangle\phi_k) \tag{E.3}$$

and transforming the variables $(u,\,v)$ into $(\rho, \triangle\phi_k)$ using the theorem of transformation of variables [82], the probability density function $P_{\triangle\phi}(\triangle\phi)$ can be obtained as

$$P_{\rho,\triangle\phi_k}(\rho, \triangle\phi_k) = P_{u,v}[\rho\cos(\triangle\phi_k), \rho\sin(\triangle\phi_k)] \left| \begin{array}{cc} \frac{\partial u}{\partial \rho} & \frac{\partial u}{\partial \triangle\phi_k} \\ \frac{\partial v}{\partial \rho} & \frac{\partial v}{\partial \triangle\phi_k} \end{array} \right|. \tag{E.4}$$

(E.4) can be rewritten as

$$P_{\rho,\triangle\phi_k}(\rho, \triangle\phi_k) = \int_0^\infty \rho P_v[\rho\sin(\triangle\phi_k)] P_\alpha(\alpha) P_\beta(\rho\cos(\triangle\phi_k) - \alpha) d\alpha. \tag{E.5}$$

It can be shown that if u is independent from v, then ρ will be independent from $\triangle\phi_k$. The probability density function $P_{\triangle\phi_k}(\triangle\phi_k)$ is then given by

$$P_{\triangle\phi_k}(\triangle\phi_k) = \int_0^\infty P_{\rho,\triangle\phi_k}(\rho, \triangle\phi_k) d\rho. \tag{E.6}$$

and hence

$$P_{\triangle\phi_k}(\triangle\phi_k) = \int_0^\infty \int_0^\infty \rho P_v[\rho \sin(\triangle\phi_k)] P_\alpha(\alpha) P_\beta[\rho \sin(\triangle\phi_k) - \alpha] d\alpha d\rho. \quad \text{(E.7)}$$

VITA

Surname: Wang ***Given Names:*** Nanyan

Place of Birth: Hongan, Hubei, P.R.China

Educational Institutions Attended

University of Victoria	1999 to 2005
Huazhong University of Science and Technology	1996 to 1999
Huazhong University of Science and Technology	1991 to 1995

Degrees Awarded

M.S.	Huazhong University of Science and Technology	1999
B.E.	Huazhong University of Science and Technology	1995

Journal Publications

1. N. Y. Wang, P. Agathoklis, and A. Antoniou, "Analysis of beamformer configurations for DS-CDMA systems", *IEEE Transactions on Signal Processing*, Vol. 53, No. 3, pp. 945-956, March, 2005.
2. N. Y. Wang, P. Agathoklis, and A. Antoniou, "A new DOA estimation technique based on subarray beamforming," Accepted for publication in *IEEE Transactions on Signal Processing* with minor revisions.
3. N. Y. Wang, P. Agathoklis, and A. Antoniou, "A subspace multiuser beamforming algorithm for the downlink in mobile communications," submitted to *IEEE Transactions on Circuit and Systems, Part II.*

Conference Publications

1. N. Y. Wang, P. Agathoklis, and A. Antoniou, "Pilot-aided DOA estimation for CDMA communication systems," *Proc. IEEE International Symposium on Circuits and Systems*, pp. 1441-1444, Kobe, Japan, May, 2005.
2. N. Y. Wang and P. Agathoklis, "A new high-resolution-and-capacity DOA estimation technique based on subarray beamforming," *Proc. IEEE Asilomar Conference on Signals, Systems, and Computers*, vol. 2, pp. 2345-2349, Pacific

Grove, CA, USA, Nov. 2004.

3. N. Y. Wang, P. Agathoklis, and A. Antoniou, "A subspace multiuser beamforming algorithm for downlink of mobile communications," *Proc. IEEE International Symposium on Circuits and Systems*, vol. 3, pp. 381-384, Vancouver, BC, Canada, May 2004.
4. N. Y. Wang, P. Agathoklis, and A. Antoniou, "A new beamforming and power control scheme for wireless mobile communications," *Proc. IEEE Pacific Rim Conference on Communications, Computers, and Signal Processing*, pp. 438-441, Victoria, BC, Canada, Aug. 2003.
5. N. Y. Wang, P. Agathoklis, and A. Antoniou, "A weighted beamforming algorithm for the downlink in mobile communication systems," *Wireless 2003*, vol. 2, pp. 569-574, Calgary, AB, Canada, July 2003.
6. N. Y. Wang, P. Agathoklis, and A. Antoniou, "Analysis of beamformer configurations for DS-CDMA systems," *Proc. IEEE Vehicular Technology Conference*, pp. 1347-1351, Vancouver, BC, Canada, Sept. 2002.
7. N. Y. Wang, P. Agathoklis, and A. Antoniou, "Analysis of MMSE beamformer for DS-CDMA systems," *Proc. IEEE Pacific Rim Conference on Communications, Computers, and Signal Processing*, vol. 1, pp. 128-131, Victoria, BC, Canada, Aug. 2001.
8. N. Y. Wang, L. S. Zhou, Y. Li, and H. J. Hu, "An embedded stability control system for Gezhouba hydropower plant," *Proc. The 13th Annual Central-south China Conference on Power Systems*, vol. 2, pp. 291-295, Dongguan, Guangdong, China, Nov. 1998.
9. Y. Li, L. S. Zhou, N. Y. Wang, and H. J. Hu, "A new application of GPS in automation devices for power systems," *Proc. The 13th Annual Central-south China Conference on Power Systems*, vol. 1, pp. 27-31, Dongguan, Guangdong, China, Nov. 1998.